Master's thesis

NTNU
Norwegian University of Science and Technology
Faculty of Information Technology and Electrical Engineering
Department of Engineering Cybernetics

Edmond Baloku Vigre

Atmospheric Correction for HYPSO-1 Data

Master's thesis in Cybernetics and Robotics
Supervisor: Tor Arne Johansen
Co-supervisor: Sivert Bakken
June 2023

NTNU
Norwegian University of
Science and Technology

Edmond Baloku Vigre

Atmospheric Correction for HYPSO-1 Data

Master's thesis in Cybernetics and Robotics
Supervisor: Tor Arne Johansen
Co-supervisor: Sivert Bakken
June 2023

Norwegian University of Science and Technology
Faculty of Information Technology and Electrical Engineering
Department of Engineering Cybernetics

NTNU
Norwegian University of
Science and Technology

HYPSO-1 Data Analysis

Atmospheric Correction for HYPSO-1 Data

TTK4900 - 30.0 SP

Edmond Baloku Vigre

2023

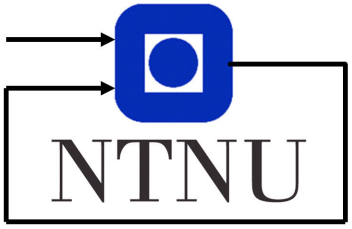

Department of Engineering Cybernetics

Summary

This Master's thesis investigates the application of the ACOLITE atmospheric correction on HYPSO-1 satellite data, comparing it with two other correction methods (6S and ELF), and analyzing the effectiveness of a newly introduced calibration method. The research aims to derive accurate data for environmental applications, such as monitoring harmful algal blooms, by evaluating and comparing the performance of different correction algorithms.

The study demonstrates that ACOLITE outperforms the 6S and ELF methods in terms of alignment with ground station data. Despite challenges encountered, including negative reflectance values at lower wavelengths and output variations, ACOLITE, with its dark spectrum fitting algorithm emerges as a more suitable choice for atmospheric correction of HYPSO-1 data. However, the analysis also highlights the need for a more extensive dataset, particularly captures over various type water bodies, to comprehensively evaluate ACOLITE's performance.

In addition to ACOLITE, this thesis examines a newly introduced calibration method for HYPSO-1 captures. Preliminary comparisons between the old and new calibration coefficients, in line with ground station data, indicate potential improvements in the accuracy of the atmospheric correction process. However, further validation with a larger dataset is necessary to confirm these findings.

Overall, the research underscores the promising results of ACOLITE for HYPSO-1 data correction and the potential for enhanced accuracy with the new calibration method. It emphasizes the importance of ongoing investigation and improvements in certain aspects, while acknowledging the challenges encountered during the study. By contributing to find an optimal method for atmospheric correction of HYPSO-1 data, this thesis serves as a valuable reference for future research in this domain.

Until another correction method that performs better and suits HYPSO-1 data even more is found, ACOLITE is the best fit for atmospheric correction of HYPSO-1 data. However, future work of the pre-processing steps is required to address the negative reflectance values around 400-500 nm. In addition, the new calibration method should be further validated with a larger dataset to confirm its efficacy. Lastly, a matchup analysis with other satellite missions, such as Sentinel or Landsat, would provide a valuable comparison benchmark for assessing the accuracy of ACOLITE for HYPSO-1 data.

Sammendrag

Denne masteroppgaven undersøker bruken av ACOLITE for atmosfærisk korreksjon på HYPSO-1 data, sammenligner den med to andre korreksjonsmetoder (6S og ELF), og analyserer forskjellene til en ny versjon av HYPSO-1 kalibreringen. Denne oppgaven har som mål å utlede nøyaktige data for miljøapplikasjoner, som overvåking av skadelige algeoppblomstringer, ved å evaluere og sammenligne ytelsen til ulike korreksjonsalgoritmer.

Oppgaven viser at ACOLITE presterer bedre enn 6S og ELF når det sammenlignet med data fra bakkestasjoner. Til tross for utfordringer som negative reflektanseverdier i lavere bølgelenger og variasjoner i resultatene, viser ACOLITE med sin DSF algoritme seg å være et mer egnet valg for atmosfærisk korreksjon av HYPSO-1-data. Imidlertid påpeker analysen også behovet for et mer omfattende datasett, spesielt med variasjon av ulike typer vanntyper, for å fullstendig evaluere ACOLITE sin ytelse.

I tillegg til ACOLITE, undersøker denne oppgaven en ny kalibreringsmetode for HYPSO-1 data. Foreløpige sammenligninger mellom gamle og nye kalibreringskoeffisienter, i tråd med data fra bakkestasjoner, indikerer potensielle forbedringer i nøyaktigheten av den atmosfæriske korreksjonsprosessen. Imidlertid er ytterligere validering med et større datasett nødvendig for å bekrefte disse funnene.

Totalt sett understreker forskningen lovende resultatene av ACOLITE for korreksjon av HYPSO-1-data og potensialet for forbedret nøyaktighet med den nye kalibreringsmetoden. Det legges vekt på viktigheten av kontinuerlig undersøkelse og forbedring av visse aspekter, samtidig som det erkjenner utfordringene har blitt møtt. Ved å bidra til å finne en optimal metode for atmosfærisk korreksjon av HYPSO-1-data, tjener denne oppgaven som en verdifull referanse for fremtidig forskning på dette området.

Inntil videre funn av en annen korreksjonsmetoder som passer bedre til HYPSO-1 data for både land- og vannapplikasjoner, er ACOLITE den beste løsningen for atmosfærisk korreksjon. Imidlertid kreves det fremtidig arbeid med forbehandlingsprosedyrene for å håndtere negative reflektanseverdier rundt 400-500 nm. I tillegg bør den nye kalibreringsmetoden valideres ytterligere med en større datasett for å bekrefte effektiviteten. Til slutt ville en sammenligningsanalyse med andre satellittoppdrag, som Sentinel eller Landsat, gi en verdifull referanse for å vurdere nøyaktigheten til ACOLITE for HYPSO-1-data.

Preface

This thesis marks the end of my time at the Norwegian University of Science and Technology (NTNU), a period of significant learning and development. I appreciate the knowledge and skills I have gained here, which have played a critical role in the completion of this work and is the foundation of my upcoming working life.

I want to express my thanks to my supervisor, Sivert Bakken. His guidance and expertise have been crucial during this process, and his support has been greatly appreciated. He has allowed me to explore my interests and provided me with the freedom to pursue my ideas. I am grateful for his patience and encouragement throughout this journey.

Being a part of the SmallSat Lab at NTNU has been an important part of my experience. Team members have shown their interest in helping people new to a satellite project like this. I am thankful for the opportunity to contribute to this project and for the cooperation of the team members I have worked with.

I would also like to thank Quinten Vanhellemont for his help and cooperation to add support for the HYPSO-1 satellite in ACOLITE. His work has been a valuable contribution to this project and for the future of the HYPSO-1 mission.

Contents

Acronyms and Abbreviations

AOT Aerosol Optical Thickness.

BoA Bottom of Atmosphere.

FRM Fiducial Reference Measurement.

HAB Harmful Algae Bloom.

Rrs Remote sensing reflectance.

RRVP Railroad Valley Playa.

SZA Solar Zenith Angle.

ToA Top-of-Atmosphere.

VIIRS Visible Infrared Imaging Radiometer Suite.

VNIR Visible and Near-Infrared wavelengths.

VZA View Zenith Angle.

Introduction

Contents

In January 2022, the Norwegian University of Science and Technology (NTNU) sent the Hyperspectral Smallsat for Ocean Observation - HYPSO-1 into orbit aboard a SpaceX Falcon-9 rocket from Florida. The purpose of this satellite is to observe the ocean and coastal areas from an altitude of 500 km, using both visible and near-infrared wavelengths ranging from 400-800 nanometers [1]. This marked the first time a Norwegian university had launched a research satellite [2].

The main focus of HYPSO-1 is to detect phytoplankton and algae blooms which are not all harmful, but harmful algae blooms (HABs) or cyanobacteria can have negative effects on the ocean's ecosystem and marine environment. HABs can be identified by their colour in the ocean, appearing as red, green, or brown tides with wavelengths ranging from 400-700 nm [1].

To achieve its mission, HYPSO-1 uses hyperspectral remote sensing. This technique involves analyzing the full spectrum of light within the wavelengths of 400-800 nm, rather than just the red, green, and blue components in each spatial image pixel. The intensity of each pixel in the image is analyzed in multiple layers based on the number of bands available on the hyperspectral camera. With 120 bands, this satellite can provide a wealth of information about an image.

1.1 Motivation

Over the last decades in Norway, there has been much investment in marine technology to prevent fish in fish pens from being killed by the HABs. The wild fish in the sea often retreats to the deeper ocean away from these blooms, but as the fish in the fish pens are trapped, it is hard for them to do anything. Figure 1.1 shows HABs hitting a fish farm in Ballangen, Norway, where eight million salmon died because of the algae and phytoplankton blooms. The Norwegian government has allocated millions of NOKs in the past years to fight this. The satellite will be able to detect harmful algae and phytoplankton, which can be vital for marine industries and the ecosystem, especially in Norway, where the fish industry is a big part of the economy [3] [4].

Figure 1.1: Harmful algae hitting a salmon pen in Ballangen, Norway. Image from [4], with permission from Ballangen Sjøfarm.

While the HYPSO-1 satellite has the potential to provide valuable information about harmful algal blooms (HABs) and phytoplankton in the ocean, accurate and reliable data can only be obtained by correcting for atmospheric effects. Atmospheric correction is a necessary step in remote sensing, as it corrects for atmospheric effects such as absorption and scattering of light caused by atmospheric gases and particles, which can lead to errors in the measurement of the radiance at the sensor.

For example, the presence of aerosols in the atmosphere can cause scattering of light, leading to a reduction in the amount of light that reaches the sensor. This can result in an underestimation of the true radiance, and thus, an underestimation of the concentration of phytoplankton or HABs. Similarly, the presence of water vapour in the atmosphere can lead to the absorption of certain wavelengths of light, leading to errors in the measurements.

Therefore, without atmospheric correction, the data obtained from HYPSO-1 may not accurately reflect the true distribution of phytoplankton and HABs in the ocean. Furthermore, as the Norwegian fish industry is a significant contributor to the economy, accurately monitoring and predicting HABs and phytoplankton blooms can help to prevent the economic losses associated with fish deaths caused by these blooms. Thus, the implementation of atmospheric correction in the analysis of HYPSO-1 data is crucial to improving our understanding of these phenomena and their impact on the marine ecosystem and the economy.

1.2 Problem Formulation

The expanding field of hyperspectral remote sensing offers plenty of detailed images. These images provide valuable insights into various applications including vegetation monitoring, mineral mapping, water quality analysis or finding HABs. However, the pre-processing stage of these hyperspectral images presents challenges.

Raw hyperspectral images are subjected to a variety of atmospheric disturbances, such as scattering, absorption, and the presence of sun glint. These disturbances distort the image quality and compromise the authenticity of the data, particularly in hyperspectral water images.

Atmospheric correction methods, including empirical line fits, 6S, dark spectrum fitting, look-up tables and a lot more methods, have been developed to address these issues. However, they each have their limitations and can yield unsatisfactory results. In this thesis, the open-source software ACOLITE which uses the dark spectrum fitting method will be used to perform the atmospheric correction. Another key issue is the accurate georeferencing of these hyperspectral images, which, if not achieved correctly, can lead to substantial inaccuracies in data analysis and interpretation.

A primary question that arises in this context is, "How does the atmospheric correction performed by ACOLITE impact the accuracy of reflectance values derived from HYPSO-1 data compared to ground station data for water applications?". Additionally, a comparative assessment between different correction algorithms could provide insights into their efficiency, leading to another research question, "How do different atmospheric correction algorithms compare in their accuracy of deriving reflectance from HYPSO-1 data?"

Lastly, understanding the variance in the accuracy of the atmospheric correction of HYPSO-1 satellite data between land and water could provide valuable information. This prompts the research question, "How does the atmospheric correction performed by ACOLITE impact the accuracy of reflectance values derived from HYPSO-1 data compared to ground station data for land applications?".

1.3 Objective and Tasks

The objective of this thesis is to develop and evaluate a method for atmospheric correction of HYPSO-1 captures, with a focus on hyperspectral water images.

To achieve this, the following tasks will be undertaken:

- **Deepen Understanding of Background Theory:** A exploration of hyperspectral remote sensing, the impact of atmospheric factors, and existing pre-processing and atmospheric correction methods are necessary to recognize disparities and potential areas for improvement.

- **Review and Evaluate Existing Pre-processing and Georeferencing Techniques:** A evaluation of current pre-processing techniques, atmospheric correction methods, and geo-

referencing techniques is crucial to understand their limitations and identifying potential enhancements.

- **Implement HYPSO-1 support for ACOLITE:** This task will involve incorporating the HYPSO-1 satellite data within the ACOLITE software. Support for each satellite or sensor is needed to be added individually to ACOLITE. This task will be done in collaboration with the person responsible for ACOLITE..

- **Test and evaluate:** The task consists of validating the results of the atmospheric correction performed by ACOLITE. To answer the research questions, atmospheric correction over water and land application is needed to be performed. As well as comparing the results from ACOLITE with the results from 6S and ELF.

- **Conclude:** The final task will involve summarizing the results of the atmospheric correction performed by ACOLITE and comparing the results with those obtained from different methods. The results will be discussed to find a conclusion and future work will be precised.

Background theory

Contents

2.1 Hyperspecral Remote Sensing

Hyperspectral remote sensing is a method that analyzes the spectrum of light on each pixel, rather than relying on the traditional approach of observing images in red, green or blue. The images captured by the satellite are divided into multiple spectral bands, with this particular satellite boasting 120 bands and utilizing a push-broom imager to create a single hyperspectral cube, where you can represent a continuous spectrum for a single point on the image.

The significant advantage of hyperspectral remote sensing lies in the level of analysis that can be performed on specific objects. This is because we can detect unique objects by their colour signature, which is obtained from the spectrum of light captured in the detailed images on multiple bands. The focus of this particular satellite is on the VNIR wavelengths (400-800 nm).

Each band on the hyperspectral imager represents a single measurement that contributes to the continuous spectrum of the object's reflectance. Figure 2.1 presents an example of a hyperspectral cube, where each band is a layer of a different colour. The red box in the cube represents one pixel, and we can analyze the desired spectrum of light for that specific pixel.

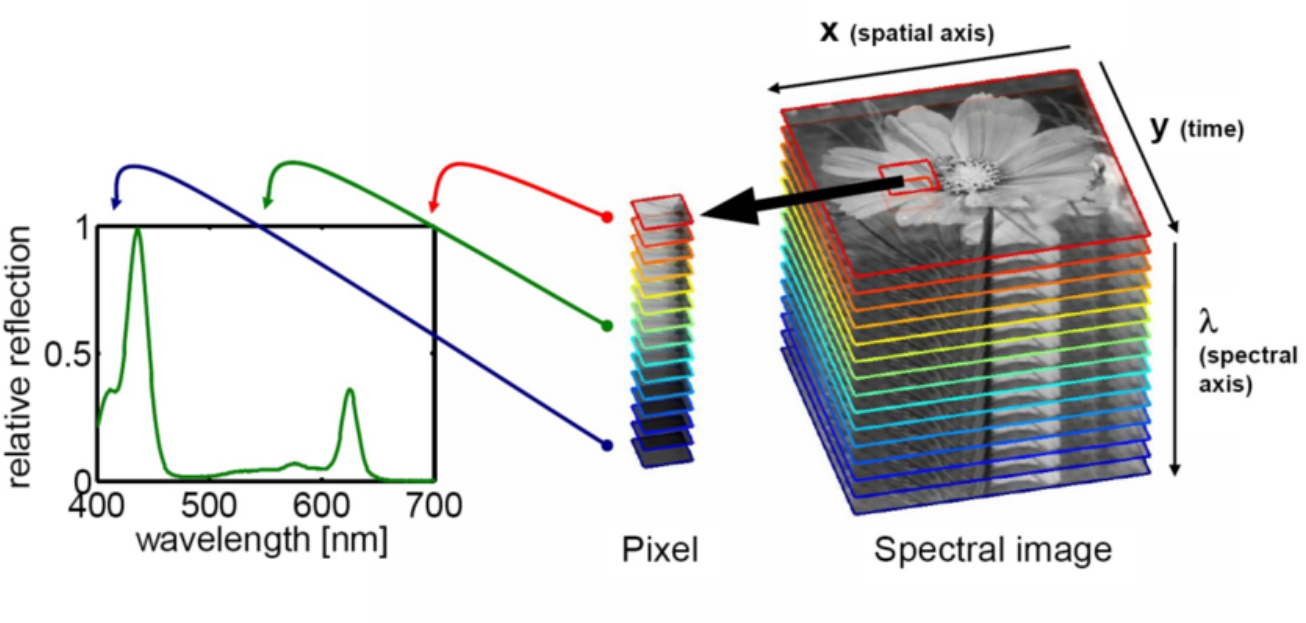

Figure 2.1: Hyperspectral cube with each wavelength for one pixel, figure from [5]

The utilization of hyperspectral remote sensing is also useful for monitoring processes such as chlorophyll, which indicates the abundance of HABs. The chlorophyll indicators can appear as red, green, or brown tides in the ocean on hyperspectral images. The different colours of the HABs result from the type of algae. For example, red tides indicate HAB-type dinoflagellates, green tides indicate HAB-type cyanobacteria and brown tides indicate HAB-type diatoms [6]. Different types of HABs have different negative impacts on the environment and human health, and we can identify the colourful tides by analyzing images using the mentioned method.

Figure 2.2a below, to the left, shows an extensive phytoplankton bloom in Vancouver, Canada. Figure 2.2b below, to the right, shows that we can use the data from the image to check the chlorophyll concentration in this area. The higher the chlorophyll concentration, the more intense the red colour, which again indicates the phytoplankton bloom.

The image to the right was generated using a basic algorithm that first identifies water by differentiating between subtle variations in reflectance across the light spectrum. After water is identified, a simple algorithm estimates the chlorophyll-a concentration in the water. The estimation of chlorophyll-a concentrations is based on the average reflectance at three particular spectral bands. These bands were chosen due to their known association with chlorophyll-a absorption and reflection properties. The average reflectance value at these bands is indicative of the relative amount of chlorophyll-a in the water, and therefore, the density of phytoplankton blooms.

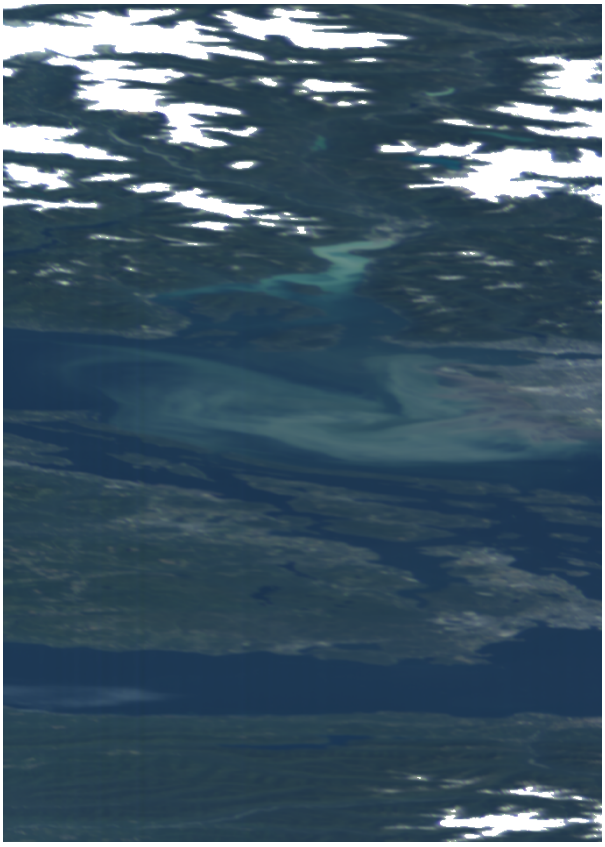

(a) The hyperspectral image of Vancouver, Canada, taken by HYPSO-1 22.07.2022

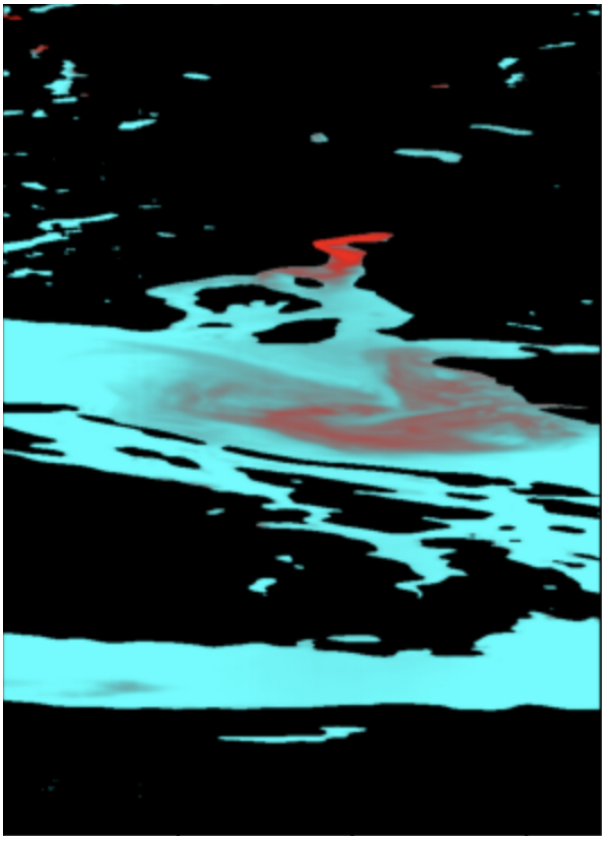

(b) Image shows chlorophyll; more intense red signifies higher levels.

Figure 2.2: The images exemplifies how we can use hyperspectral remote sensing to detect chlorophyll concentration in the ocean

This estimated chlorophyll-a concentration is subsequently normalized and used to assign an RGB colour value for visualization purposes. The resulting image portrays regions of high chlorophyll-a concentration as shades of red and lower concentrations in a bluish hue, providing a visually intuitive representation of phytoplankton distribution.

While the image and algorithm employed in this study illustrate the capabilities of HYPSO-1 in detecting phytoplankton blooms, it's essential to highlight that a more advanced algorithm could potentially increase the precision of these chlorophyll-a concentration estimates. Further work could explore different spectral bands or more complex chlorophyll-a estimation models to refine the algorithm and achieve higher accuracy.

The method of capturing these images is through the use of a push-broom scanner, which is also known as an along-track scanner. The scanner operates by sequentially scanning multiple lines in the along-track direction and requires high spectral and spatial resolution to minimize the spectral mixing effect and blur in the image pixels. This can be challenging to achieve, as the imager is moving at high speeds and the satellite is in orbit. HYPSO-1 overcomes this issue by tilting

the hyperspectral imager backwards as it translates forward, resulting in overlapping pixels that improve the spatial resolution. Figure 2.3 illustrates how the push-broom scanner scans along-track, creating a cube in the x direction with pixels in the y and λ cross-track direction [1].

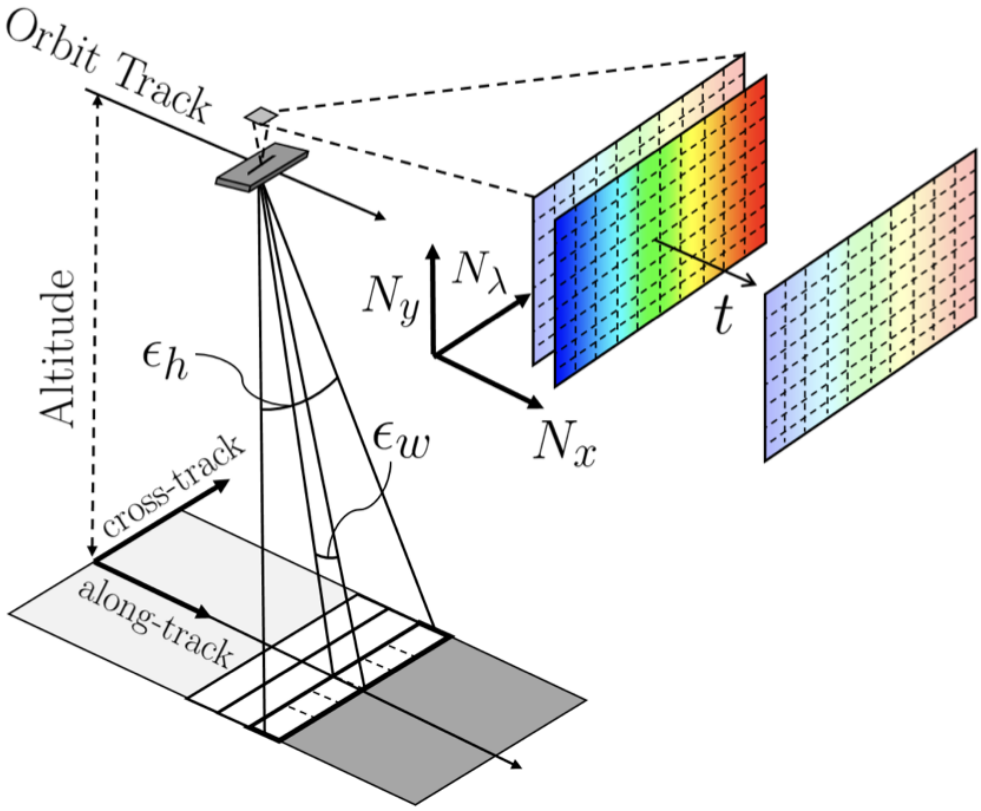

Figure 2.3: The figure shows how the push-broom scanner scans along-track, figure from [1]

2.2 Atmosphere and Atmospheric Correction

A challenge in hyperspectral remote sensing is the impact of atmospheric conditions on the quality of images. The atmosphere acts as a complex medium that can absorb, scatter, and reflect light. This can create difficulties in image analysis as the light reflected from the target object may differ from the light reflected from the atmosphere. The only source of natural light for hyperspectral imaging is the sun. Figure 2.4 depicts the absorption and scattering of radiation from the sun on its way to the surface and on its way back to the hyperspectral imager.

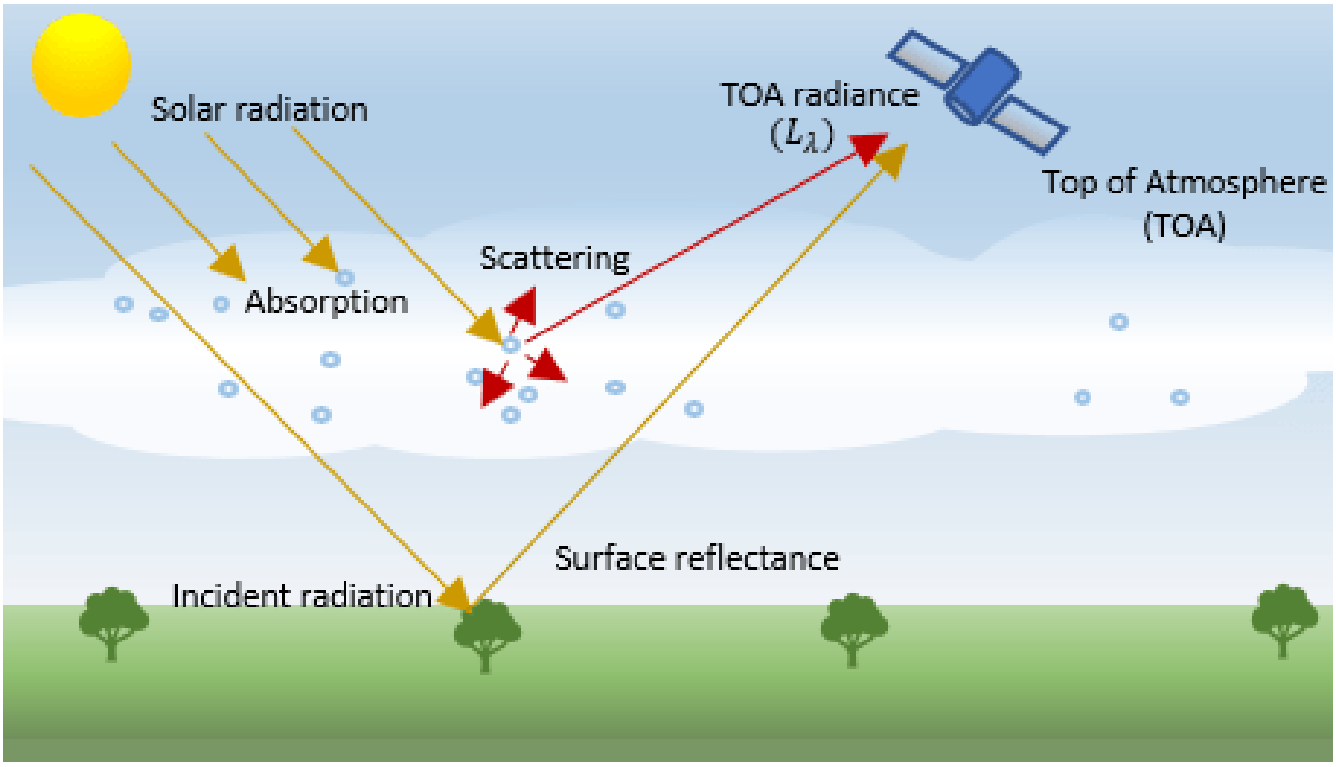

Figure 2.4: An illustration of the atmospheric effects on hyperspectral imaging, figure from [7]

2.2.1 Scattering and Absorption

The atmosphere consists of different particles and gases causing different atmospheric effects. Scattering takes place when aerosols, particles or gases interact with electromagnetic radiation. Aerosols consist of solid or liquid particles suspended in the air, often as a result of human activity. The scattering effect varies depending on different factors, such as the wavelength of the radiation, the distance between the how far the radiation travels through the atmosphere and the prosperity of particles and gases. As much as 90% of the ToA radiance is caused by scattering of the sunlight radiation [8]. There are different types of scattering depending on the wavelengths of the radiation, as for HYPSO-1 the most relevant types are Rayleigh- and aerosol scattering due to these types usually occurring around the same wavelengths that HYPSO-1 operate in.

Aerosol scattering takes place if the radiation passes through particles that are much larger than the wavelengths of the radiation [9]. Rayleigh scattering takes place when the radiation passes through particles that are much smaller than the wavelength of the radiation. These particles could be dust or nitrogen and oxygen molecules in the upper atmosphere. This phenomenon is scattering the shorter wavelengths such as the blue of the VNIR spectrum and this is what causes the sky to be blue during the day [10][11][12]

Absorption is a phenomenon where aerosols and molecules absorb electromagnetic radiation at different wavelengths. This causes some wavelengths to lose light intensity and may result in wavelengths are not properly transmitted or reflected. The molecules responsible for this phe-

nomenon consists mostly of ozone, carbon dioxide and water vapour. The ozone layer absorbs ultraviolet radiation which works as a protective layer so humans do not burn their skin. The carbon dioxide and water vapour along with a couple of more gases that are associated as greenhouse gases are responsible for absorption around the infrared (IR) electromagnetic radiation which is also causing thermal heating on Earth. The amount of radiation that is absorbed varies with the concentration of these gases, the wavelengths and the intensity of the radiation [11].

2.2.2 Sun Glint

Sun glint occurs on an image when the sun is reflecting off the surface of the ocean at the same angle the satellite sensor views it and causes a bright spot of light on an image. This causes a high surface reflectance to be reflected to the hyperspectral imager around the longer wavelengths in VNIR and may disrupt an image. The sun glint may as well cause loss of data on specific pixels due to saturation of the sensor [13]. Another issue is that the bright sun glint may be mistaken as clouds which may lead to difficulties as well.

Figure 2.5 below, is taken by the VIIRS satellite in 2018 [14], and the white cloudy-like area in the middle is sun glint. This image illustrates how sun glint is a problem for not only hyperspectral imaging but also for other types of optical remote sensing.

Figure 2.5: The image captured by VIIRS in 2018 shows the sun glint effect, image from [14].

2.2.3 Challenges with Hyperspectral Water Images

Hyperspectral imaging faces challenges in capturing accurate data in both land and water environments, but water-based imaging presents additional difficulties due to the unique properties of water and general weather. These challenges are quite relevant for HYPSO-1 because of its mission of capturing hyperspectral images over coastal- and ocean water. More often and so will there be a dynamic environment in the water that could cause disturbances. Disturbances such as waves, currents and tides, as well as the presence of HABs, may exist in one image and may not exist in the next. The presence of these disturbances may lead to inconsistent images from time to time. Another challenge that differs from land to water is the presence of sun glint in the water as explained in the subsection above. There are as well challenges with land surfaces due to weather, vegetation and industrial growth, however, these factors are generally much slower and more predictable than those in the ocean and water.

In figure 2.5 there are some dark spots in the middle of the image where there appears to be no sun glint. At these dark spots, there are no wind waves which causes the ocean to operate as a mirror and removes the sun glint from the image in those areas. This shows as well how the dynamic environment in the ocean may cause different results at different times [14].

These challenges for water bodies can lead to difficulties in the calibration and validation of hyperspectral images because of the available fiducial reference measurements (FRMs) from a ground station. If the FRMs are unstable and inaccurate, it could lead to difficulties in analysing results. It is desirable to have FRMs available over specific areas with reflectance measurements inside the same hour as the HYPSO-1 capture to have the most accurate validation of the corrected data. This will be covered in more details in the following chapter.

The properties and challenges with water can affect the Signal-to-Noise Ratio (SNR), which is a measure of the instrument's ability to resolve spectral signatures and is impacted by correlated signal noise and uncorrelated image sensor noise. While a high SNR is desirable for better radiometric accuracy and improved atmospheric correction, it is important to ensure this is not achieved at the expense of spectral resolution. Over-processing of data, such as aggressive spectral binning or smoothing to boost SNR, can make it difficult to distinguish between different spectral bands or wavelengths and to discern fine details of the spectrum.

2.2.4 Top of Atmosphere

The light received by the hyperspectral imager on a satellite can be represented by the total Top of Atmosphere (ToA) radiance, which is a complex and challenging quantity to predict due to the atmospheric challenges mentioned above. According to [1], the total ToA radiance can be expressed as:

$$L_{tot}^{ToA} = L_{atm}^{ToA} + t_{dir}L_{sg} + t_{diff}L_{wc} + t_{diff}L_{water} \tag{2.1}$$

where:

- L_{tot}^{ToA} represents the total radiance at the top of the atmosphere
- L_{atm}^{ToA} represents the combined radiance of Rayleigh, aerosol, and Rayleigh-aerosol interaction scattering, including sky background reflection and scattering
- t_{dir} and t_{diff} represent the direct and diffuse transmittance along the optical path, governed by wavelength
- L_{sg} represents the surface-based specular reflection of sun glint radiance transmittance
- L_{wc} represents the sun and sky radiance reflected by whitecaps and foam
- L_{water} represents the water-leaving radiance

2.3 Pre-Processing Hyperspectral Images

Four different main levels are defined by NASA explaining how much satellite data is processed [15]. Level 0 data is the raw unprocessed data and the payload data are at full resolution. At this level, the data may contain various types of noise or errors. For HYPSO-1 this is raw data where the intensity of light is represented in digital counts and yet not processed.

Level 1 consists of three sublevels. Level 1A is still unprocessed data at full resolution, but with the addition of ancillary information containing radiometric and geometric coefficients, as well as georeferencing parameters for calibration. These coefficients and parameters are calculated but not applied to the Level 0 data. At Level 1B the L1A data are processed to sensor units and the coefficients are applied. Level 1C data have new variables that describe the spectrum of light. At this level, the data has been calibrated.

Level 2 data has the data processed to geophysical variables at the same resolution and location. This level is achieved by applying atmospheric correction to remove the effects of the atmosphere, clouds and water vapour causing attenuation. Level 3 data maps variables on uniform space-time grid scales. Level 4 is the final level where you have some result analysis or model output.

Spectral calibration is part of processing level 0 data into level 1 data and is a critical step in hyperspectral remote sensing, as it ensures the accurate determination of the spectral band centres for all samples in a hyperspectral data cube. Specifically, the case of a dispersive imaging spectrometer is typically addressed, involving the characterization of the centre wavelength for each element of a two-dimensional focal plane array to correct any potential spatial-spectral distortion [16].

Another crucial step part of processing level 0 data into level 1 data is to perform radiometric calibration. This calibration process is estimating the ToA spectral radiance corresponding to the spectral calibrated wavelengths. The intensity of light is represented by the use of digital count in the raw images captured by HYPSO-1. This is mainly due to the sensor, as well as it is the simple

way to represent the intensity of light. Converting the digital count to radiance is needed to be done to have the correct unit for an atmospheric correction, as during the atmospheric correction process, the ToA radiance is used to calculate the surface reflectance [7][16].

2.4 Atmospheric Correction Methods

The atmospheric effects pose a challenge for HYPSO-1, reducing the satellites accuracy in its main objective, namely to detect HABs. Ideally, radiative transfer models would incorporate built-in atmospheric correction methods. However, real-time satellites may not be able to accommodate these methods due to their complexity and computational demands [1]. There are a variety of methods for atmospheric correction, ranging from simple to complex, which can be applied after data is transferred from the satellite to the ground station. These methods can under- or overcorrect the ToA radiance, leading to varying accuracy.

There are many different methods to perform atmospheric correction, whereas some or more advanced and some simpler and different results may be achieved. The methods can be divided into two categories, empirical and physical. The empirical methods have a more statistical analysis approach trying to find an empirical relationship between sensor measurements and atmospheric parameters and do not take the physical properties of the atmosphere into account. Physical methods are based on the theoretical physics of the atmosphere and the interaction between the atmosphere and light.

2.4.1 Empirical Line Fits

Empirical Line Fits (ELF) is a widely used method for atmospheric correction that is based on the assumption that the spectral reflectance of a target surface can be accurately measured in the field. The ELF method involves the creation of a linear relationship between the measured radiance from a ground station and radiance derived from a satellite capture, which is then used to derive the atmospheric correction coefficients for the remote sensing data [17]. Ideally, the ground station measurement is taken at the same location and time as the satellite capture.

The linear relationship is defined by a slope and an intercept. The slope of this relationship represents the rate at which the satellite's measurements change as the ground station's measurements change, while the intercept represents the value of the imager's measurements when the ground station's measurements are zero. From [16], the slope is defined by equation (2.2) below, and the intercept is defined by equation (2.3):

$$\hat{a}(\lambda) = \frac{L_2(\lambda) - L_1(\lambda)}{\rho_2(\lambda) - \rho_1(\lambda)} \tag{2.2}$$

$$\hat{b}(\lambda) = \frac{L_1(\lambda)\rho_2(\lambda) - L_2(\lambda)\rho_1(\lambda)}{\rho_2(\lambda) - \rho_1(\lambda)} \tag{2.3}$$

where:

- $\rho_1(\lambda)$ and $\rho_2(\lambda)$ are radiance values from two pixels from the imager
- $L_1(\lambda)$ and $L_2(\lambda)$ are the corresponding ground station measurements

Together, the slope and intercept allow the ELF technique to convert the imager's measurements to values of sea-surface radiance, which can be used to calculate the water-leaving radiance of a body of water. The corrected water-leaving radiance is then applied to all pixels of the image and is found using the following equation:

$$\hat{\rho}_i(\lambda) = \frac{L_i(\lambda) - \hat{b}(\lambda)}{\hat{a}(\lambda)} \tag{2.4}$$

2.4.2 6S

The Second Simulation of a Satellite Signal in the Solar Spectrum (6S) is a radiative transfer model frequently employed for atmospheric correction of satellite images. It simulates the transmission and reflection of solar radiation through the Earth's atmosphere. This method takes into account both absorption and scattering phenomena induced by atmospheric constituents such as gases and aerosols. Notably, 6S considers the effects of molecular and aerosol scattering, gas absorption, and surface reflectance characteristics.

One of the essential features of the 6S method is the use of Look-Up Tables (LUTs). LUTs represent pre-computed simulations under a variety of atmospheric and surface conditions, which simplifies the retrieval process. This design enables the model to be computationally efficient while maintaining a high degree of accuracy [18].

The 6S model's flexibility and versatility have resulted in its wide adoption in the correction of images from diverse satellite platforms. It has been successfully used to correct images from the Landsat series and the Sentinel-2 MultiSpectral Instrument, among others, providing reliable and satisfactory results. This method enables accurate retrieval of surface reflectance, a critical variable in various remote sensing applications, from monitoring land use change and vegetation health to assessing water quality and urban expansion [19][20].

The 6S model continues to evolve, with updates and improvements aimed at enhancing performance and extending its applicability to newer sensors and different atmospheric correction challenges. These continuous developments are a testament to the 6S method's robustness and its vital role in advancing remote sensing science.

2.4.3 Dark Spectrum Fitting

The Dark Spectrum Fitting (DSF) approach for atmospheric correction in optical satellite imagery for aquatic applications. The DSF algorithm creates a dark spectrum using multiple dark targets

in the scene to estimate the atmospheric path reflectance using the best-fitting aerosol model. The processing allows for a seamless atmospheric correction for full and merged scenes, making it suitable for a wide range of environments, including clear and turbid coastal waters, inland waters and land. ACOLITE is an open-source software for atmospheric correction of satellite data that uses the DSF method. The use of ACOLITE will be further explained in the next chapter.

The essence of the algorthm used by ACOLITE starts by converting the satellite's Top of Atmosphere (ToA) radiance to ToA reflectance using the following equation:

$$\rho_{ToA} = \frac{\pi \cdot L_{ToA} \cdot d^2}{F0 \cdot cos(\theta_s)} \tag{2.5}$$

where L_{ToA} is the ToA radiance, d is the Earth-Sun distance, F0 is the mean extraterrestrial solar irradiance given by [21] and θ_s is the solar zenith angle. The ρ_{ToA} is then corrected for atmospheric gas transmittance (t_{gas}) to obtain the corrected ToA reflectance using the equation:

$$\rho_{ToA} = \frac{\rho_{ToA}}{t_{gas}} \tag{2.6}$$

The corrected ToA reflectance is then modelled according to the equation proposed by [22] with the use of Lookup Tables (LUTs). The LUTs consist of data such as atmospheric path reflectance,ρ_{path}, two-way diffuse atmospheric transmittance, t_d, and the spherical albedo of the atmosphere,S, used in the proposed equation:

$$\rho_{ToA} = \rho_{path} + \frac{\rho_s \cdot t_u \cdot t_d}{1 - \rho_s \cdot S} \tag{2.7}$$

After estimating the AOT and applying the correction, surface level reflectance (ρ_s) is computed. Finally, if wanted, the remote sensing reflectance is obtained by dividing the corrected ρ_s by π. [23][24].

2.4.4 Look-Up Tables

The use of Look-Up Tables (LUTs) is commonly used across various atmospheric correction methods. LUTs are sensor-specific precomputed radiative transfer functions that contain information about various atmospheric and surface conditions. This is heavily used because it is computationally expensive to find a radiative transfer model and it can take up to several hours to build LUTs [25], while if you have predefined LUTs you can emulate them to perform a time-saving and more efficient atmospheric correction. The LUTs usually only need to be built once, and then they can be emulated for future use. Even for empirical methods that do not specifically use radiative transfer models, they can still use LUTs to retrieve pre-calculate information about atmospheric

properties such as aerosol thickness, water vapour or other pre-calculated properties that can be used to achieve a better performing atmospheric correction.

Methods and Tools

Contents

3.1 ACOLITE

ACOLITE is an open-source software that uses the Dark Spectrum Fitting (DSF) method combined with Look-Up Tables (LUTs) to perform atmospheric correction, funded by various projects by the Belgian Science Policy Office STEREO program and by the European Community's Seventh Framework Programme [26]. It was first released around 2018 mainly for the multispectral Landsat and Sentinel-2 satellites, but has since been continuously developed with improvements and added support for hyperspectral satellites and sensors. It uses the DSF method to estimate aerosol optical thickness (AOT), atmospheric path reflectance, transmittances and spherical albedo. The software is mainly for use in water applications, especially turbid and productive waters, but can be applied on clear water and land as wel. ACOLITE performs an atmospheric correction and transforms the level 1 processed data into level 2 data. A geolocated and atmospheric corrected NetCDF file is created as output along with RGB images of the corrected data.

This software has shown promising results for other satellites and is a good candidate for the atmospheric correction of the HYPSO-1 data. The person responsible for the software has to create support for each satellite and sensor to be able to use specific satellite data with the software. I reached out to the person responsible for the software and asked if it was possible to add support for HYPSO-1 data. He was very enthusiastic about the idea and through active communication and collaboration, we were able to successfully integrate HYPSO-1 satellite data into ACOLITE. The open-source code is available on GitHub [26].

After cloning the software from GitHub it is possible to launch ACOLITE by running the Python script **launch_acolite.py** located in the repositorary. Figure 3.1 below, shows the user interface of the software. To be able to process HYPSO-1 data, you have to select a NETCDF4 (.nc) HYPSO-1 data file and select a folder to output the results. You do as well have the option to select a region of interest by either typing in boundaries in south, north, west and east or by providing a polygon file with the desired region of interest. In the ACOLITE manual [27], it is a list of different algorithms that you can type in the L2W parameters field for the retrieval of different parameters, parameters such as **Rrs_*** for remote sensing reflectance retrieval. This L2W parameter will be used in the validation process. It is possible to save the settings file with the chosen parameters to be easily restored next time. The atmospheric correction process is started by clicking on **Run processing**. The software will then start processing the data and output the results in the selected output folder. This process is completed on all the captures that will be used for the validation in the following chapter.

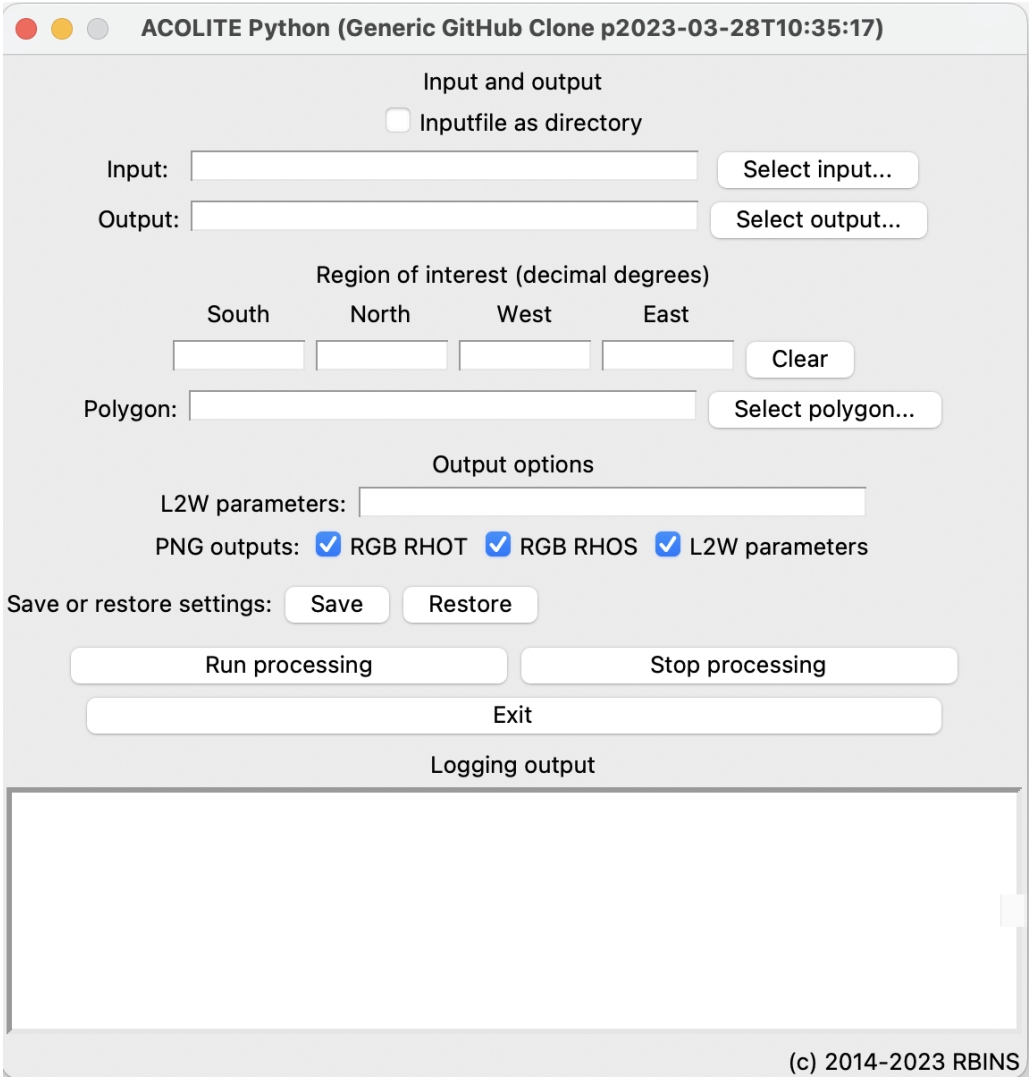

Figure 3.1: The figure shows the graphical user interface of ACOLITE

The input to ACOLITE is as mentioned needed to be a NETCDF4 file format (.nc), which is not generated in the raw HYPSO-1 data. This has to be generated by using the script **h1data_processing.py** created by the HYPSO-1 team member, Sivert Bakken. This script takes the raw data folder as input, performs radiometric- and spectral calibration and generates a .nc file [28] which can be used in ACOLITE.

3.2 Ground Stations

It is necessary to compare the remote sensing reflectance captured and processed by HYPSO-1 and ACOLITE with reference measurements from ground-based stations to validate the correction that is performed. The reference measurements are often referred to as Field Radiometric Measurements (FRMs) as mentioned earlier. These instruments can capture a wide variety of data,

from atmospheric properties, such as aerosol content and humidity, to terrestrial attributes, like the reflectance of the earth's surface or water-leaving radiance in bodies of water.

Two different ground station networks will be used - Aerosol Robotic Network (AERONET) and the Radiometric Calibration Network (RadCalNet). These networks provide valuable reference measurements that aid in validating the correction performed on the remote sensing reflectance data captured by the HYPSO-1. They are chosen due to the matchup with HYPSO-1 captures over the ground station from these networks. These networks have sites equipped with different instruments, offering a broad range of parameters for comparison, validation, and calibration of satellite data. However, in this thesis the focus for the validation will be primarily be on water-leaving radiance, ToA and BoA reflectance measurements, given their relevance to the validation of optical properties of water and land.

In the following sections and chapters, three ground stations will be further explained and used for validation. Figure 3.2 below, shows three markers of the geographical location of the ground stations. The top right marker is the Acqua Alta Oceanographic Tower (AAOT) outside of Venice, Italy. The upper left marker is Railroad Valley Playa (RRVP) in Nevada, United States. The marker at the bottom is Gobabeb, Namibia.

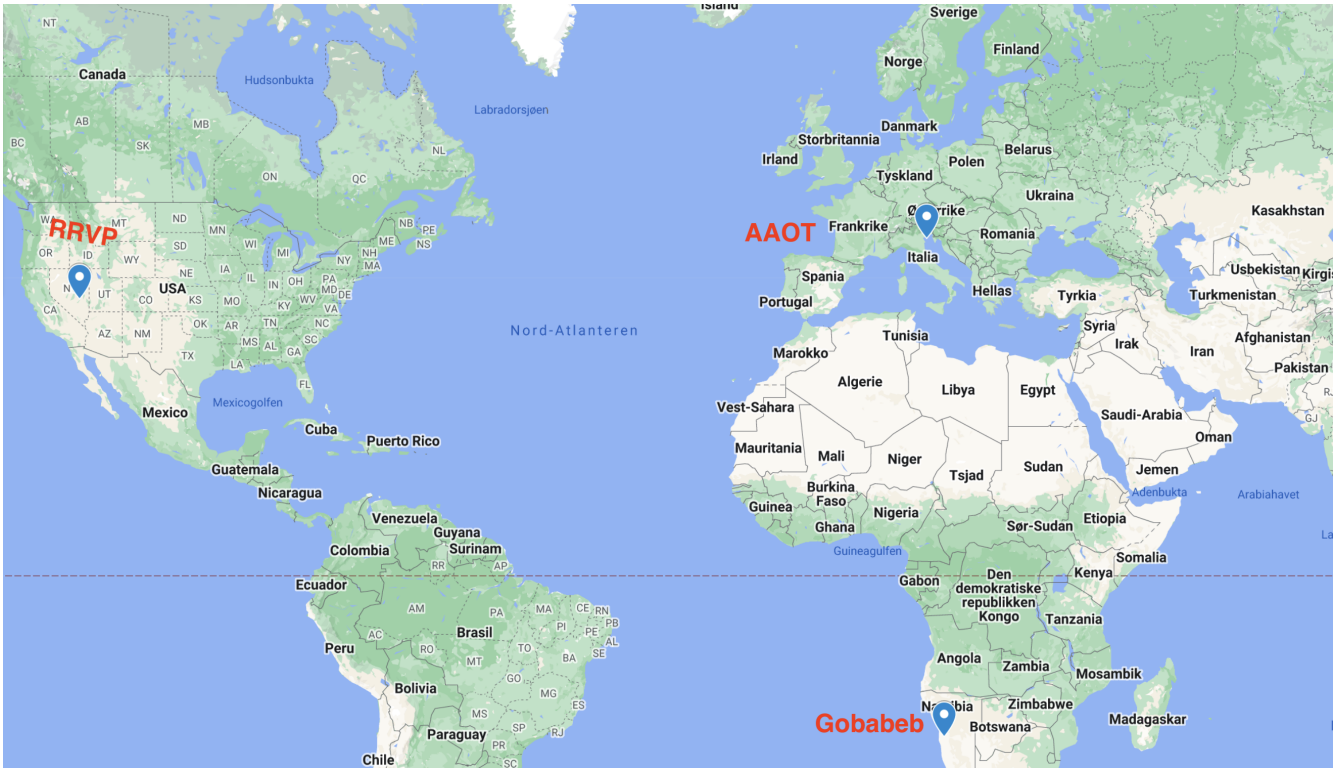

Figure 3.2: The map shows the location of the three ground stations that will be used for validation. Top right is AAOT, top left is RRVP and bottom is Gobabeb.

3.2.1 AERONET

One widely used network of ground stations is the Aerosol Robotic Network (AERONET). AERONET was established in 1993 as a collaboration between NASA and PHOTONS and currently consists of hundreds of sites around the world. Each site is equipped with different instruments, which measure different parameters, where the water-leaving radiance is the one that will be used for this validation. The water-leaving radiance is the radiance that is leaving the surface of the water and going into the atmosphere. It is an important parameter for remote sensing of the ocean, as it provides the possibility of validation of the optical properties of the water [29].

The Acqua Alta Oceanographic Tower (AAOT) outside of Venice, Italy is a good source to use for validation [30]. HYPSO-1 has 120 bands ranging from 400-800 nm, which is the same range as the AAOT station. However, the AAOT station does not have this many measurements for the water-leaving radiance varying in different wavelengths. AAOT has twelve different measurements from 400-1020 nm, where only the first nine are interesting for HYPSO-1. The wavelengths available are 400, 412, 443, 490, 510, 560, 620, 667, 779 [nm].

The data available from the AAOT station can be categorized into three different processing levels. Level 1.0 data are unscreened and raw data. Level 1.5 data are cloud-cleared and quality controlled, but the data may not have its final calibration applied. Level 2.0 data are automatically cloud-cleared and quality assured with pre-field and post-field calibration applied [31]. In general, it is always desired to use the level 2.0 data, but the level 1.5 data from AAOT is only raised to level 2.0 when the instrument is returned to the laboratory every 12 months. This happens every June and is thus too late to be used for this thesis.

In dialogue with the site manager for the AAOT site, it was precised that the difference between level 1.5 and level 2.0 data is often small and negligible, but some level 1.5 data may be excluded from level 2.0 data because of poor quality. To be able to use the level 1.5 data, the data can be compared with the level 2.0 data to see the differences. HYPSO-1 currently have a couple of captures over this ground station. Level 1.5 and level 2.0 data from AAOT are compared a year before but on the same day and month of the HYPSO-1 captures. The AAOT data for the previous year may not necessarily be comparable to the AAOT data that will be used for the validation but is most likely the best option for comparison due to many of the factors affecting the water-leaving radiance is more likely to be the same at the day and month of the previous year. This is done to see if it is possible to use the level 1.5 data on the same day as the HYPSO-1 captures.

Data Level Comparison

Data from 07/02/2022 and 08/02/2022 will be used for data comparison. The water-leaving radiance data has been downloaded from the AAOT website [31]. The data that is downloaded has to be converted from water-leaving radiance to Remote sensing reflectance (Rrs) to use the same unit as the output from ACOLITE. Rrs is a measure of the ratio of the upwelling radiance leaving the water's surface to the downwelling irradiance that arrives from the sun. This is done by dividing the water-leaving radiance on the mean extraterrestrial solar irradiance given from [21].

The level 1.5 (blue) and level 2.0 (orange) data for 07/02/2022 are plotted on top of each other

to illustrate the differences at the different wavelengths in figure 3.3 below. It is noticeable that there is no difference in all the measurements except the measurement at 13:46. This is typically one of the measurements that would probably be removed or calibrated when raising level 1.5 to level 2.0. Upon initial inspection, the Rrs values seem to contain variability across different wavelengths. However, the scale provided by the y-axis reveals that the actual difference between these values is relatively minor, as the absolute magnitudes of these variations are quite low.

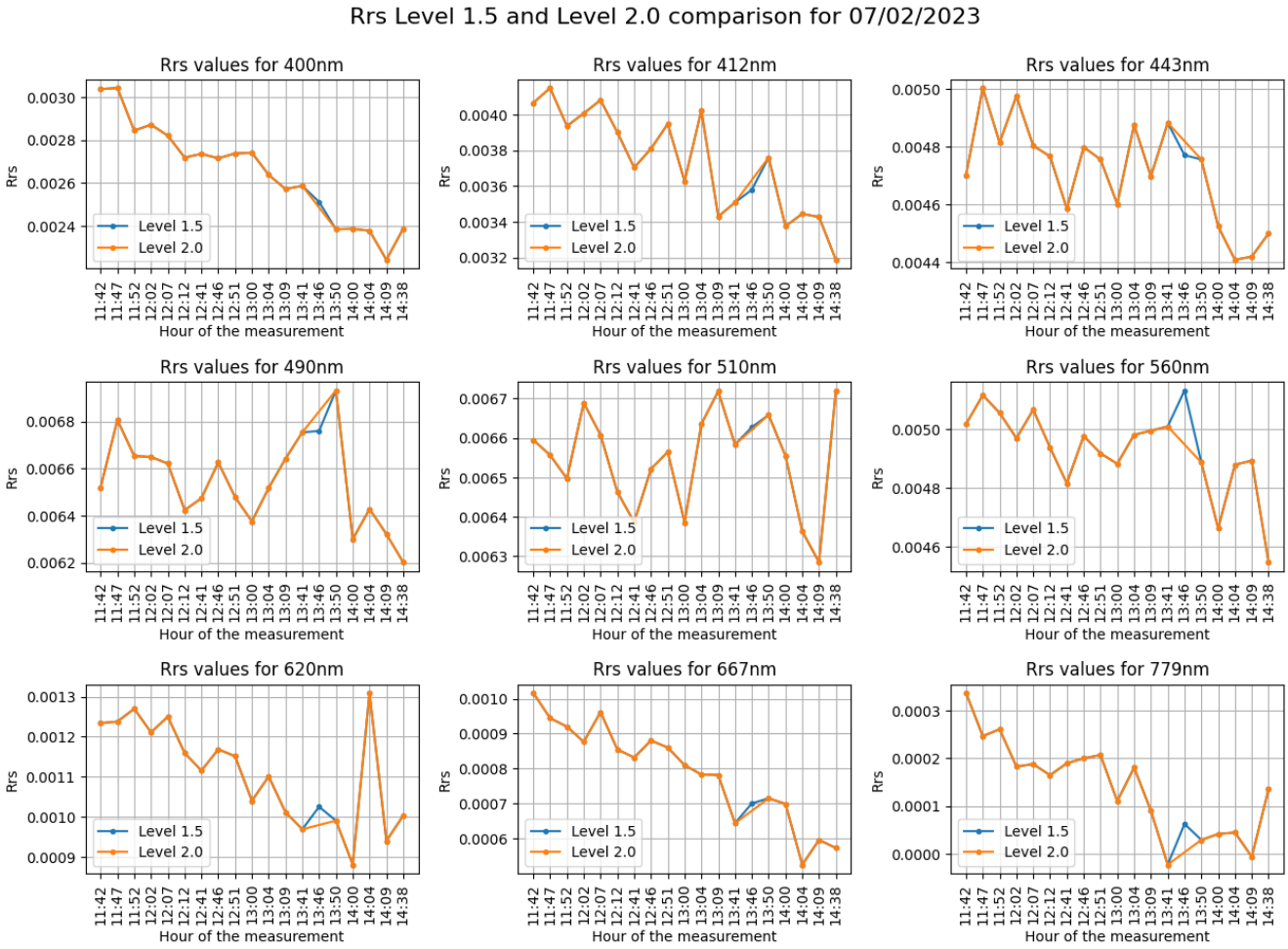

Figure 3.3: Comparison of level 1.5 and level 2.0 data from AAOT on 07/02/2022.

The data for 08/02/2022 is plotted on top of each other in figure 3.4 below. In this dataset, we have almost twice as many measurements as in the previous figure. Even with twice as many measurements, there is absolutely no difference at all between level 1.5 and level 2.0 data.

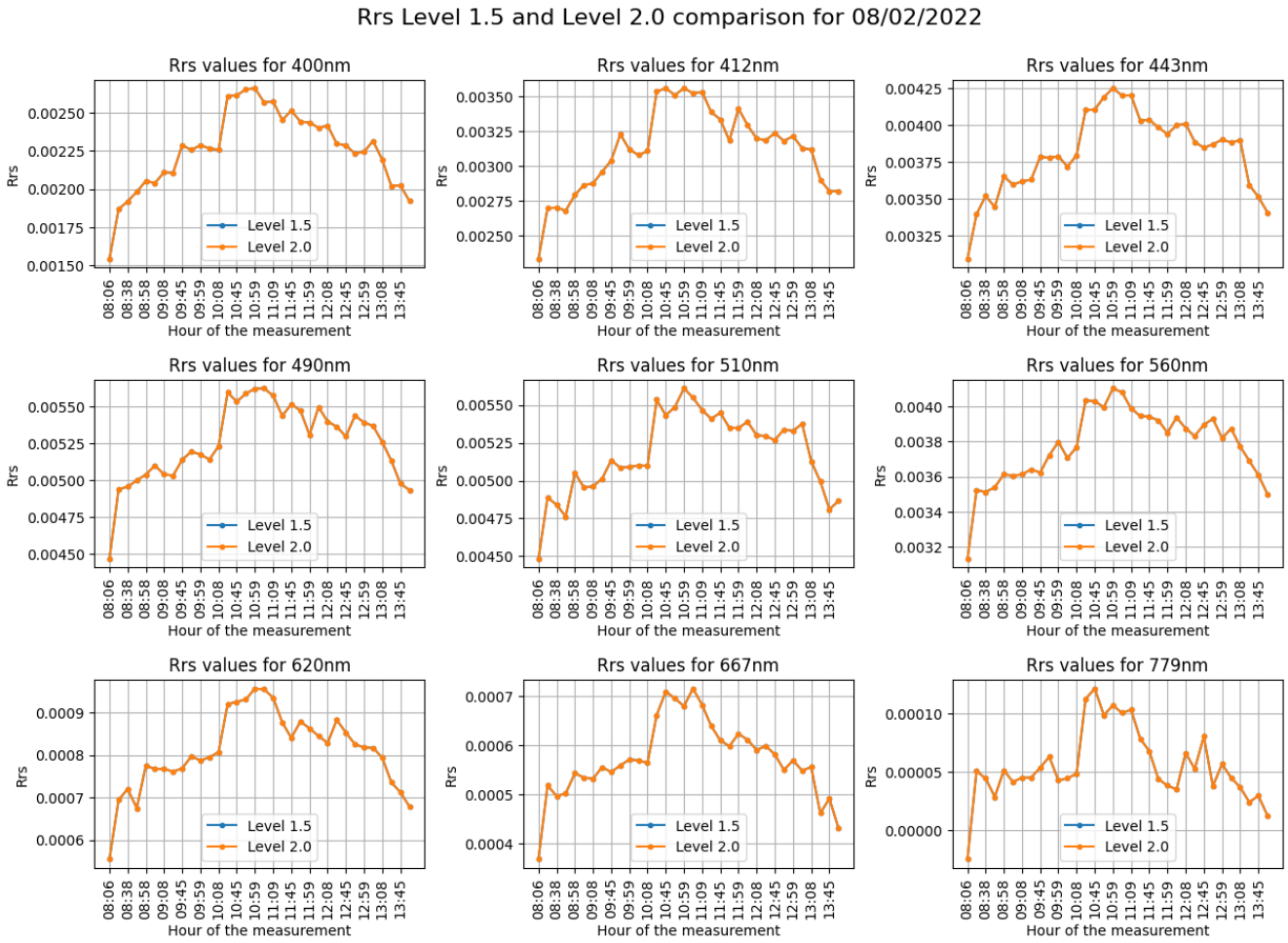

Figure 3.4: Comparison of level 1.5 and level 2.0 data from AAOT on 08/02/2022.

The analysis conducted on the Rrs values of different dates revealed that there exist insignificant variations between the level 1.5 and level 2.0 data. This suggests that the level 1.5 data is suitable for validating the atmospheric correction results produced by the ACOLITE. Nonetheless, it is worth considering that the level 1.5 data may contain measurement errors and may not be as precise as the level 2.0 data.

3.2.2 RadCalNet

The Radiometric Calibration Network (RadCalNet) is a radiometric calibration network that was developed by researchers at the University of Arizona to provide accurate and consistent calibration data for Earth-observing imagers operating in the visible to shortwave infrared spectral range. The network consists in May 2023 of five radiometric calibration sites located around the world that use a common set of calibration targets and procedures to ensure uniformity of data [32].

The need for RadCalNet arose from the fact that existing calibration methods for remote sensing imagers often result in inconsistent and unreliable data due to variations in the calibration process

and environment. RadCalNet aims to provide a standard calibration method that can be used by multiple satellite missions and sensors, reducing the need for individual calibration efforts and improving the consistency and accuracy of the data produced. [32].

RadCalNet test sites offer nadir-view ToA reflectance data at 30-minute intervals from 9 am to 3 pm local standard time, covering a spectral range of 400 nm to 2500 nm with a resolution of 10 nm. This data is derived from ground-based nadir-view reflectance measurements and atmospheric measurements, including surface pressure, columnar water vapour, columnar ozone, aerosol optical depth, and the Angstrom coefficient. The correction to the top-of-atmosphere is performed by using Modtran for all sites uniformly [33].

MODerate resolution atmospheric TRANsmission (MODTRAN) is a widely used computer code that allows research scientists in government agencies, commercial organizations, and educational institutions to predict and analyze optical measurements through the Earth's atmosphere. MODTRAN is an essential component of many operational and research sensor and data processing systems, particularly those that involve the correction of atmospheric effects [34].

While the AERONET ground station in Venice will be used for validation of the atmospheric correction in water applications, the BoA and ToA reflectance data available at the RadCalNet portal will be used for validation of atmospheric correction over land applications. RadCalNet has measurements of the BoA reflectance and converts it to ToA reflectance. HYPSO-1 has several captures over two of the RadCalNet ground station, namely Railroad Valley Playa in the United States and Gobabeb in Namibia.

Railroad Valley Playa is a desert in Nevada, United States at the coordinates 38.497° North, −115.69° East [33]. This ground station is not ideal to use for validation of atmospheric correction over land with the use of ACOLITE. This is due to there might not be too many dark pixels at the captures, which is what ACOLITE needs to have because of the dark spectrum fitting method it uses. However, it is one of the few ground stations where HYPSO-1 has several captures of and ground truth are available at the capture time.

Gobabeb is also a heavy sand and desert ground station, however, it is located next to the ocean at the coordinates −23.6002° North, 15.11956° East [33]. Because of its location next to the ocean, this might change the results of the atmospheric correction over a desert area. Ideally, a ground station that is located in a more vegetated location would be preferred. However, HYPSO-1 does not have a lot of captures over such a ground station where ground truth is available at the capture time.

The water-leaving radiance is converted to remote sensing reflectance for the Venice validation, as this validation is for water applications. For the land application both BoA and ToA reflectance will be used for the validation of the atmospheric correction of Railroad Valley Playa and Gobabeb.

Work and Results

Contents

The accuracy of the comparison between HYPSO-1 captures and ground station measurements are highly dependent on the timing of the captures. To ensure precision, the HYPSO-1 captures should be around the same time as the ground station measurements. AAOT, Venice measures several times a day, from 08:00 to 16:00, which provides sufficient opportunities for HYPSO-1 to acquire captures close in time to AAOT measurements. RadCalNet measures every 30 minutes from 9 am to 3 pm in local standard time Additionally, weather conditions should be considered when taking HYPSO-1 captures. Cloud coverage can significantly impact the quality of the captures. In the start of the spring the maximum cloud coverage was set to 20% for the capturing of Venice to ensure fewer clouds in the images. Though after few captures were taken, the maximum cloud coverage was set to 30% to increase the number of captures.Exceeding 30% would result in too many clouds in the images, which possibly would make the captures unusable.

To improve the quality of HYPSO-1 captures over ocean areas, it is recommended to set a high minimum elevation angle to have a low off-nadir angle on the capturer. This is particularly important over ocean areas due to the significant reflection and glare from the water's surface. The high minimum elevation angle helps reduce glare and improves overall image quality. However, setting a minimum elevation of 85% resulted in infrequent captures, and it was instead set to 60% to increase the likelihood of daily captures.

An issue with performing atmospheric correction with ACOLITE is that during the process we lose vital data regarding the Rrs values below approx 500 nm. The Rrs values are negative, which may be caused by either too low ToA calibration or that there may be an overestimation of the aerosol optical depth. Consequently, validation points at 400, 412, and 443 nm may not be used in the validation process, leaving only six valid control points.

4.1 Georeferencing

One important issue with the HYPSO-1 captures is that there are small offsets in the geolocation of the captures. In each capture, there is information regarding the latitude and longitude for every pixel. These latitudes and longitudes do not match up perfectly with the actual location of the pixels. This is a problem when trying to pinpoint the exact location of the which pixels the ground station is located at. Figure 4.1 below left, shows a raw capture of Venice on top of a map, whilst the image to the right has the transparency reduced to show the misalignment to the map underneath. The red lines in the image illustrate the offsets in the geolocation of the pixels. This small offset could result in a few kilometer, which is not acceptable when trying to pinpoint the exact location of the ground station. This could possibly disturb the validation process by comparing the wrong pixels.

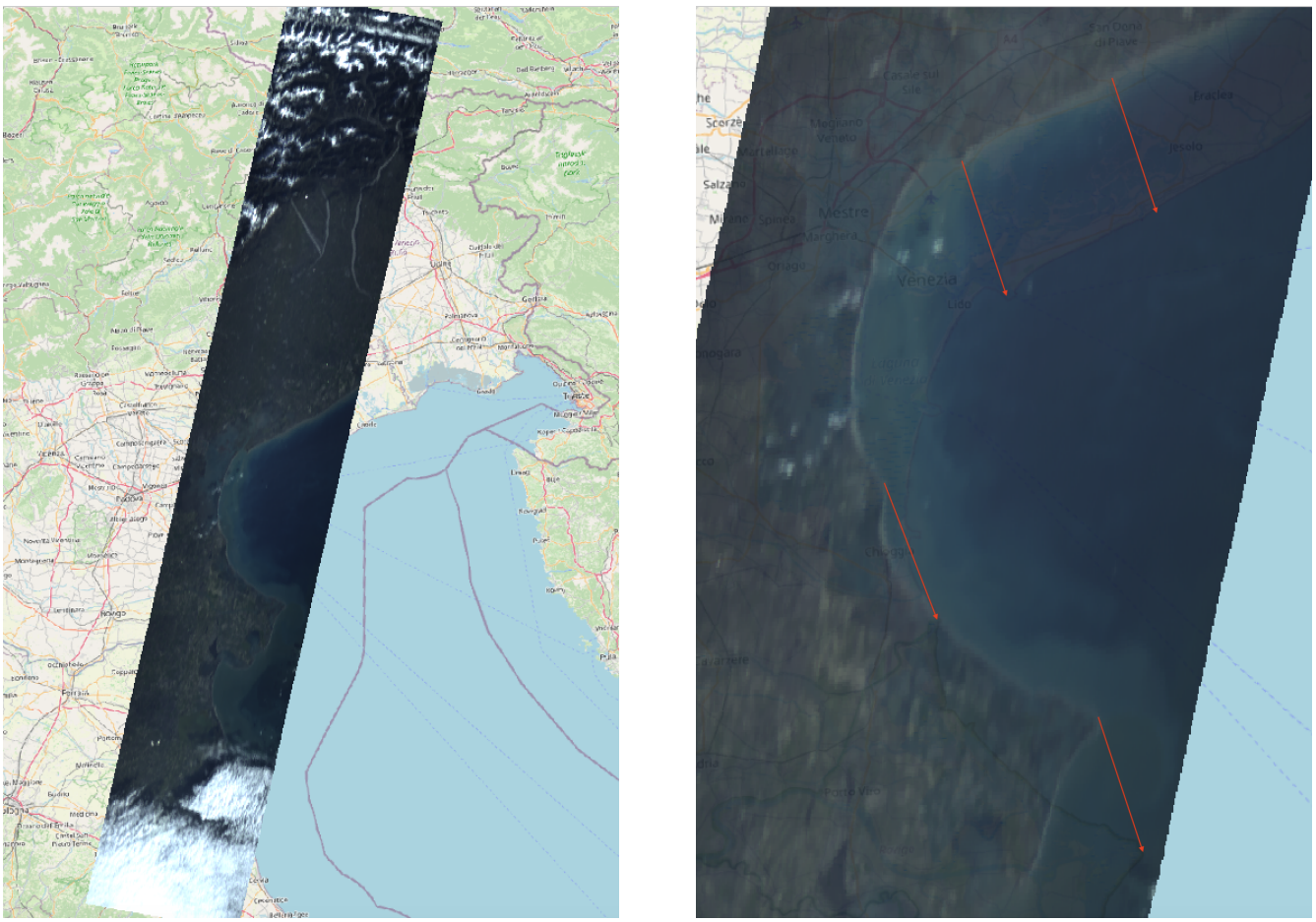

(a) (b)

Figure 4.1: The figures show the geographical offset of a raw HYPSO-1 capture of Venice.

It is possible to use various methods to geoereference capture. To handle this issue in this thesis, the Quantum Geographical Information System (QGIS) is used to georeference the captures. QGIS is a free and open-source cross-platform desktop geographic information system application

that supports viewing, editing, and analysis of geospatial data [35]. QGIS has an indirect georeferencing tool where you use a set of ground control points (GCP) to georeference an image. The control points are manually chosen points that are known in both the image and the map. The control points are used to calculate the transformation between the image and the map. The transformation is then used to georeference the image.

It is possible to use a raw geotif (.tif) file that is created when the image is captured in the georeferencer. Figure 4.2 shows the result of georeferencing a raw geotiff image in Figure 4.1a using QGIS. The red dots in the image is the ground control points that are used to georeference the image. This method of georeferencing is also performed on a raw geotif (.tif) file generated from the capture, the result of this is the same as in the image below.

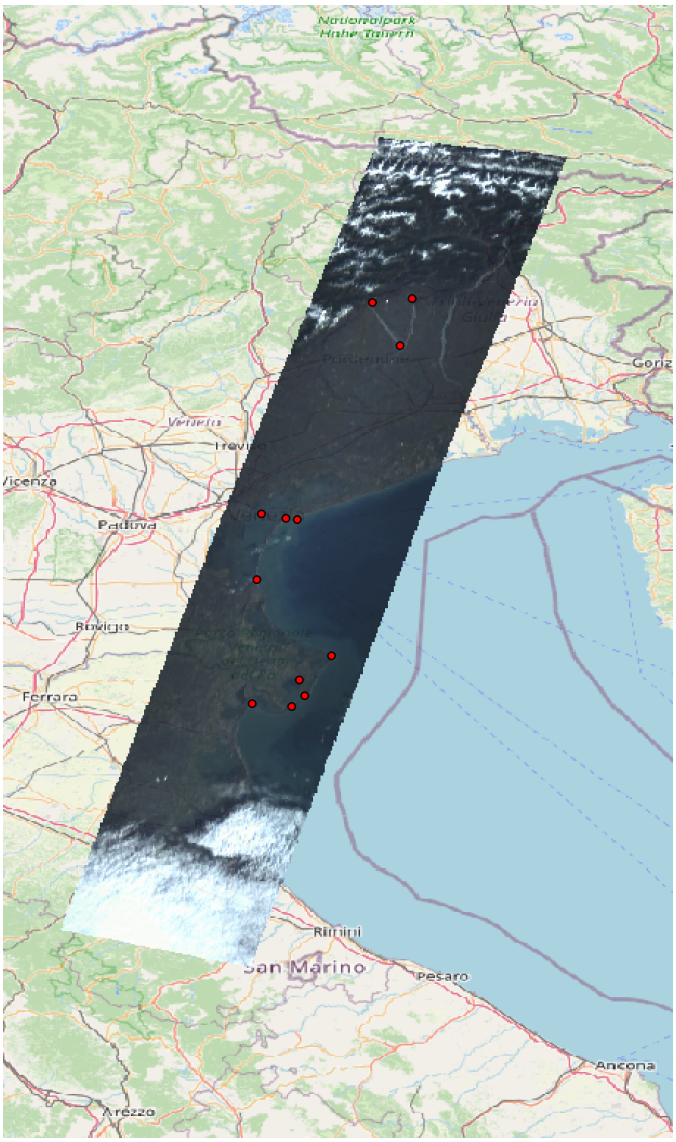

Figure 4.2: The image shows the results of georeferencing using QGIS. The red dots are the GCPs.

The image is now georeferenced and by studying the image by adjusting the transparency in QGIS, it is possible to see that the geolocation of the pixels is now more accurate. The ground control points can be extracted with the specified offset in x and y for each ground control point, which can be used to calculate the offset of any pixel of interest. The pixel of interest for the following validation chapter is the location of the ground station. It is necessary to pinpoint the location of the ground station as exactly as possible for the most accurate comparison.

The first step to finding the correct pixel of interest is to do a polynomial transform. This transformation is between the image coordinates and the geospatial coordinates based on the ground control points. The transformation can be used directly from the python library **scikit-image**. The next step is to find the geospatial coordinates for a given set of image coordinates using the polynomial parameters obtained in the transformation. The following formulas are used:

$$x' = c_{0,0} + c_{0,1} \cdot x + c_{0,2} \cdot y + c_{0,3} \cdot x^2 + c_{0,4} \cdot x \cdot y + c_{0,5} \cdot y^2 \tag{4.1}$$

$$y' = c_{1,0} + c_{1,1} \cdot x + c_{1,2} \cdot y + c_{1,3} \cdot x^2 + c_{1,4} \cdot x \cdot y + c_{1,5} \cdot y^2 \tag{4.2}$$

where,

- x and y are the original coordinates of the image.
- x' and y' are the transformed coordinates of the image.
- c_0, n is the coefficients of the polynomial transform to calculate the x' coordinate.
- c_1, n is the coefficients of the polynomial transform to calculate the y' coordinate.

This will be used later in this chapter to pinpoint the location of the ground stations. This location will be used to compare the reflectance measured by HYPSO-1 and the reflectance measured by the ground station.

4.2 Venice

Figure 4.3b below illustrate the result of performing an atmospheric correction on a raw HYPSO-1 capture of Venice, Italy, shown in figure 4.3a. The atmospheric corrected image shows a clear and vast difference in the two images by taking a quick look at it. However, it is important to see the difference in the remote sensing reflectance before and after the correction. This is because the colour representation can be manipulated quite easily by selecting any of the 120 available bands to represent an RGB image. It is thus important to see the difference in the light that is reflected.

(a) The image is a raw capture from HYPSO-1 of Venice, taken 07/02/23.

(b) The image is the atmospheric corrected image of the raw capture of Venice.

Figure 4.3: The figures show the location of the ground station and the result of performing an atmospheric correction on a raw HYPSO-1 capture of Venice.

The raw capture from HYPSO-1 has the light intensity represented in the form of a digital count. By processing the raw capture to level 1B by performing a radiometric and spectral calibration the intensity is represented in radiance at the top of the atmosphere. This is the processing level that is used as input to ACOLITE. The first output available from ACOLITE is ToA reflectance which can be compared to the ToA radiance by diving the ToA radiance on the mean extraterrestrial solar irradiance given by [21].

Figure 4.4 illustrates the ToA reflectance of the closest water pixel close to the AAOT ground station. The figure shows that there has been a correction and the reflectance has been lowered, which is expected when performing an atmospheric correction as the light is scattered and absorbed by the atmosphere as explained in section 2.2. While the figure shows promising results, it needs to be further compared to ground station measurements to ensure that the correction is as correct as it can be.

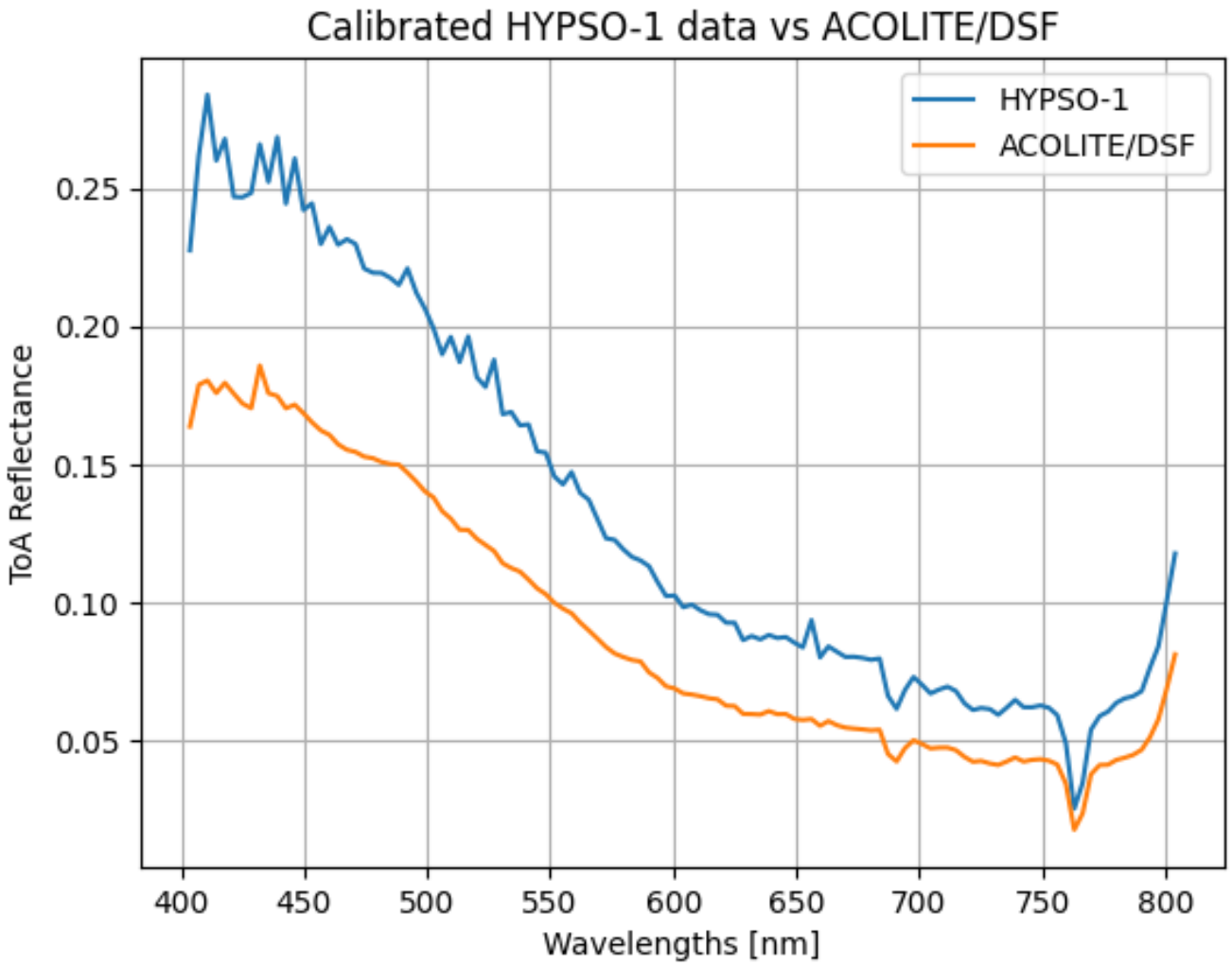

Figure 4.4: The plot illustrates that the ToA reflectance has been lowered after performing an atmospheric correction.

It is noticeable that from around 760-770 nm there is an unusual drop and rise in the reflectance. This is due to oxygen and water vapour absorption around these wavelengths, where there is low gas transmittance. Because of the absorption, there is only a specific amount of radiation that is let through the atmosphere, resulting in a reduced light reflected by the satellite [36].

After 770 nm there is a rise in the reflectance that can be explained by a term called the red edge. This happens because of the strong absorption of red light by chlorophyll, which results in low reflectance in the red portion of the spectrum, followed by a sudden increase in reflectance as the wavelength moves into the NIR region [37]. From around 760-800 nm the low gas transmittance and the red edge will be the case for all figures in this chapter where reflectance is looked at. The data around this point is not considered proper data to use as validation.

In the following subsection three captures of Venice will be looked at further in detail. Table 4.1

below, shows information regarding the data at the acquisition time which can impact the captures in different ways.

When taking a satellite capture over a water application, it is generally desirable to have low SZA (Solar Zenith Angle) and VZA (View Zenith Angle). Low SZA means that the sun is directly overhead, which reduces the number of atmospheric effects and increases the amount of light that reaches the ocean surface. Low VZA means that the satellite is viewing the ocean surface at a more direct angle, which also reduces atmospheric interference and improves image quality. However, it is not always possible to have low SZA and VZA at the same time, as the satellite is not always directly overhead the area of interest.

Date(dd/mm/yyyy)	Time(hh:mm)		SZA (deg)	VZA (deg)	Wind Speed (m/s)
	HYPSO-1	AAOT			
21/09/2022	09:31	09:28	49.2	16.4	6
07/02/2023	09:58	10:01	64.0	44.1	6
08/02/2023	09:45	10:04	64.6	22.3	5
04/05/2023	09:44	09:51	34.5	22.4	3

Table 4.1: Data overview of AAOT comparison with HYPSO-1. SZA (Solar zenith angle) is the angle between the sun and the zenith direction, while VZA (View zenith angle) is the angle between the viewing direction of HYPSO-1 and the zenith direction. Wind speeds are retrieved from local weather stations

4.2.1 Venice - 21st of September 2022

It was measured 20 out of 30 days at the AAOT station in September 2022 and for each day there are about 30 measurements from approximately 08:30 to 13:30. The 21st of September 2022 there were exactly 30 measurements of the water-leaving radiance. This radiance is converted to remote sensing reflectance by dividing the water-leaving radiance on the mean extraterrestrial solar irradiance given by [21].

The Rrs are illustrated in figure 4.5 below. It is notable that all 30 measurements almost have quite similar Rrs values and differ by small margins, especially from around 550 nm. The highest difference is from 450 - 500 nm. The closest AAOT measurement to the HYPSO-1 capture is at 09:28:02. This measurement is in the middle of all other captures, and does not seem to be an outlier.

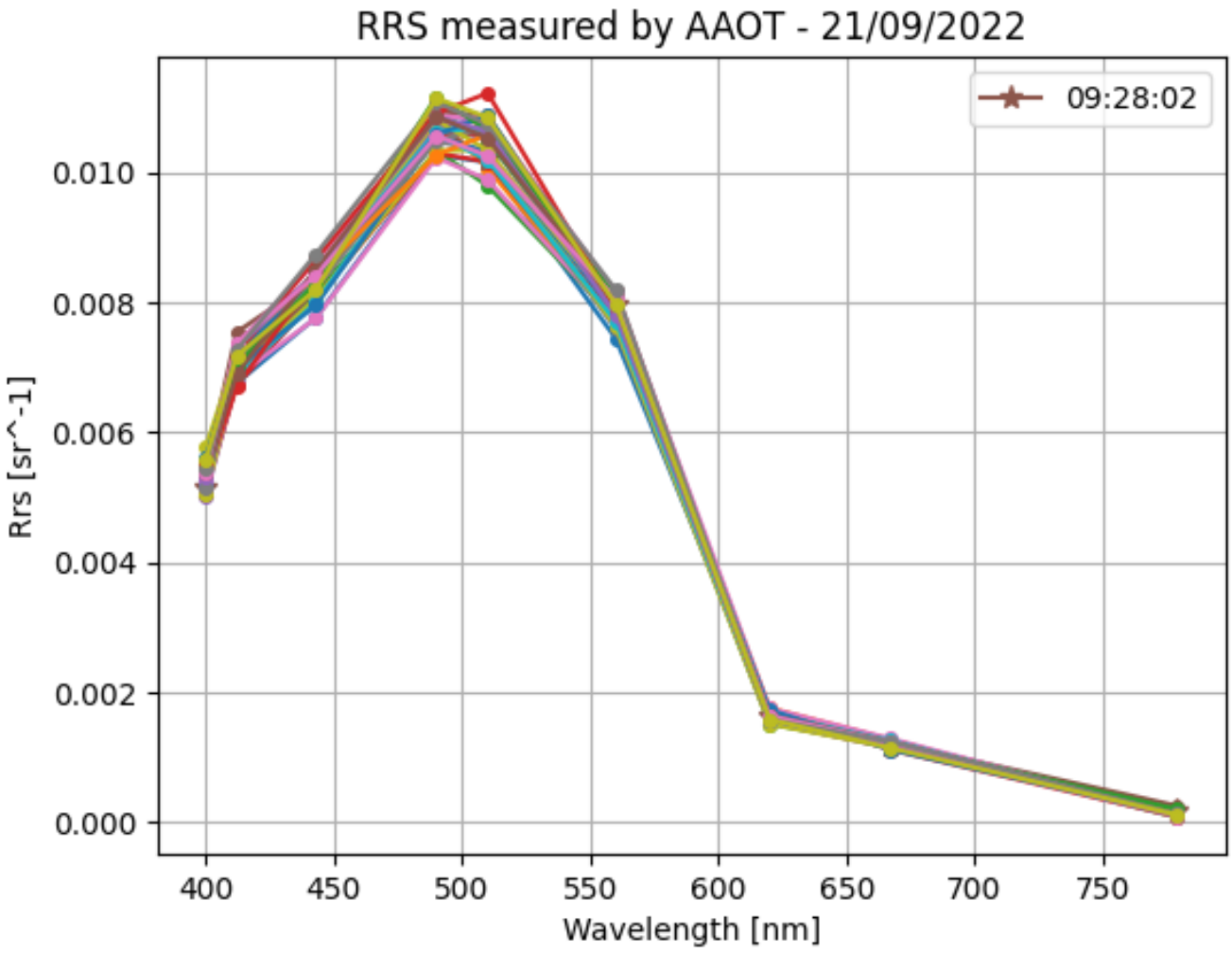

Figure 4.5: The figure shows 30 measurements of the surface reflectance on the 21st of September 2022 at the AAOT station.

To achieve the most accurate comparison of the data, it is desirable to use the pixels from the HYPSO-1 capture closest to the ground station. Figure 4.6 displays the five closest pixels to the ground station, where the Rrs values measured by HYPSO-1 are very similar, but differ by a small margin at some wavelengths. One pixel or two in difference because of incorrect georeferencing will not have a large impact on the comparison, but if the difference is larger, the comparison will be less accurate.

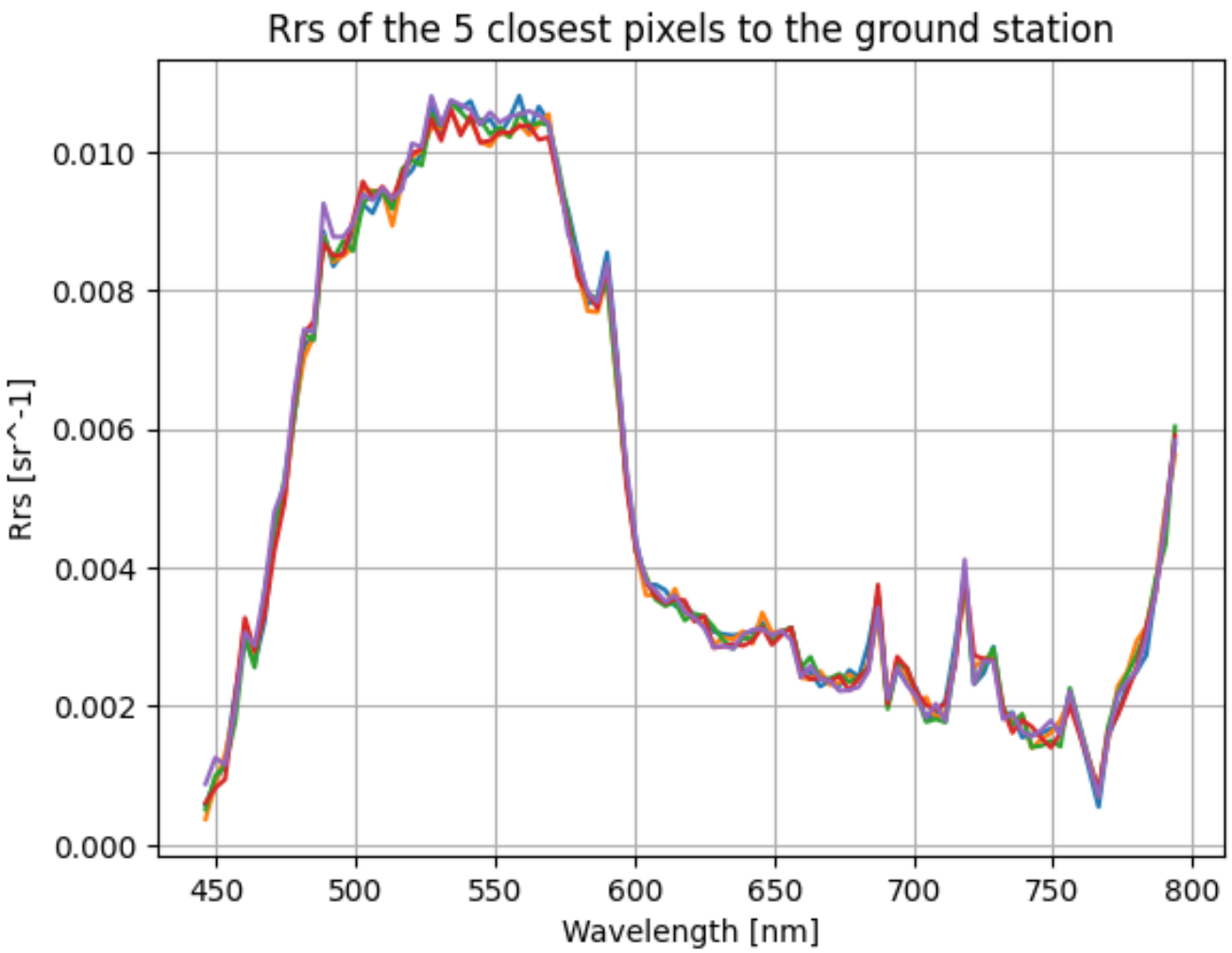

Figure 4.6: The figure illustrates the five closest pixels from the HYPSO-1 capture to the AAOT ground station.

In figure 4.7 the mean Rrs values measured this day (blue) and the closest Rrs value from the AAOT station (orange) from figure 4.5 is compared to the atmospheric corrected HYPSO-1 capture (green). The figure shows that there is almost no difference between the mean Rrs measure and the measure at 09:28:02. However the graphs show that there is a large amount of difference between the AAOT station and the HYPSO-1 capture. The difference is especially large from 450 - 600 nm, where the Rrs values from the HYPSO-1 capture look to be shifted to the right. From around 600-750 the HYPSO-1 measurements are about 0.001 - 0.0015 higher than the measured AOOT values.

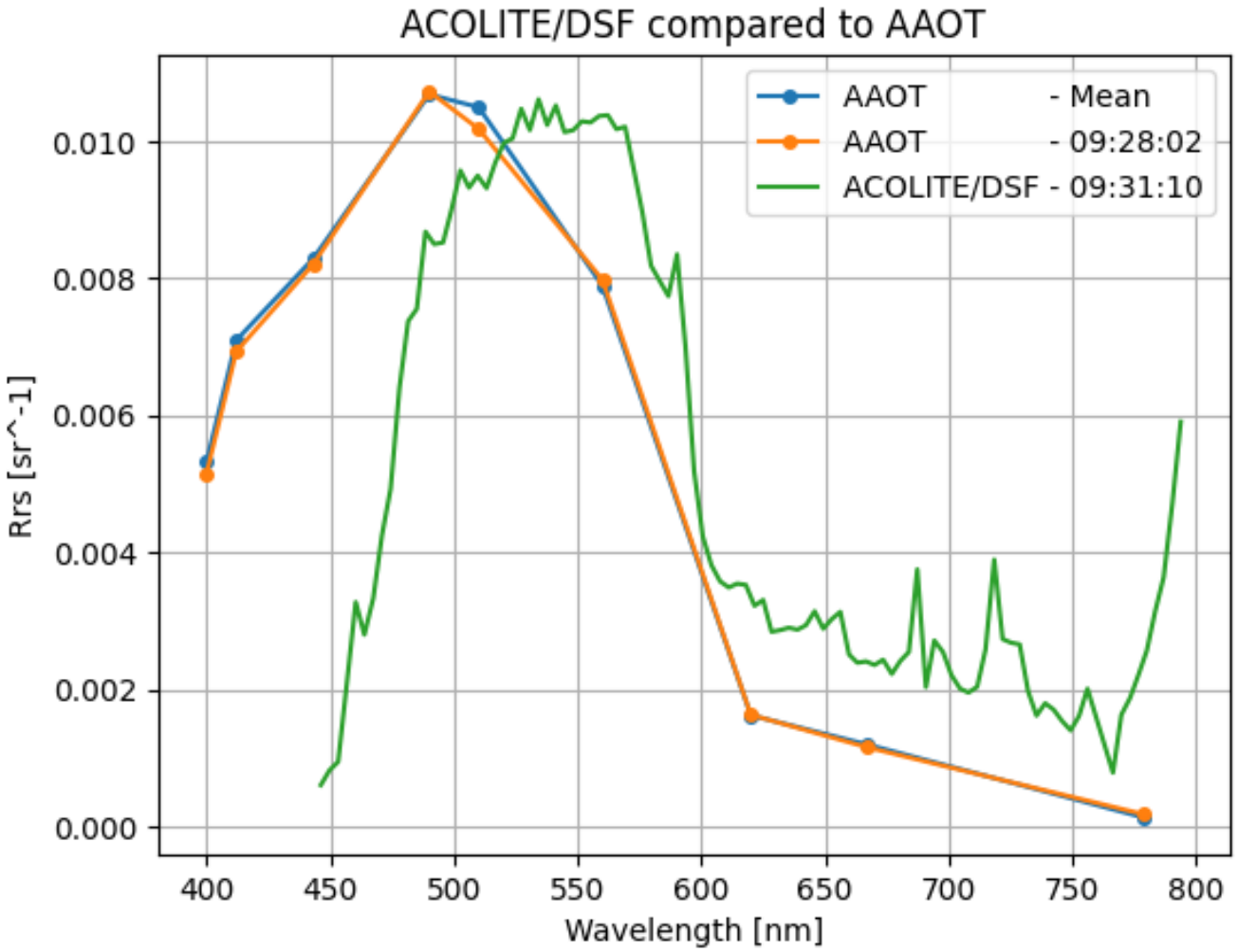

Figure 4.7: The figure illustrates the comparison of the mean Rrs values and the closest measurement from the AAOT station to the Rrs values from the HYPSO-1 capture.

This mismatch could have happened because of various amount of factors, such as atmospheric effects, wind speed and direction. This could also be the effect of ACOLITE' correcting because some HYPSO-1 data may trigger something in the algorithm. It could also be the result of incorrect georeferencing, meaning the chosen pixel is not close enough to the grouud station. This needs to be further investigated in other captures to see if this persists on other days as well.

4.2.2 Venice - 07th of February 2023

In February 2023 there were 15 days of measurements at the AAOT station and two captures from HYPSO-1. The two captures were taken on the 7th and 8th of February 2023, both these days there are measurements taken by the AAOT station. The 7th of February there were taken 32 measurements from 09:41 until 14:38. The time of the HYPSO-1 captures is 09:58:04, while the closest AAOT measurement is at 10:00:01.

32 measurements taken on the 7th of February is shown in figure 4.8, where the circles on the lines represent the wavelength of the measurement, and the red line with stars represents the measurement closest to the HYPSO-1 capture. The graph shows that while the Rrs signature of the measurements is similar, the Rrs values differ across wavelengths, with the Rrs values of the closest measurements to HYPSO-1 having some of the highest Rrs values across all wavelengths.

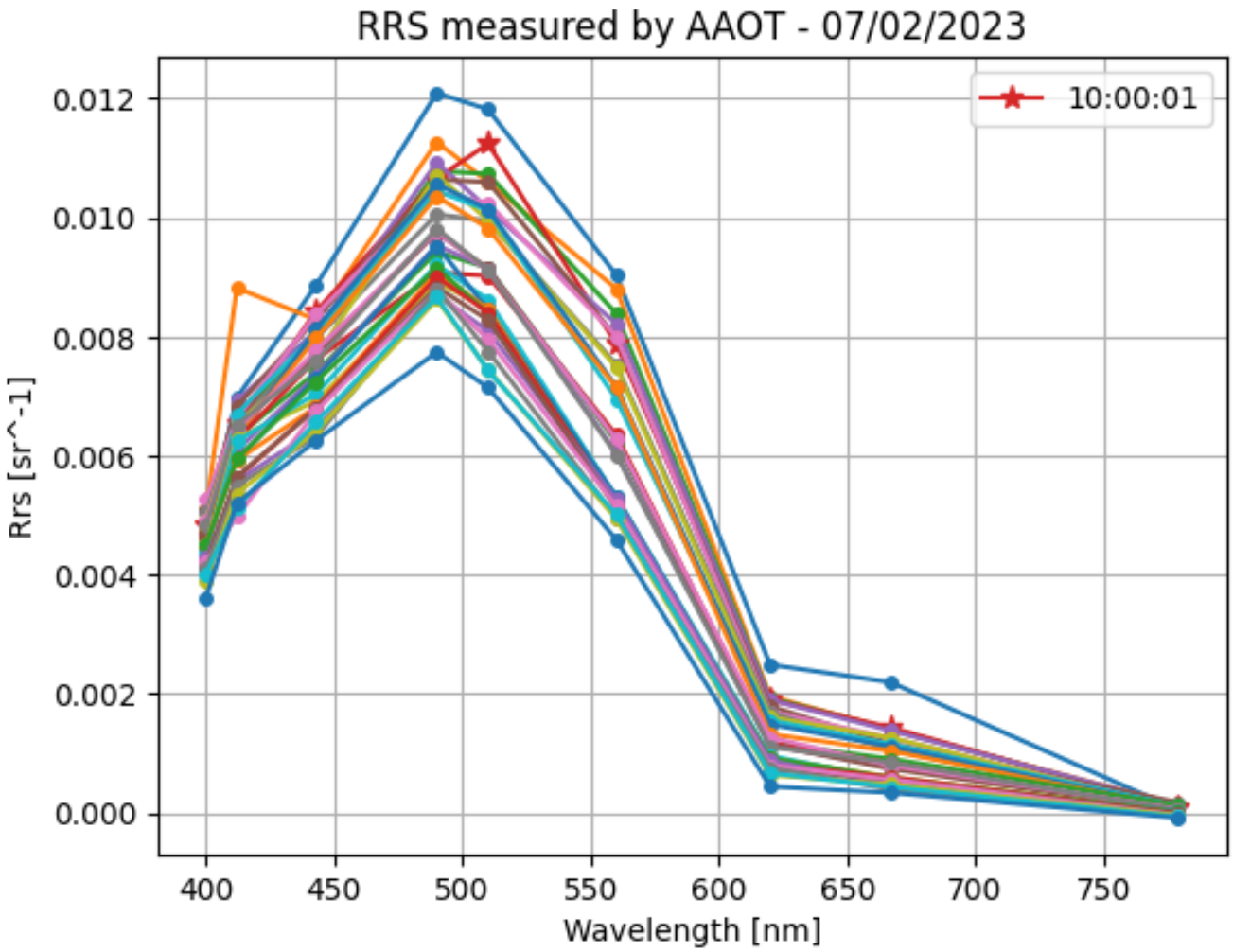

Figure 4.8: The figure illustrates the 32 measurements that are taken on the 7th of February 2023 at the AAOT station.

The closest latitude and longitude coordinates are found to be 45.31462° North and 12.50911° East, respectively. Notably, these coordinates correspond to a pixel located in close proximity to the AAOT station, which is geographically positioned at 45.31390° North and 12.50830° East [30]. Figure 4.9 displays the five closest pixels to the ground station, where it can be seen that most of the reflectance values are very similar around the ground station.

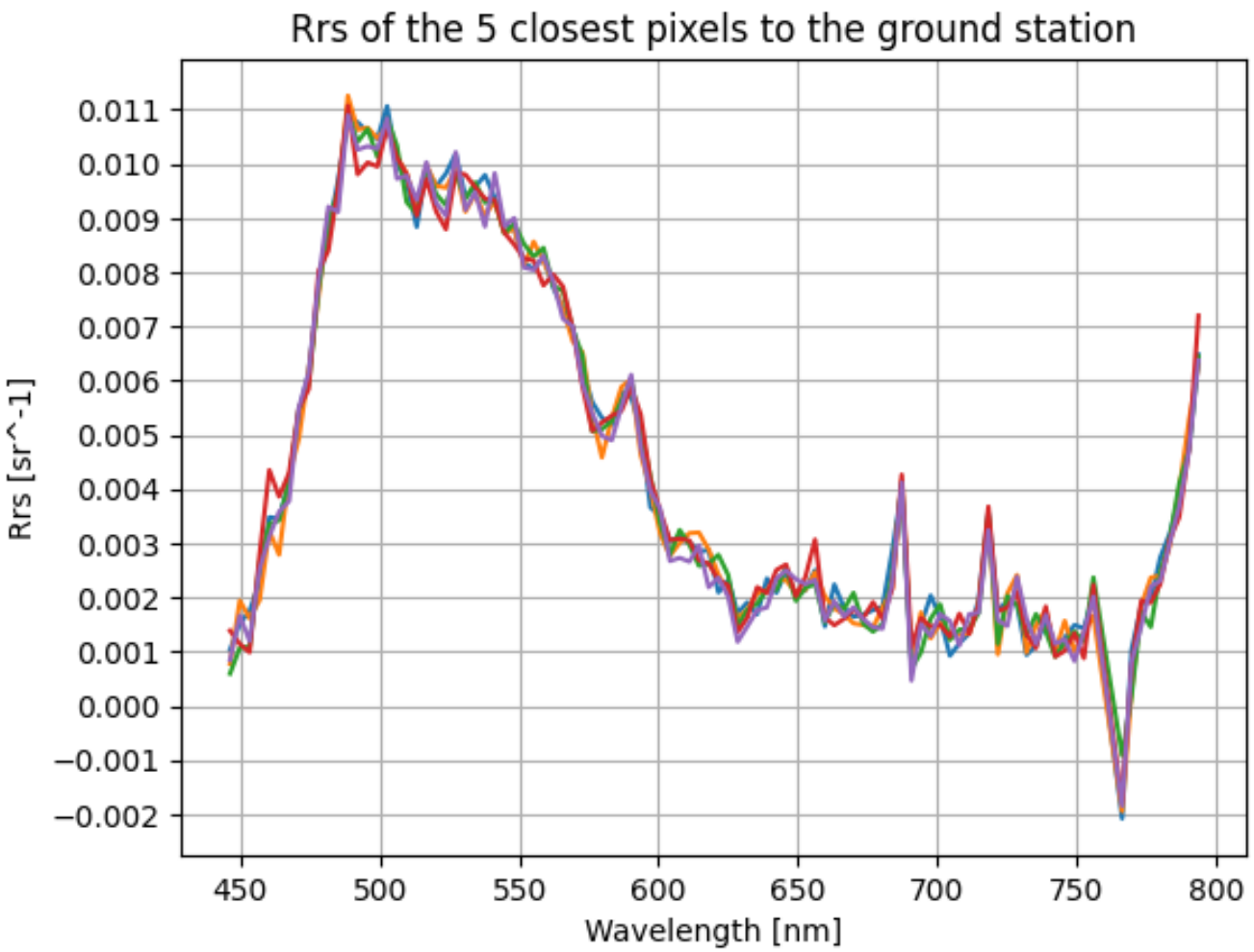

Figure 4.9: The figure illustrates the closest pixels from the HYPSO-1 capture to the AAOT ground station.

During the five hours of measurement at the AAOT station, the Rrs values fluctuated to some extent. The mean Rrs value for February 7th is illustrated by the blue line in figure 4.10, which compares the mean Rrs values from the AAOT station to the Rrs values from the HYPSO-1 capture. Although comparing the mean Rrs values may not be the most accurate way to compare the data due to potential minute-to-minute variations, it provides a good indication that the Rrs values measured by HYPSO-1 are consistent throughout the day and not only at a specific time.

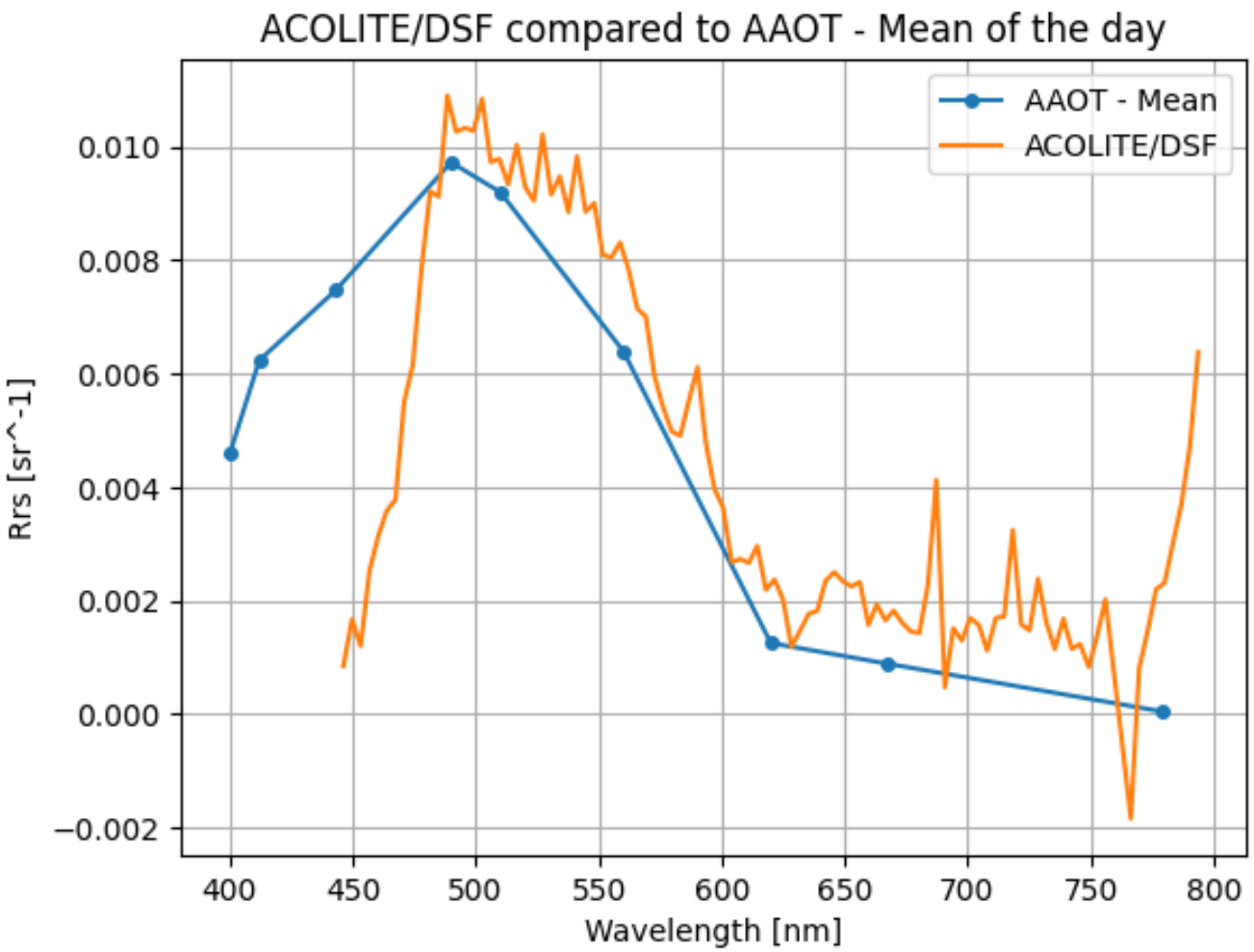

Figure 4.10: The figure illustrates the comparison of the mean Rrs values from the AAOT station to the Rrs values from the HYPSO-1 capture.

Figure 4.11 below, illustrates the AAOT measurement at 10:00:01 compared to the result from ACOLITE. Comparing from around 475 nm, it is evident that both the AAOT and HYPSO-1 data match up until around 750 nm. Although the HYPSO-1 values spike and vary more due to more measurement points, they match very well with the AAOT data. However, at the last measurement point, the HYPSO-1 data decreased and then increased significantly from approximately 760-800 nm due to the oxygen absorption and the red-edge, while the AAOT data decreased from the second last control point.

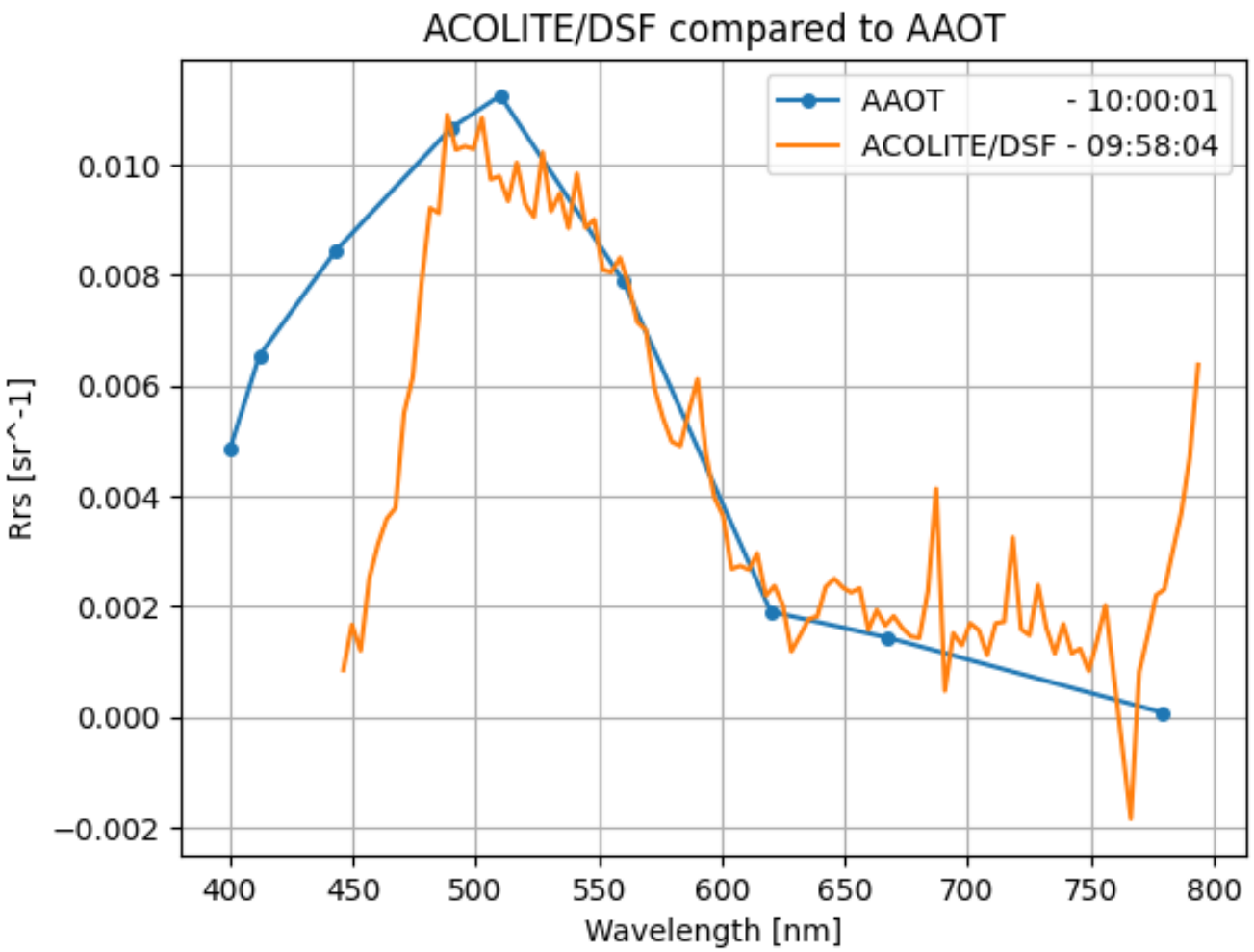

Figure 4.11: The figure illustrates the comparison of the closest measurements from the AAOT station to the closest pixels from the HYPSO-1 capture.

Figure 4.11 shows more promising results than the correction of the capture taken 21st of September 2022. Reasons for this could be either this capture has only two minutes difference from the ground station measurement, better georeferencing, impact of the combination of SZA and VZA or a combination of various factors.

4.2.3 Venice - 08th of February 2023

The 8th of February 28 measurements were taken from 08:35 until 14:38. The time of the HYPSO-1 capture was 09:44:36, while the closest AAOT measurement is at 10:04:43.

Figure 4.12 below shows the 28 measurements of the Rrs measured by AAOT. The circles on the lines illustrate the wavelength of the measurement, while the red line at the top with stars illustrates the measurement closest to the HYPSO-1 capture. While the closest measurement point to HYPSO-1 the 7th of February had some of the highest Rrs values at all wavelengths,

the image below shows that the closest measurement for this capture has some of the lowest Rrs values at all values. As for this day, there are still differences in the highest and lowest measured Rrs at each wavelength, as expected. The highest difference is around 0.004 at 510 nm, while the lowest difference can be found at 779 nm. This could be because of different weather conditions throughout the day, the presence of specific water substances which can vary in concentration from time to time or other factors.

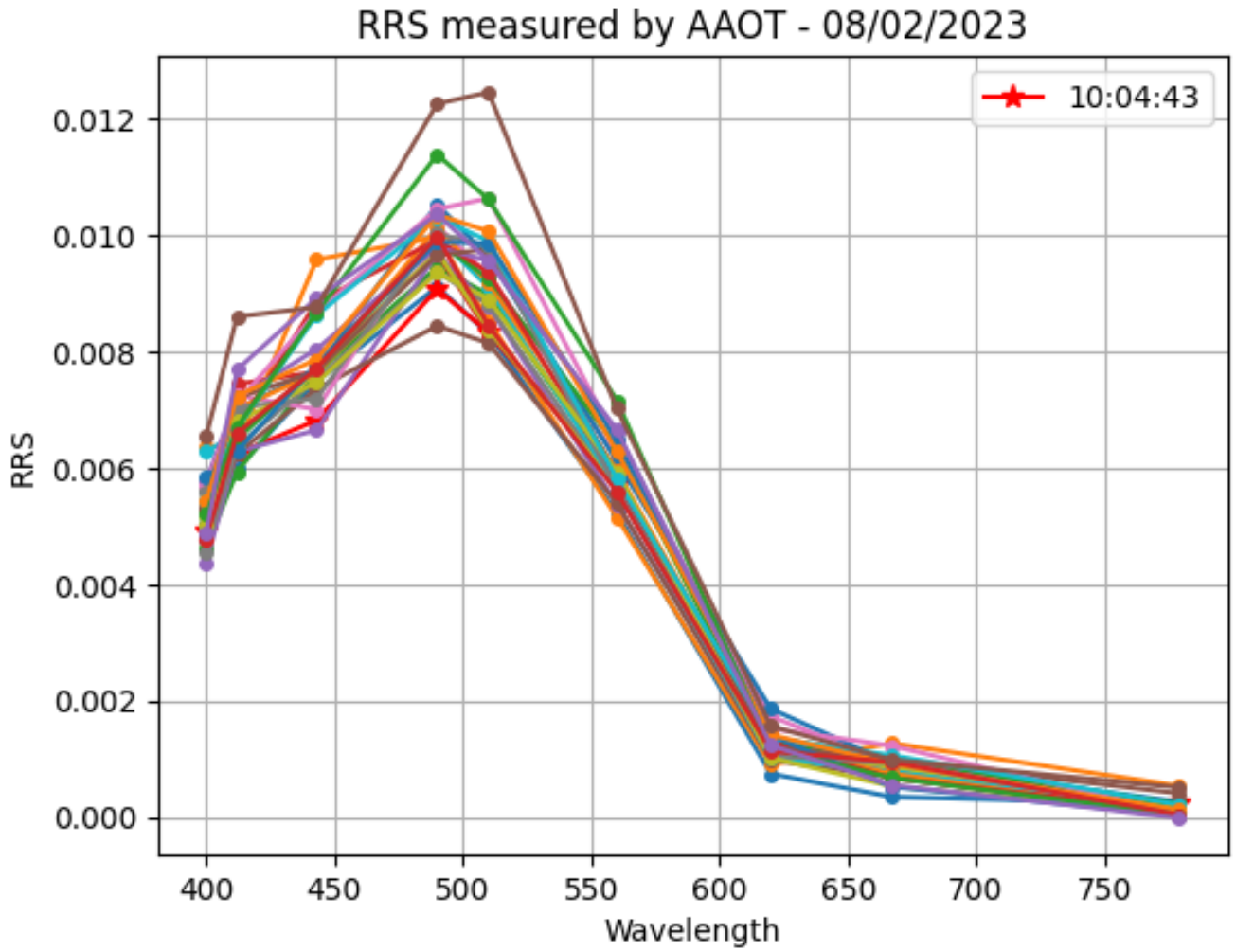

Figure 4.12: The figure illustrates the 32 measurements that are taken on the 8th of February 2023 at the AAOT station.

The five closest pixels in the HYPSO-1 capture are found with the same method as for the two previous captures. For the 8th of February, the closest pixel is found at 45.31406° North, 12.50870° East, while the ground station is located at 45.31390° North, 12.50830° East. This pixel is like the 7th of February extremely close to the ground station and is therefore a good pixel to compare the data from.

In figure 4.13 below, it is shown that the mean measurements from AAOT have somewhat higher

reflectance values below 560 nm, and onwards the values are relatively similar. The AAOT measurement at 10:04 is almost identical to the HYPSO-1 measurements from 475 - 670 nm. The 20-minute time difference could impact the accuracy of the comparison, but the results are still promising in the sense that the Rrs values are relatively similar.

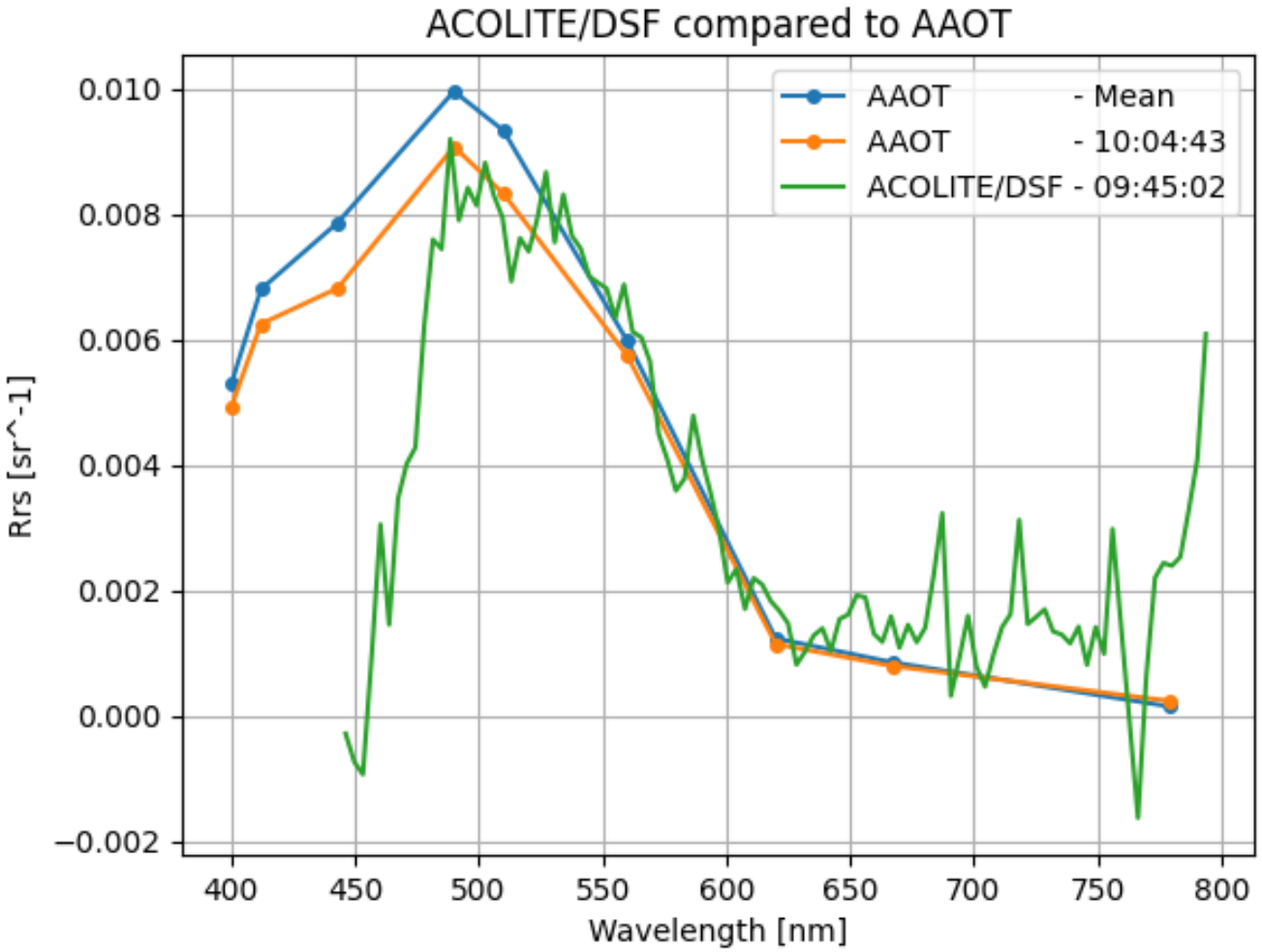

Figure 4.13: The figure illustrates the comparison of the mean Rrs values and the closest measurement from the AAOT station to the Rrs values from the corrected HYPSO-1 capture.

This corrected HYPSO-1 capture of Venice shows promising result like the previous capture from around 475 - 675/750 nm. It is evident that the Rrs values below 475 nm and above 760 nm is not useable for all the captures, which makes a loss of lot of the available data. However, the available data is still promising and can be used for further analysis.

4.2.4 Venice Combined

It is preferred to have as many captures as possible of Venice to have the best foundation to make an overall conclusion regarding the performance of ACOLITE. Overall six captures have

been taken, whereas only four of them are valid. The satellite did not orient towards Venice for two captures taken at the end of May 2023. From February, there have been minor errors with the capture target system, unfavourable weather conditions, and operational bugs that have led to fewer captures than expected and needed. In comparison of the PRISMA satellite's validation of atmospheric correction with ACOLITE in 2021/2022, a total of 12 captures were used in the validation process [38].

Figure 4.14 below, illustrates the combination of all atmospheric correctioon results of HYPSO-1 data over Venice. The Rrs values are extracted from the closest pixels to the AAOT station. The figure shows that the Rrs values are very relatively similar throughout the captures, with some differences from capture to capture at wavelength to wavelength. Notably, the last three captures have equal signatures compared to the first capture, with spikes at the same wavelengths. The biggest difference between the captures are around 500 - 600 nm, which is also where the ground measurement varied the most. A sign of consistency in the atmospheric correction is promising and preferred in the validation

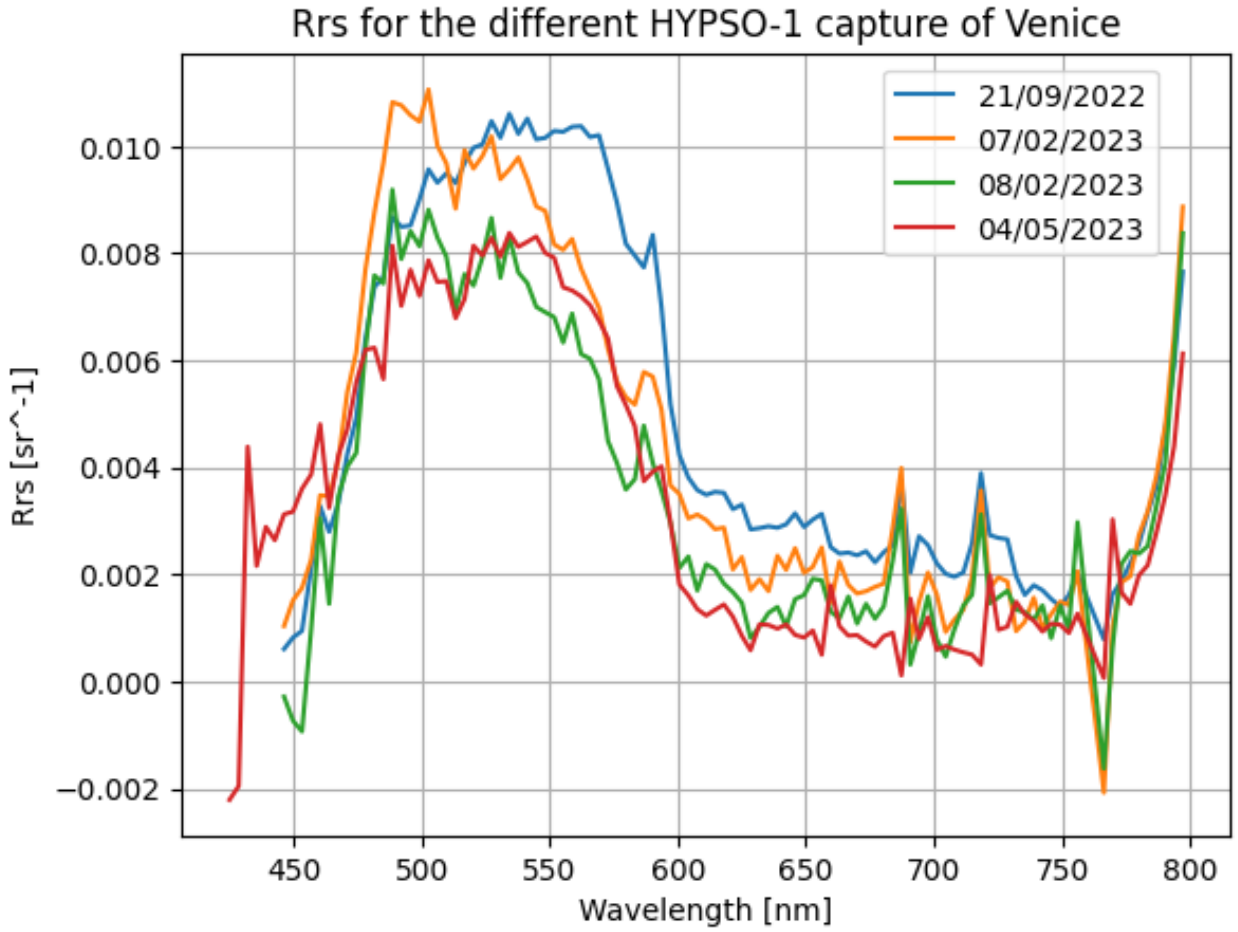

Figure 4.14: The figure illustrates the Rrs values of the pixels closest to the AAOT station from the different Venice captures.

Figure 4.15 below, illustrates the four atmospheric corrected captures over Venice compared to the ground station data from AAOT. A more detailed evaluation was performed in the previous section regarding the different captures, whereas one additional capture is included here, ideally, even more, would be included. The last three are relatively close to the ground station measurement from around 475 - 600 nm, and then there are more varying results from 600-750 whereas some are more aligned with the ground truth than other.

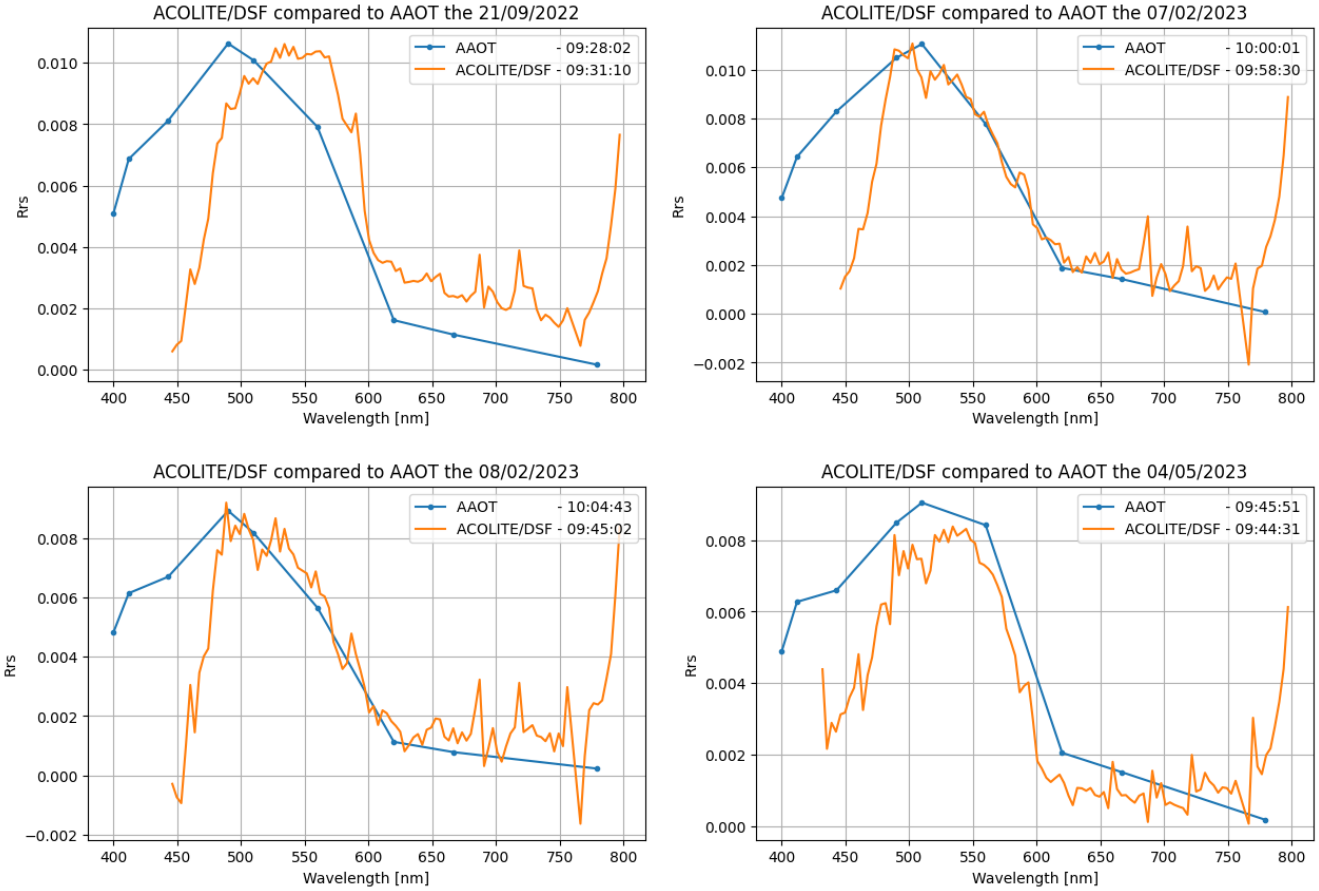

Figure 4.15: The figure compares the closest pixels from the Venice captures to the closest measurements from the AAOT station.

In interpreting the results of these four captures, it is apparent that the atmospheric correction is relatively consistent with the ground truth data, signifying a promising outcome. Taken into account that the atmospheric correction is a complex process and this is the first validation process for a somewhat new satellite. The results are promising, and the results may have been even better with better georeferencing, leading to a better pixel selection. Even one pixel in difference does change the Rrs values, even if the difference in the values is small from pixel to pixel, a larger error in pixel selection could lead to a larger uncertainty in the Rrs values.

Statistical measures can be used to evaluate the results of the atmospheric correction. These include the coefficient of determination (R^2), which is the square of the Pearson correlation coef-

ficient, indicating the shared variance between the hyperspectral data and the reference data. It provides an overarching view of the correlation and linear relationship between our interpolated hyperspectral data and the reference data. Root Mean Squared Deviation (RMSD) and Mean Absolute Deviation (MAD) are used to find the deviations from the reference values. Lastly, Mean Absolute Percentage Deviation (MAPD) is used, which gives an insight into the relative size of the prediction errors, hence allowing a comprehensive understanding of the quality and reliability of the remote sensing data. The formulas are given in the following equations:

$$R^2 = \left(\frac{\sum_{i=1}^{n}(x_i - \bar{x})(y_i - \bar{y})}{\sqrt{\sum_{i=1}^{n}(x_i - \bar{x})^2 \sum_{i=1}^{n}(y_i - \bar{y})^2}} \right)^2 \tag{4.3}$$

$$\text{RMSD} = \sqrt{\frac{1}{n}\sum_{i=1}^{n}(x_i - y_i)^2} \tag{4.4}$$

$$\text{MAD} = \frac{1}{n}\sum_{i=1}^{n}|x_i - y_i| \tag{4.5}$$

$$\text{MAPD} = \frac{100\%}{n}\sum_{i=1}^{n}\left|\frac{x_i - y_i}{x_i}\right| \tag{4.6}$$

$$\tag{4.7}$$

where:

- n is the total number of data points.
- x_i and y_i represent individual observed values of HYPSO-1 reflectance and ground truth reflectance values, respectively.
- $\bar{x}$ and $\bar{y}$ denote the mean values of x_i and y_i, respectively.

Figure 4.16 below, show a comparative study of the remote sensing reflectance (Rrs) obtained from AAOT and ACOLITE/DSF for four HYPSO-1 captures. In each subplot, the scatter plot displays the correlation between the Rrs values from AAOT and ACOLITE/DSF, colour-coded by the corresponding wavelengths. A 1:1 reference line (grey dashed) and the line of best fit (black) are also included. At the upper left of each plot, a variety of statistical parameters presented in the equations above are provided. These metrics help to quantify the overall agreement between the ground truth and the HYPSO-1 data. As the AAOT data only have 9 data points originally, these were quadratic interpolated to match 90 of the available bands from HYPSO-1, leaving some uncertainty in the scatterplots. Only the bands representing the wavelength 446 - 756 nm are chosen to be analyzed, this is because everything below 446 has negative reflectance values and above 756 nm is the effect of gas absorption and red-edge. The complete spectrum could be included in the scatterplot, but it was chosen not to be included to get a better analysis of the data that is usable.

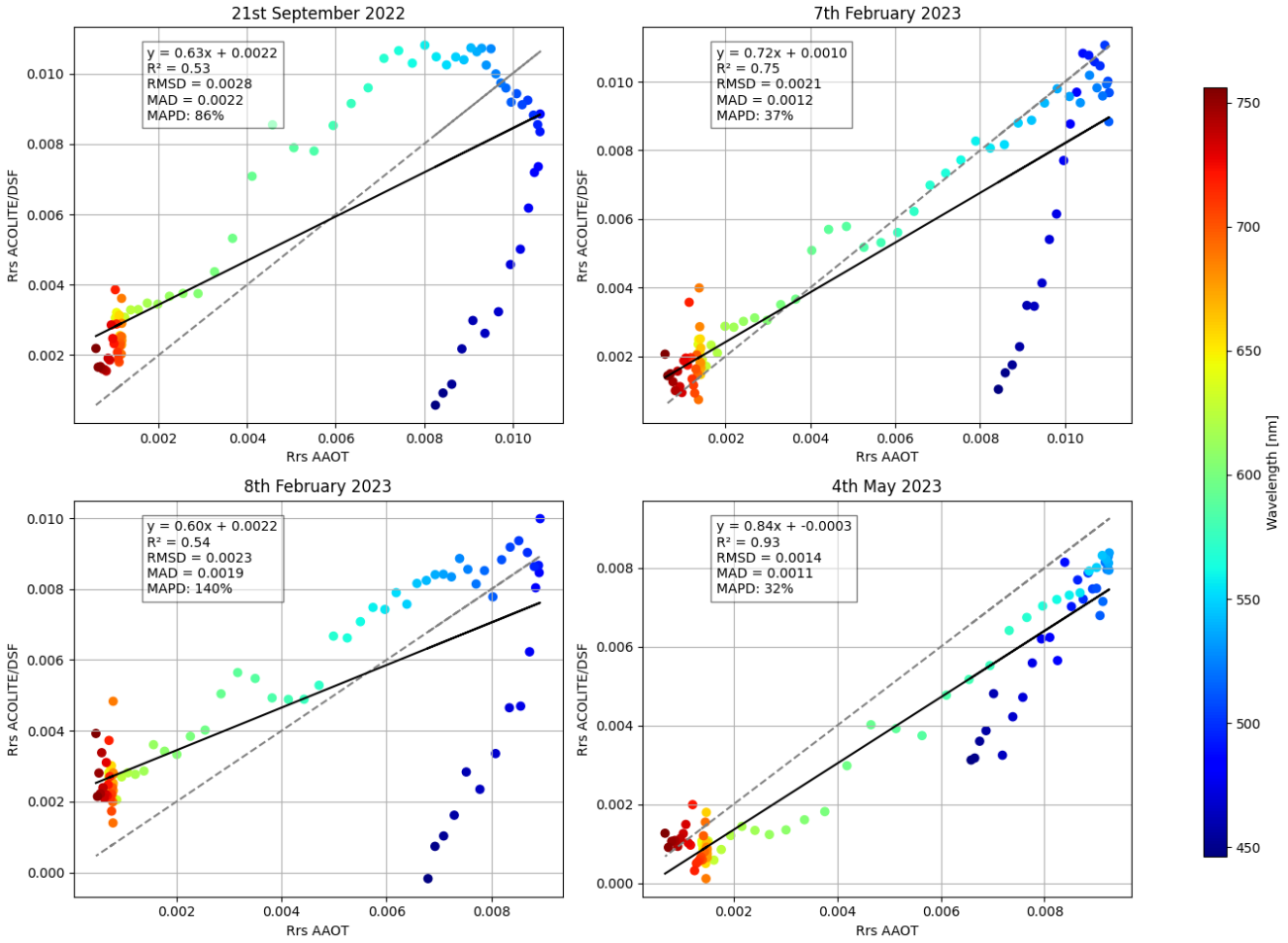

Figure 4.16: Scatterplots of interpolated ground station Rrs versus HYPSO-1 Rrs processed using ACOLITE/DSF.

For the satellite capture on 21st September 2022, the coefficient of determination (R^2) was 0.53, suggesting that 53% of the variance in the dependent variable can be explained by the independent variable. The root mean square deviation (RMSD) value was 0.0028, denoting a moderate level of deviation between HYPSO-1 and ground truth. The mean absolute deviation (MAD) was 0.0022, and the mean absolute percent deviation (MAPD) was 86% both indicating a relatively high average deviation in the HYPSO-1 data.

On 7th February 2023, the observed R^2 was 0.75, indicating a strong relationship between the HYPSO-1 and ground truth. The RMSD was 0.0021, which is lower than that of the previous capture, indicating improved accuracy, which was also seen at the detailed analysis. Both the MAD (0.0012) and MAPD (37%) were lower, suggesting that the overall accuracy of the capture improved.

On 8th February 2023, the R^2 value was 0.54, and the RMSD was 0.0023. These values are comparable to those observed in September 2022, suggesting a similar level of accuracy. The MAD

was 0.0019, and the MAPD was 140%, both of which are relatively high, indicating increased deviation in the HYPSO-1 data.

For the capture on 4th May 2023, the R^2 value was 0.93, suggesting that 93% of the variance can be explained by the model, indicating a very strong fit. The RMSD was 0.0014, the lowest among all the captures, suggesting excellent accuracy. Both the MAD (0.0011) and the MAPD (32%) were the lowest among all the captures, indicating high accuracy and precision.

In conclusion, the results from the four satellite captures exhibit varying levels of accuracy and precision. It is evident that there are quite many outliers below 475 nm as expected due to the Rrs values being very low compared to the ground truth. The measurements improved the higher the wavelengths and overtime of the captures, with the most recent capture on 4^{th} May 2023 providing the most accurate and precise data throughout the entire spectrum. However, looking at more specific wavelengths it is evident that the capture on 7^{th} was the most accurate one.

4.3 Railroad Valley Playa

The primary objective of the HYPSO-1 mission is focused on water-related missions, but there is still a desire to obtain imagery of land-based activities. ACOLITE, as discussed in section 3.1, is primarily designed for diverse water-related applications. Railroad Valley Playa (RRVP) is a desert in Nevada, United States, and because of how ACOLITE works this may not be a suitable ground station compare with. This is because ACOLITE is using the Dark Spectrum Fitting (DSF) method, which is dependent on the image having dark pixels. If the image does not have any or few dark pixels, the DSF method will not work properly and the result will most likely not be satisfying.

Most of the captures that were processed by ACOLITE were overcorrected, resulting in the ToA reflectance being very low after the atmospheric correction and the images were very bright and yellow. Figure 4.17 below, shows a raw capture in the left image, while the middle image is the atmospheric corrected image with default settings. It is noticeable that the middle image is very bright and yellow. This is because there are not too many clear dark pixels, which is needed for the dark fitting spectrum algorithm to work. The image to the right is the result of adjusting the aerosol optical thickness estimate in the ACOLITE settings from tiled to fixed, which reduced the brightness of the image. The RGB wavelengths used to generate the image were adjusted from (650, 560, 480) to (670, 560, 490) which changed the yellow colour to a more desert-representative colour.

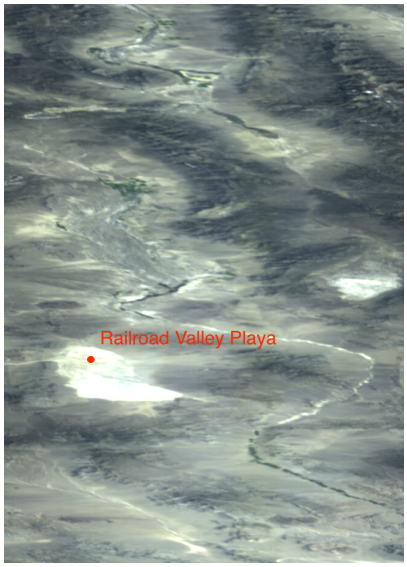

(a) A raw capture from HYPSO-1 of Railroad Valley Playa, taken 18/09/22.

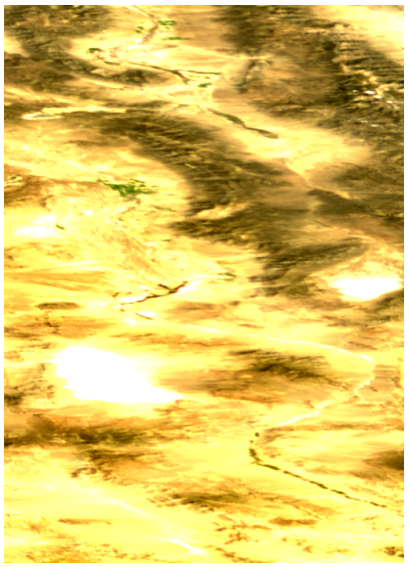

(b) Atmospheric corrected image of the HYPSO-1 capture taken 18/09/22.

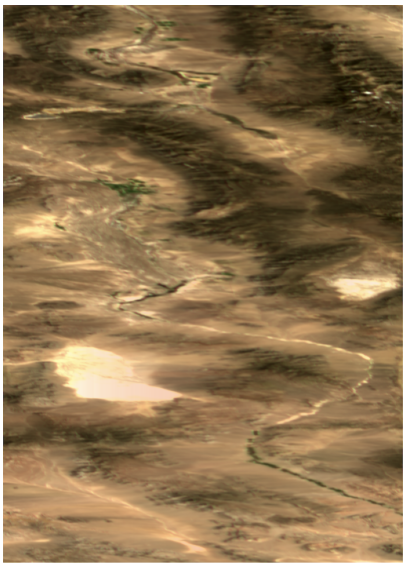

(c) Better performing atmospheric correction with adjusted settings.

Figure 4.17: The figures show the location of the ground station and the result of performing atmospheric correction on raw HYPSO-1 captures of Railroad Valley Playa.

Table 4.2 below, shows the important data regarding the SZA and VZA as well as when the HYPSO-1 capture was taken and when the RRVP measurement was done. The time of all HYPSO-1 capture matches up very well with the RRVP measurements. The biggest difference is 11 minutes the 11/10/2022, which is not too long. The first three captures in the table have quite a low VZA, while the last two captures have a very high VZA. This could impact the captures in a way such that the atmospheric scattering and absorption will increase, which in the end could make it more difficult to perform a good correction.

Date(dd/mm/yyyy)	Time(hh:mm)		SZA (deg)	VZA (deg)
	HYPSO-1	RRVP		
16/07/2022	18:02	18:00	28.9	8.3
24/07/2022	18:04	18:00	29.5	6.0
18/09/2022	18:05	18:00	42.6	1.4
11/10/2022	18:11	18:00	48.9	17.2
12/10/2022	17:58	18:00	50.9	13.3
14/10/2022	17:34	17:30	54.0	54.6
17/03/2023	18:32	18:30	44.1	57.0

Table 4.2: Data overview of the RRVP comparison with HYPSO-1. SZA (Solar zenith angle) is the angle between the sun and the zenith direction, while VZA (View zenith angle) is the angle between the viewing direction of HYPSO-1 and the zenith direction.

At the start of May 2023, HYPSO-1 has 20 captures over Railroad Valley Playa, whereas seven of them have valid data and are captured on a day when RadCalNet have BoA and ToA reflectance measurements. The reflectance is available after processing the seven HYPSO-1 captures through ACOLITE and will be used for validation. Figure 4.18 below, shows the seven different ToA reflectance after they have been atmospheric corrected in the left image and the BoA reflectance to the right.

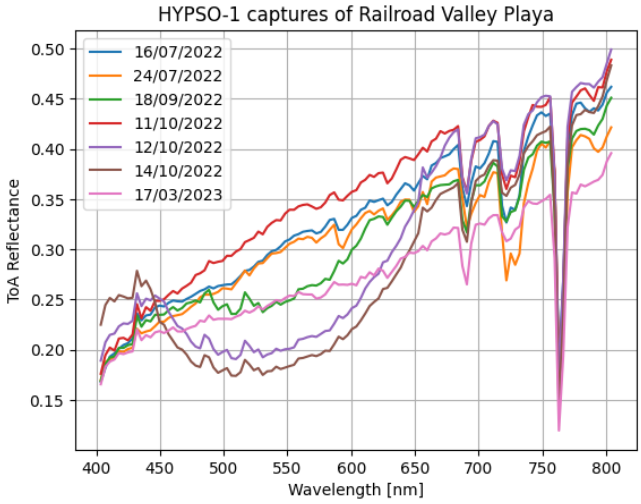

(a) The plot shows the ToA reflectance of the seven HYPSO-1 captures of Railroad Valley Playa

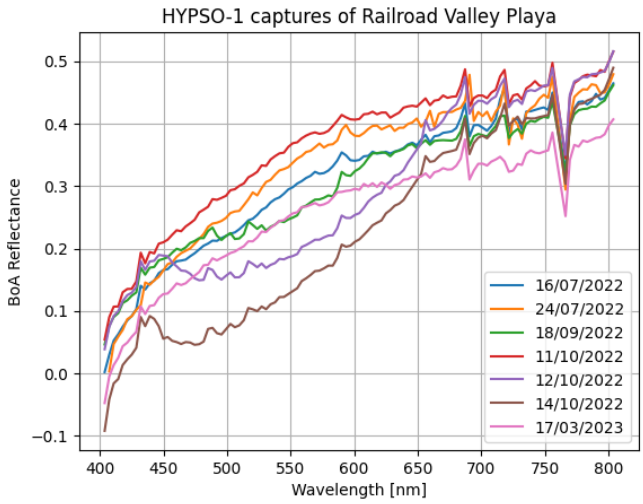

(b) The plot shows the BoA reflectance of the seven HYPSO-1 captures of Railroad Valley Playa

Figure 4.18: The figures shows ToA and BoA reflectance to the left and to the rights, respectively over the seven RRVP captures.

The signatures of the different captures are very similar, but there are some differences. Looking at ToA reflectance from the image on the left, the capture the 12^{th} and 14^{th} of October have an unusual dip from around 440 - 650 nm. This is apparent on the raw data as well and could be result of oversaturation of the satellite imager. Ideally, all of the reflectance values from the different captures should have more or less the same reflectance under perfect conditions, at least the same reflectance signature. To have perfect conditions at all captures are of course extremely difficult and is most likely not the case for these captures, which might be why there are variances in the reflectance values.

As previously mentioned the Railroad Valley Playa is mainly a desert, which causes the absence of dark pixels in the image. This might cause problems for the algorithm. The lack of dark pixels in an image result in the algorithm overestimating the aerosol optical thickness [23]. The atmospheric correction tends to overcorrect when the aerosol optical thickness is overestimated. Figure 4.19 below, shows the ToA reflectance comparison between the ground station measurement (blue), the calibrated HYPSO-1 data that is used as input to ACOLITE (orange) and the output from ACOLITE (green).

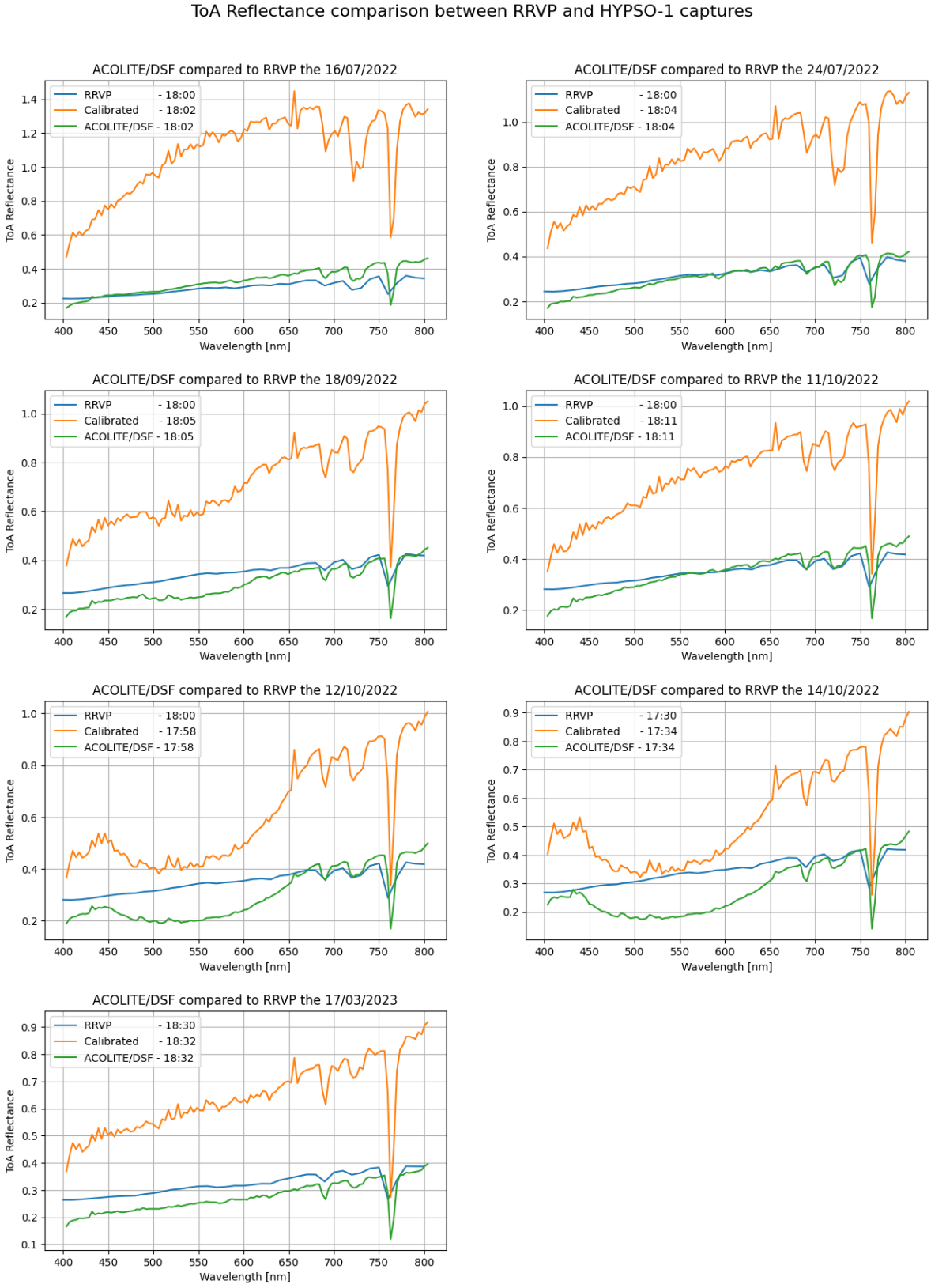

Figure 4.19: The figure illustrates the ToA reflectance comparison between the ground station measurement (blue), the calibrated HYPSO-1 data that is used as input to ACOLITE (orange) and the output from ACOLITE (green)

It can be seen that the HYPSO-1 data and the ground station data are very similar for most captures. The calibrated HYPSO-1 data used as input to ACOLITE is quite high and ACOLITE corrects a fair amount of the reflectance. The dip in reflectance at 12/10 and 14/10 as mentioned previously is also visible in this figure where the reflectance is lower from around 460-650 nm, while it matches the ground station data for the rest of the spectrum. It must be said that the ToA data available from the ground station is transformed from BoA data, which may cause some minor offsets in the data shown in the figure.

Figure 4.20 below, shows the BoA reflectance comparison between the ground station measurement (blue) and the output from ACOLITE (orange). The BoA reflectance data shows the same patterns as the ToA reflectance comparison. It is shown here as well that the 16/07 and 24/07 captures have a higher reflectance than the rest of the captures, while the captures at 18/09, 11/10 and 17/03 match up relatively well with the ground station data. The 12/10 and 14/10 captures have a lower reflectance from around 460-650 nm, while the rest of the spectrum matches the ground station data.

At first sight, it looks like the BoA is way off compared to the ToA. This is in some way an illusion since the y-axis range is much less in the BoA figure compared to the ToA figure due to the high ToA reflectance values from the calibrated HYPSO-1 data. However, ACOLITE transforms the ToA to BoA reflectance which is where data possibly could get a minor offset. It can still be seen that there is a correlation between the BoA and ToA that matches the data.

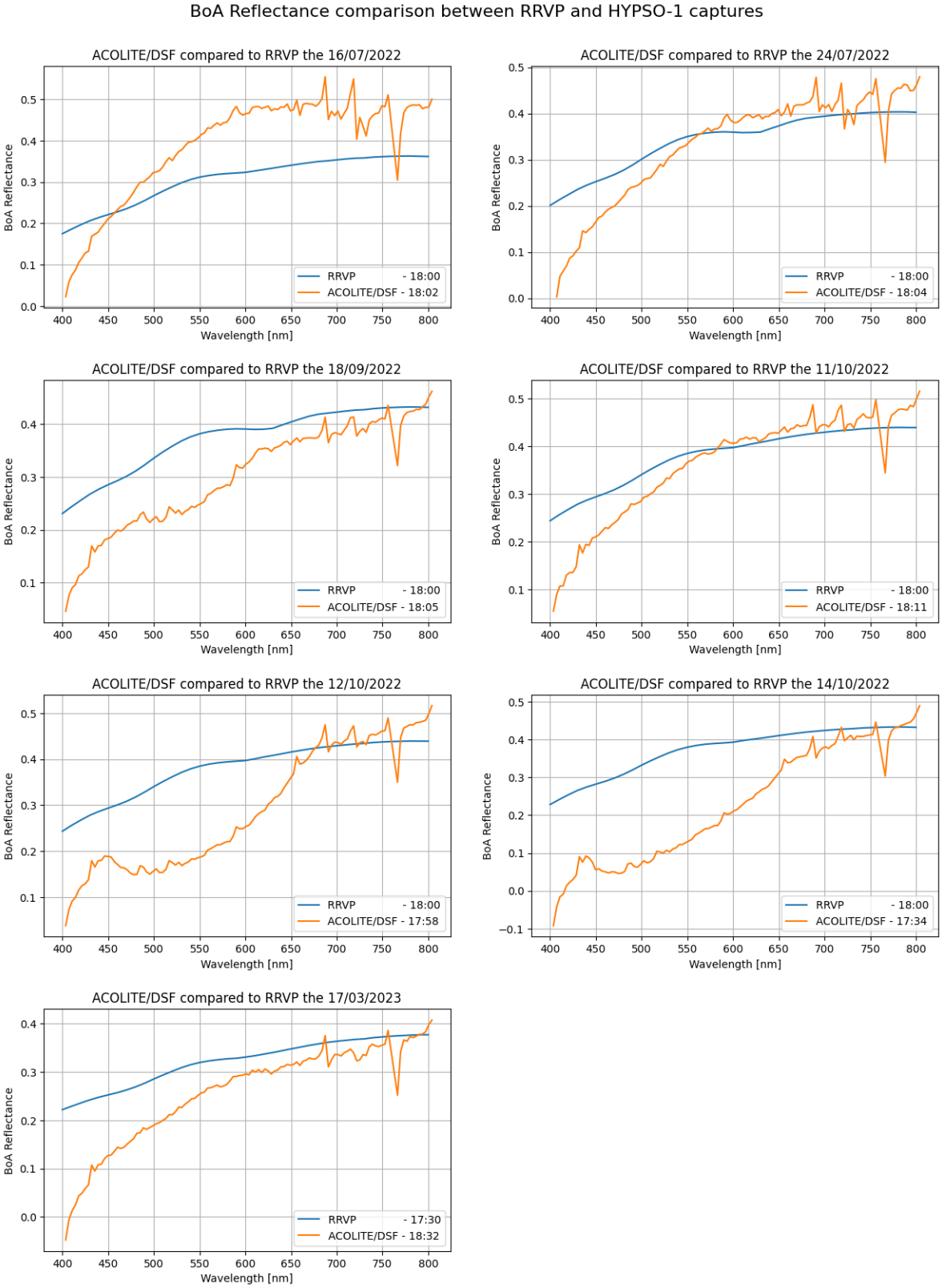

Figure 4.20: The figure illustrates the BoA reflectance comparison between the ground station measurement (blue) and the output from ACOLITE (orange)

It was shown that most of the ToA reflectance did match up with the measured ground station data, even if there are some small differences at some wavelengths. ACOLITE tends to overcorrect the BoA reflectance in three of the captures throughout the entire spectrum. For almost every capture it also overcorrects at smaller wavelengths, while the BoA reflectance from 600/650 nm is higher than the ground station data in four of the captures. It may be hard to conclude anything specific while having different behaviour in most captures. There may be factors such as a lack of dark pixels that perhaps causes the differences shown in the figures or the weather conditions at some captures. The atmospheric correction can be seen as working with small offsets, especially at lower wavelengths on the captures of Railroad Valley Playa.

4.4 Gobabeb

It is desired to validate the performance of ACOLITE on various surfaces with different vegetation and water content. Previously, the validation has been performed on the ocean outside of Venice and in a desert with few dark pixels. The next surface and vegetation that should be looked at is a land application with a more vegetated surface. There exists a lot of captures by HYPSO-1 on these applications, but there are quite a few that match up with any ground station data. This makes it hard to validate the actual result when performing the atmospheric correction. A evaluation of this type of vegetation would have been performed if there were such ground station data available.

HYPSO-1 has a lot of captures of Gobabeb, where four of them match up with ground station data. This location is very similar to Railroad Valley Playa, however, this site is located at the coastline. This means that there will be more dark pixels for ACOLITE to choose from than in Railroad Valley Playa. Figure 4.21 below, shows the raw image of Gobabeb on the left and the atmospheric corrected image on the right. The images turned originally out with a yellow colour to the desert, but by changing the RGB band combination to the same as for Railroad Valley Playa, a more true tone of the desert is shown. One big difference is that the atmospherically corrected images did not turn very bright, which is a good indication that more dark pixels help the algorithm to perform better.

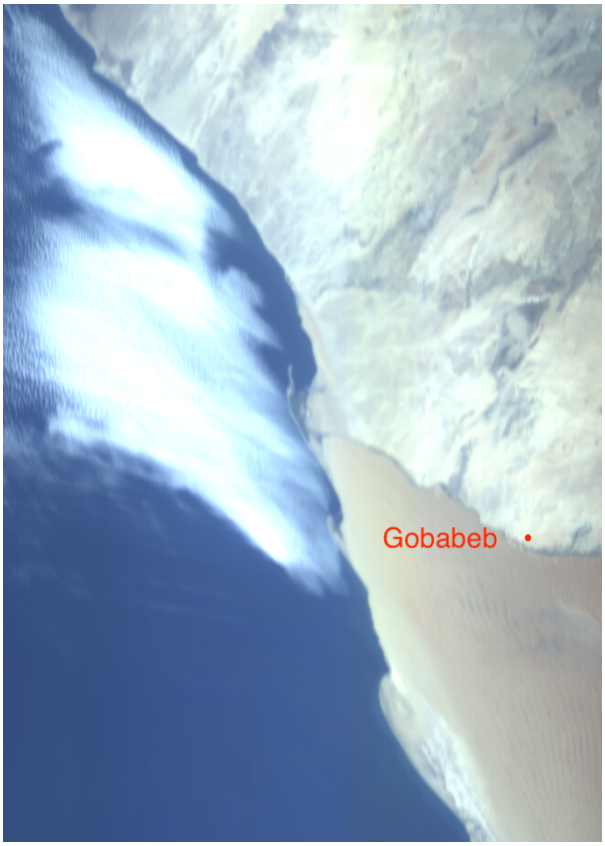

(a) A raw capture of Gobabeb captured by HYPSO-1 the 22/11/2022.

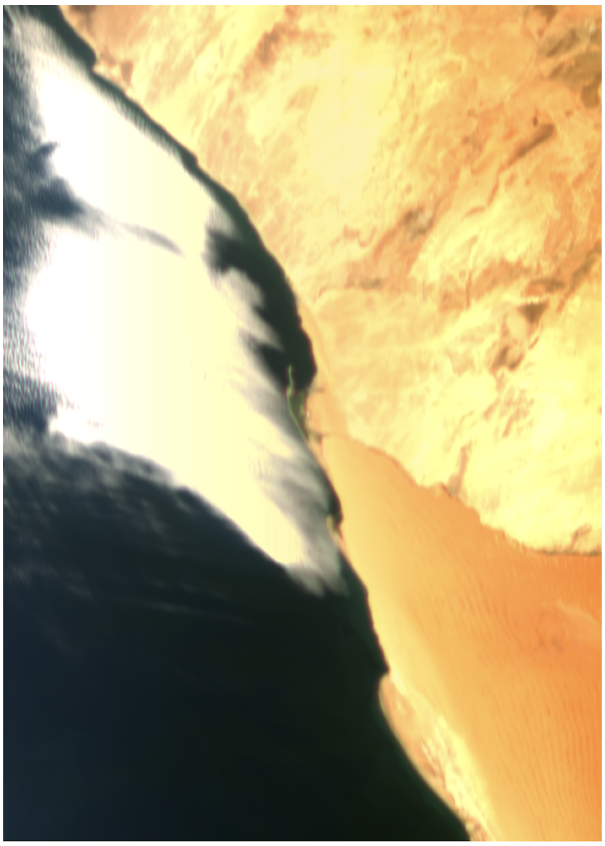

(b) Atmospheric corrected image of the Gobabeb capture the 22/11/2022.

Figure 4.21: The figures show the location of the ground station and the atmospheric corrected image of Gobabeb the 22/11/2022.

Table 4.2 below, shows the important data regarding the SZA and VZA as well as when the HYPSO-1 capture was taken and when the Gobabeb measurement was done. The time of all HYPSO-1 capture matches up very well with the Gobabeb measurements. The biggest difference is 54 minutes the 22/11/2022, which may impact the comparison. Three out of four captures in the table have quite a low VZA, while the last capture has a very high VZA. This could impact the captures in a way such that the atmospheric scattering and absorption will increase, which in the end could make it more difficult to perform a good correction.

Date(dd/mm/yyyy)	Time(hh:mm)		SZA (deg)	VZA (deg)
	HYPSO-1	RRVP		
02/09/2022	08:51	09:00	44.2	19.8
19/09/2022	08:38	09:00	41.7	18.2
22/11/2022	08:06	09:00	37.2	65.3
14/02/2023	08:41	09:00	38.1	5.7

Table 4.3: Data overview of the Gobabeb comparison with HYPSO-1. SZA (Solar zenith angle) is the angle between the sun and the zenith direction, while VZA (View zenith angle) is the angle between the viewing direction of HYPSO-1 and the zenith direction.

The capture taken the 2nd of September 2022 is almost useless due to the heavy cloud cover of the image. As shown in figure 4.22 below, almost the entire image is covered by clouds. It is however taken into the validation to exemplify how cloud cover may disrupt data. The clouds are above the ocean as well, which is also affecting the number of dark pixels available.

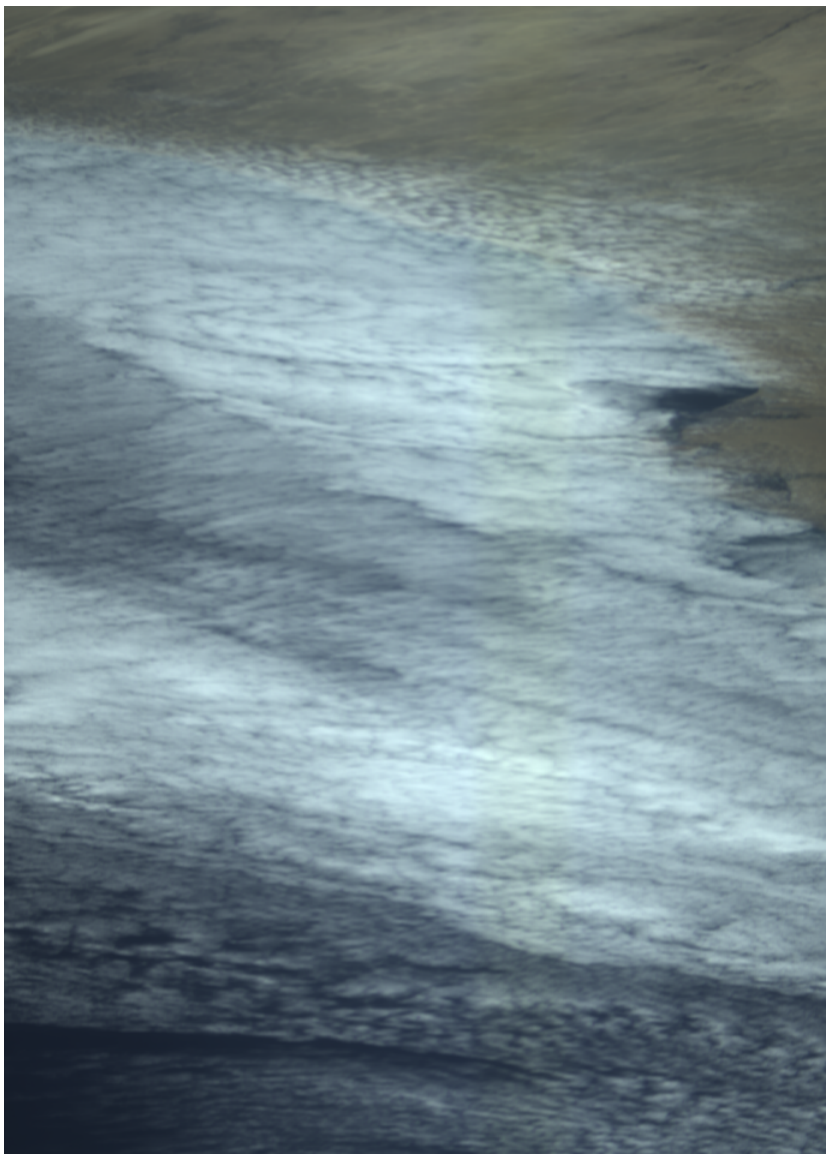

Figure 4.22: The figure illustrates heavy cloud cover of the Gobabeb capture taken 02/09/2022.

Figure 4.23 below, shows the measured ToA reflectance from the HYPSO-1 captures after atmospheric correction on the left, and the BoA on the right. The first notice is the cloud-covered capture on 02/09/2022 has about twice as high ToA reflectance values from around 400-600 nm, and still quite high values from 600-800 nm than the three other captures. The three other captures have very similar signatures and somewhat the same reflectance values, which is very promising. The cloud-covered capture has still quite a high BoA reflectance compared to the other captures. This indicates that the amount of clouds in the capture does impact the atmospheric correction in such an amount that it is not useable.

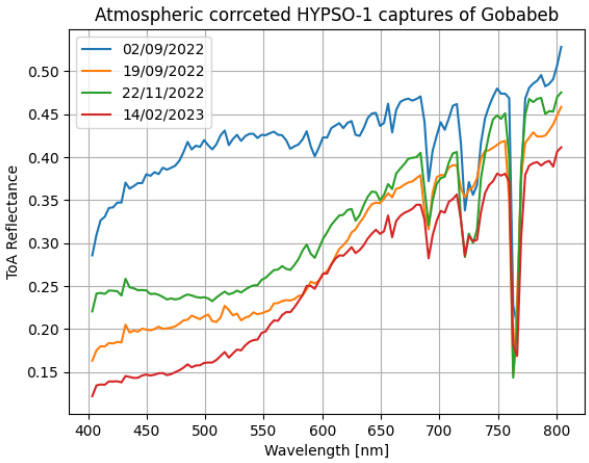

(a) The plot shows the ToA reflectance of the seven HYPSO-1 captures of Gobabeb

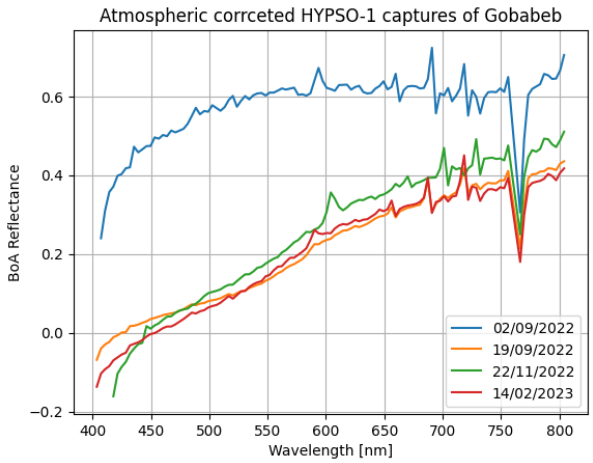

(b) Atmospheric corrected image of the Gobabeb capture the 22/11/2022.

Figure 4.23: The plot shows the BoA reflectance of the four HYPSO-1 captures of Gobabeb

Figure 4.24 below, shows the measured ground station data (blue), the calibrated HYPSO-1 data (orange) and the output of ACOLITE (green). The figure shows that the ToA reflectance values from the three useable capture of Gobabeb are close to the measured ground station data. There are some minor differences at different places on the three valid plots throughout the entire spectrum, which makes it hard to conclude anything specific at some wavelengths. It is noticeable that the 19/09 and 22/11 captures have higher ToA reflectance from around 650-750 nm.

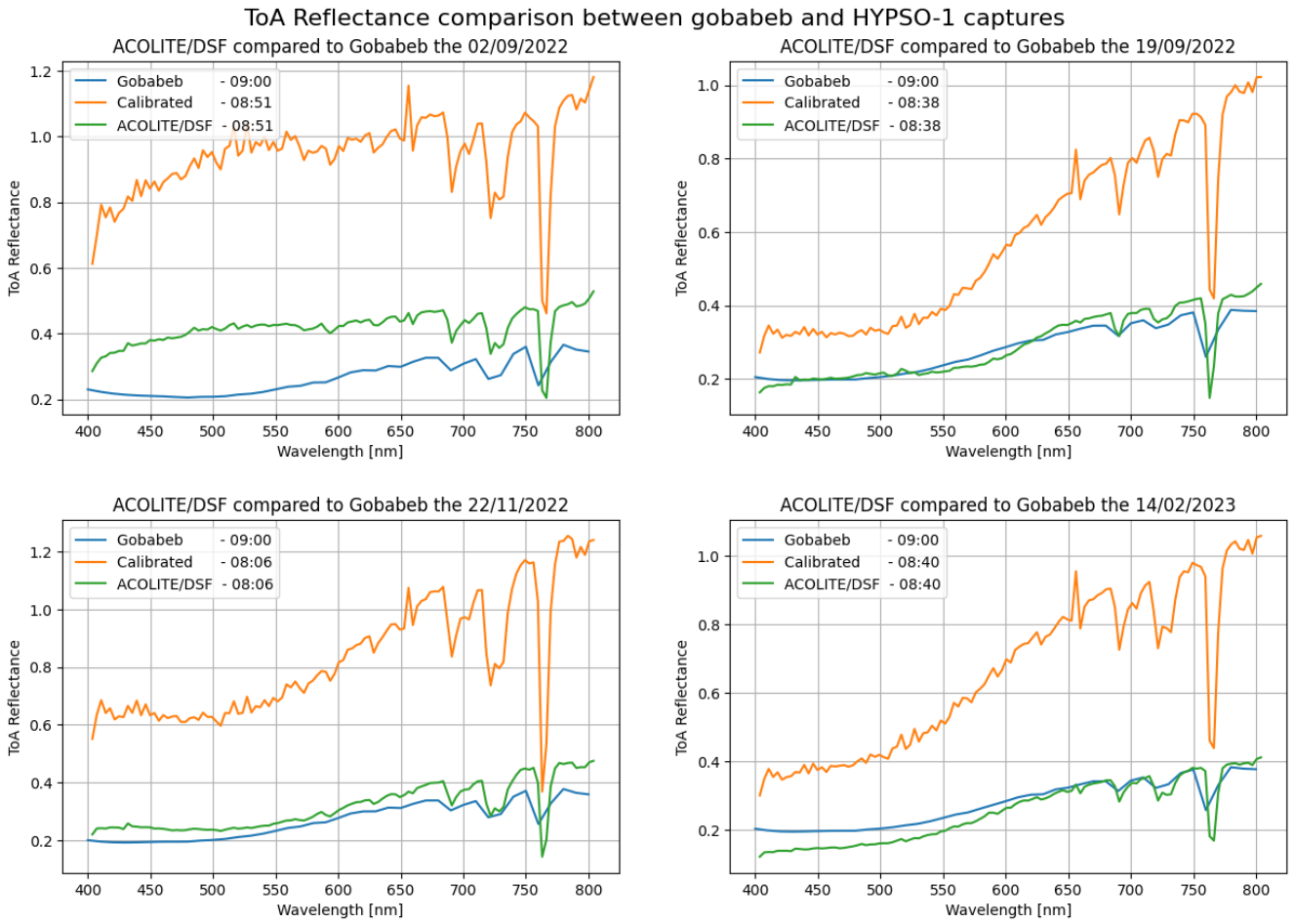

Figure 4.24: The figure compares the ToA reflectance measured ground station data (blue), the calibrated HYPSO-1 data (orange) and the output of ACOLITE (green).

The BoA plots below in figure 4.25 have been transformed by ACOLITE from Level 1 ToA reflectance to Level 2 BoA reflectance. The BoA reflectance measured from the Gobabeb ground station over a span of 5 months is about identical in all four plots. This indicates that this reflectance is the standard at this ground station. The cloud-covered capture in the first plot is still shown to illustrate the differences. The BoA reflectance from 19/09 and 14/02 is very similar in terms of both having lower values than the ground station in the entire spectrum.

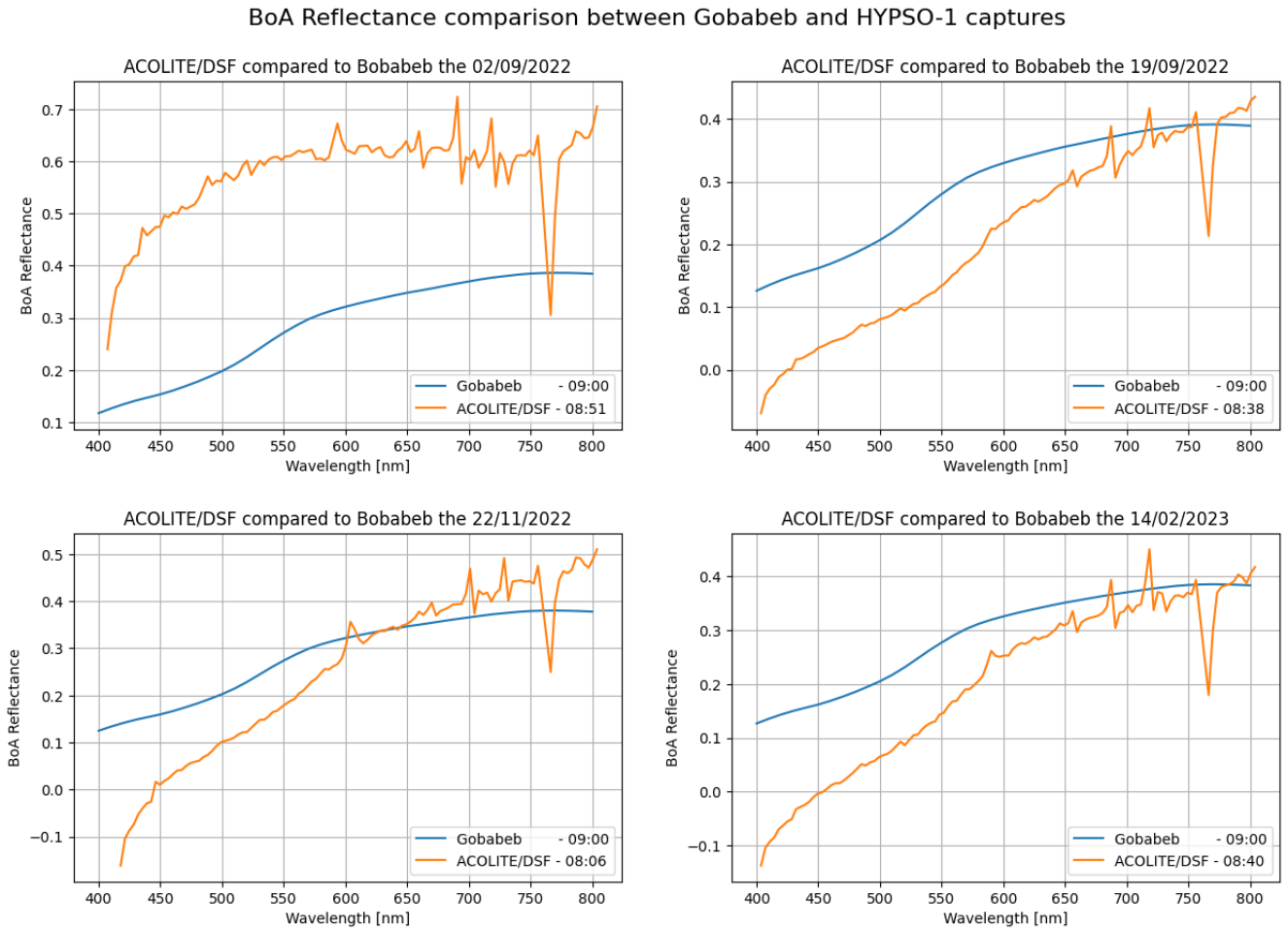

Figure 4.25: The figure compares the Boa reflectance measured ground station data (blue), the calibrated HYPSO-1 data (orange) and the output of ACOLITE (green).

It was very promising that the signature and BoA reflectance values for all three valid captures were almost similar in the entire spectrum. This was the case for the ground station data as well, with only some minor differences at some wavelengths. The differences between the accuracy of the atmospherically corrected data compared to the ToA and BoA data correlate, but the differences while comparing the BoA data were bigger. It is also evident that with the presence of more dark pixels the atmospheric correction has better accuracy to the ground station for Gobabeb compared to RRVP.

4.5 Comparison of different methods

In section 2.4 it was mentioned different methods for atmospheric correction, where the 6S method was heavily described. Alvaro Flores-Romero, an HYPSO-1 team member has created a Python script for performing atmospheric correction by the use of the 6S method. The script is first acquiring necessary parameters, such as solar zenith and azimuth angles, satellite zenith and

azimuth angles, and location coordinates among others. These parameters were used to set up the 6S model for each spectral band of the hyperspectral data. Spectral response functions (SRF) for each band were derived based on Full Width at Half Maximum (FWHM) values, and these SRFs were used to run the 6S model, obtaining outputs such as direct and diffuse solar irradiance, path radiance, and absorption and scattering transmissivities. The 6S model outputs were then employed to compute the surface reflectance for each band, replacing at-sensor radiance with atmospherically corrected reflectance values. To fill in gaps in the data due to aerosol optical thickness (AOT) variations, a linear 1-dimensional interpolation was performed.

Figure 4.26, below, offers a comparison of the results of atmospheric correction conducted via 6S and ACOLITE, against the data collected from the ground station. This comparison is made for three captures of Venice with a resolution of (956, 684). The 4th of May 2023 capture, which has a widespatial format with a resolution of (598, 1092), is currently incompatible with the 6S script. Preliminary analysis indicates that the 6S method produces higher reflectance values than ACOLITE, which itself aligns closely with the ground station data. This might be attributable to the more advanced algorithms and scripts employed by ACOLITE, which are possibly better suited to the HYPSO-1 data.

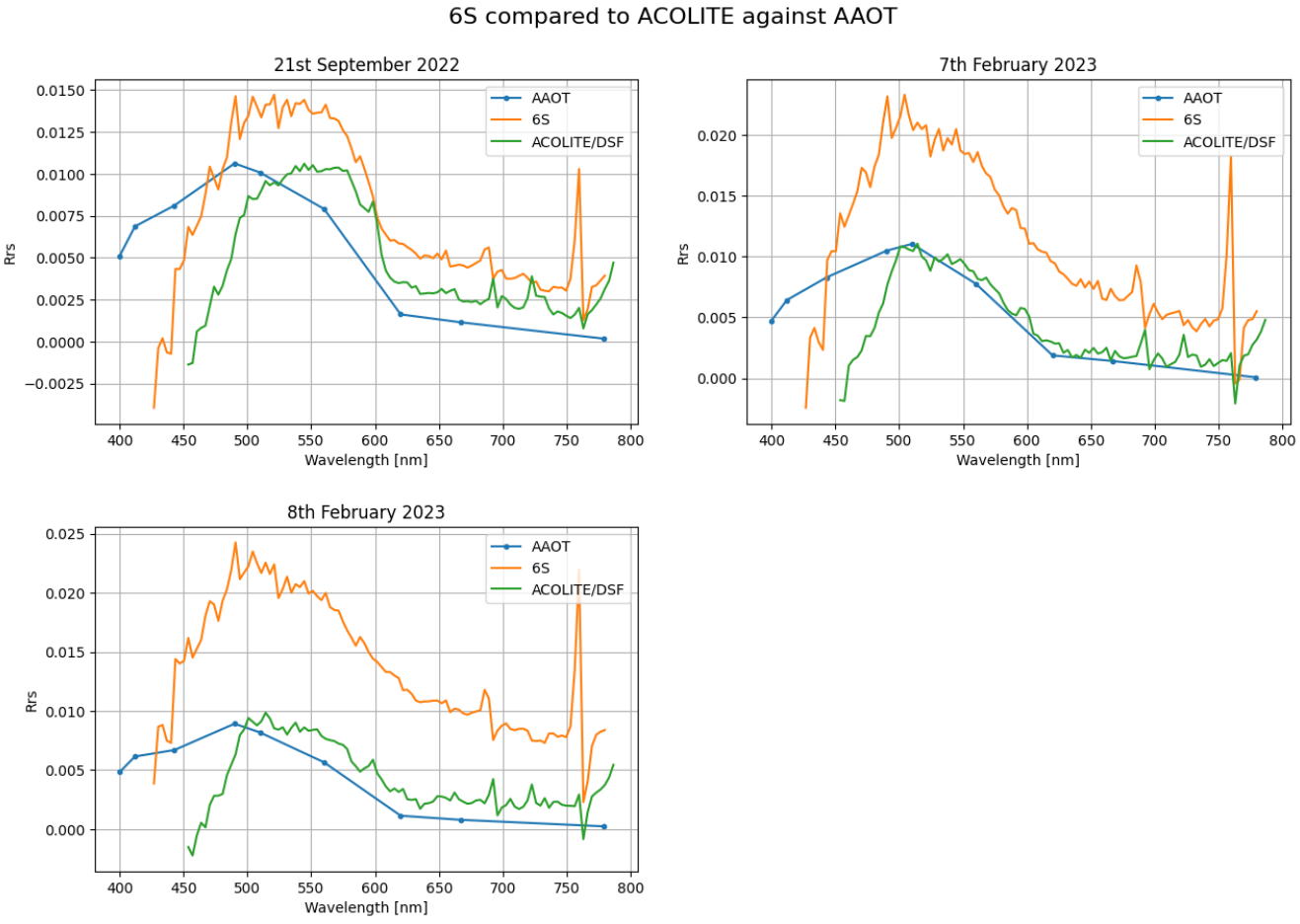

Figure 4.26: The figure delineates the contrast between the measured ground station data (blue), the data corrected by the 6S method (orange), and the data corrected by ACOLITE (green).

The 6S atmospheric correction primarily focuses on water applications, and for this reason, it is not necessary to look at the correction of land applications. Despite the ideal scenario of having more captures of Venice for evaluating atmospheric correction differences, the limited captures available are sufficient to conclude that, based on the ground station data, the 6S method is significantly less effective than ACOLITE.

A more statistical technique is the Empirical Line Fits (ELF), which was also introduced in section 2.4. The basic principle of the ELF method is to establish a linear relationship between the spectral radiance values of a base spectrum for open-ocean water and the corresponding satellite radiance values [16]. The U.S Geological Survey (USGS) has a base spectrum for open-ocean water, which is used to find the correlation, slope and intercept needed to find the linear relationship between the base truth and the HYPSO-1 data [39].

A Python plugin was developed in QGIS to execute the ELF method on HYPSO-1 data. Shortly described, the user initiates the process by inputting the HYPSO-1 raw data, which is then radiometric- and spectrally calibrated. Subsequently, the user manually inputs three pixels identified as water that is used to perform the atmospheric correction as explained in section 2.4. The plugin's initial output has the unit radiance, which is converted to Rrs values by dividing the radiance by the mean extraterrestrial solar irradiance and then by π [21].

Figure 4.27, below, illustrates the comparison between the corrected ELF data, the ACOLITE output, and the ground station data derived from AAOT. It is easily established that the ELF-corrected data diverges significantly from the ground station and ACOLITE data. The only redeeming aspect of the ELF method is that all the HYPSO-1 bands remain available post-correction. However, considering that the Rrs values deviate significantly from the ground station data, it can be concluded that the ELF method is not well-suited for atmospheric correction of HYPSO-1 data.

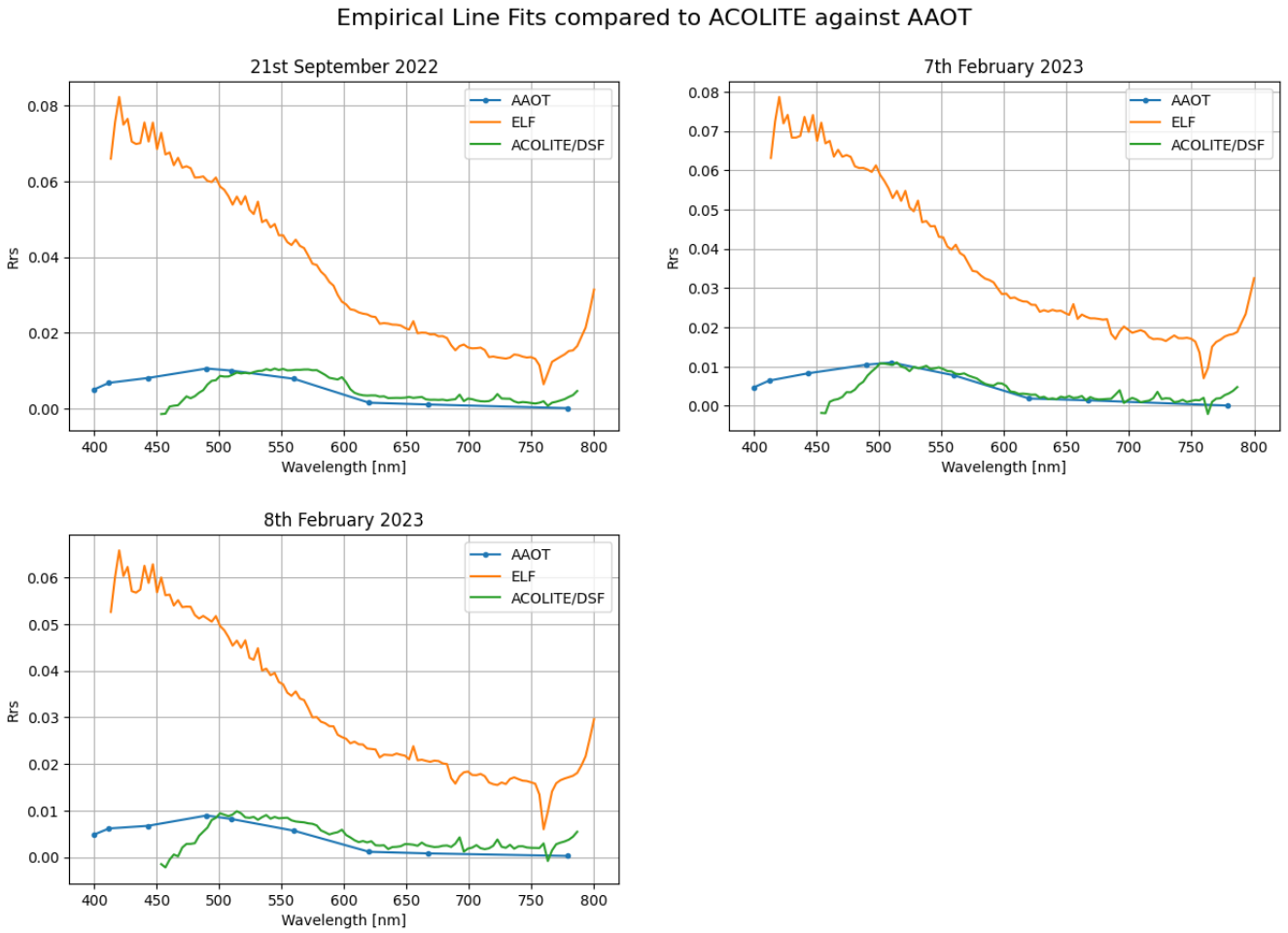

Figure 4.27: The figure presents a comparison of the measured ground station data (blue), the ELF-corrected data (orange), and the ACOLITE-corrected data (green).

4.6 New calibration coefficients

The input file used in ACOLITE is first calibrated in the script **h1data_processing.py** as mentioned at the end of section 3.1. In the middle of May 2023, a new set of calibration coefficients and a couple more calibration functions was created by the HYPSO-1 team member, Marie Henriksen. The old version of performing calibration left some stripes in the images unless an external destriping was performed on the cube afterwards. The new calibration coefficient will most likely impact the radiometric calibration which may as well impact the performance of ACOLITE. The difference will be the values of the calibrated ToA radiance from the calibrated cube, which in the end may impact the atmospheric correction.

The latest functionality performs radiometric- and spectral calibration with a new set of calibration coefficients. A smile correction is performed afterwards on the newly calibrated cube. The smile correction removes most of the vertical stripes that may disrupt the images to some extent. Then the cube is destriped for the removal of small blobs in the images. Destriping is essentially the

process of removing effects from an image without changing the original image in any way.

The capture of Venice taken 4th of May 2023 is taken in a widespatial format which changes the resolution from 956x684 to 598x1092. The new image format and the new calibration functions mean that the **h1data_processing.py** script needs to be updated accordingly. I have implemented the new calibration coefficients and the new calibration functions in the script which allows the script to process both image resolutions with the newest calibration method.

Figure 4.28 below, shows the ToA radiance of the Venice capture taken 8th of February 2023, with the old method (orange) and the new method (green) in the image to the left. In the image to the right is the ToA radiance from the new method minus the old one. The new calibration coefficients seem to have a slightly lower ToA radiance than the old calibration coefficients. Even if the differences seem quite low, they could impact the atmospheric correction in a more significant way as more components are added to the atmospheric correction.

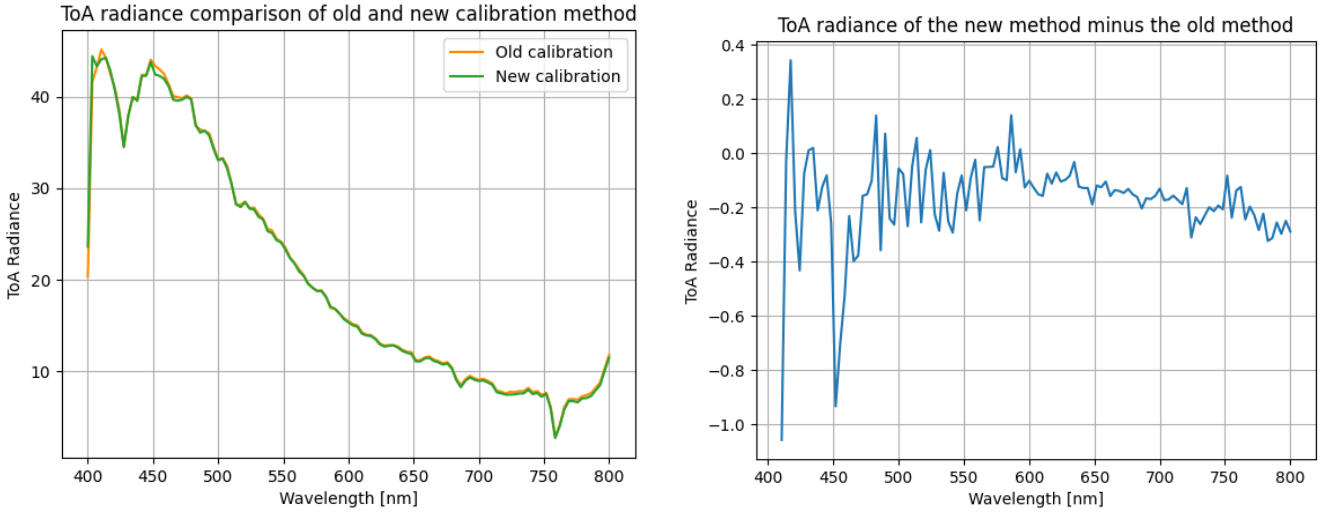

Figure 4.28: The figures show the differences in the ToA radiance from calibration with the new method versus the old method.

Figure 4.29 below, shows the difference between the old (orange) and the new calibration coefficients (green) applied on the Venice captures and compared to the AAOT ground station data (blue). The new calibration coefficients seem to improve the accuracy of the atmospheric correction on two out of three captures, namely on 21/09/22 and 08/02/23, while the 07/02/23 capture has a slightly worse accuracy. It was not possible to calibrate and perform atmospheric correction on the capture 04/05/23 until the script was updated due to the widespatial image format of this capture.

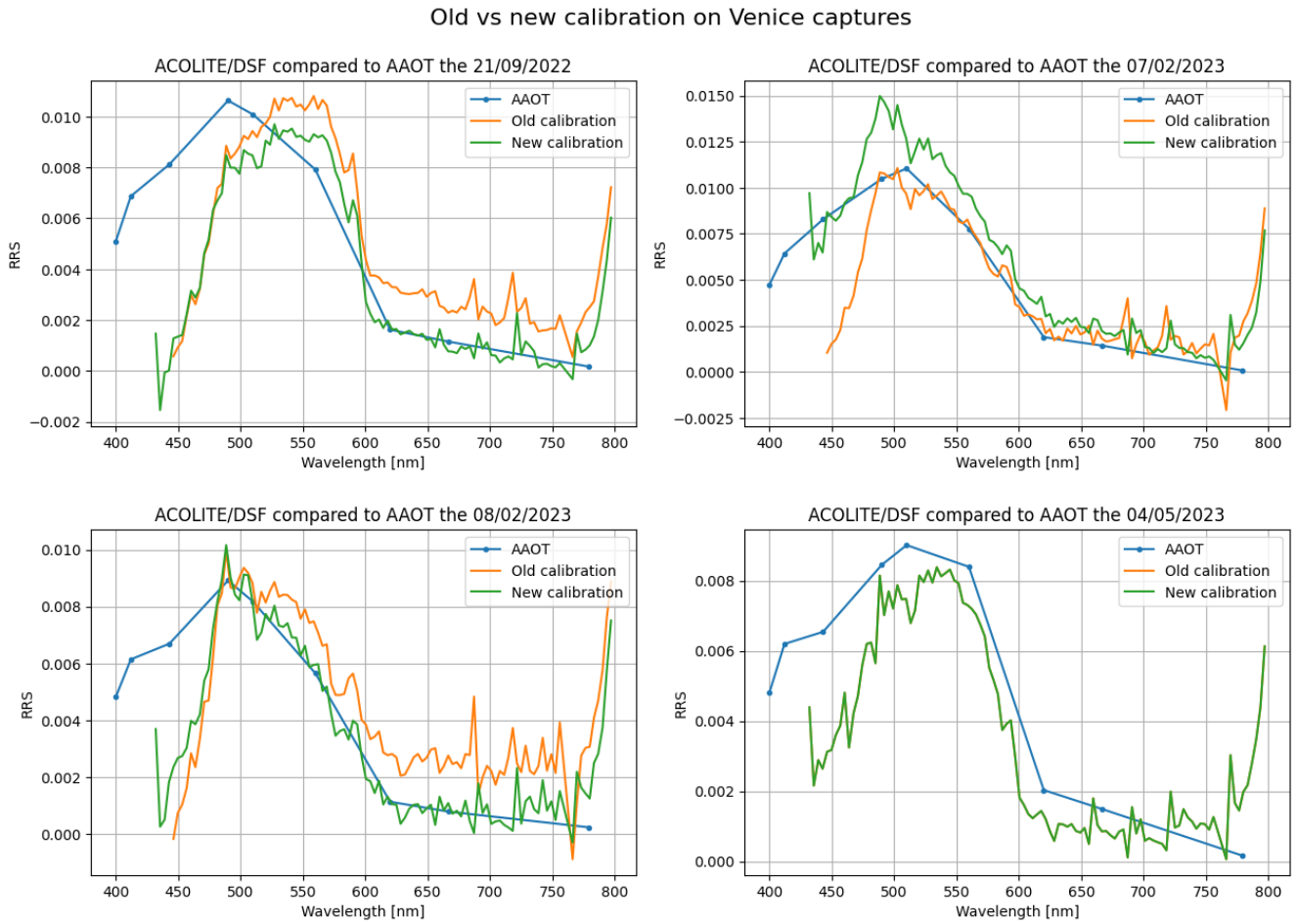

Figure 4.29: The figure compares the old (orange) and the new (green) calibration coefficients applied on the Venice captures and compared them to the AAOT ground station data.

Another positive aspect of the new calibration coefficients is that with the new calibration coefficients, it is now possible to analyse the result of four more wavelengths in the lower end of the spectrum without having negative reflectance values. The results from the new coefficients and functions indicate that the new calibration coefficients should be used in the future for the HYPSO-1 captures.

To have more confidence in the new calibration coefficients, it would be beneficial to have more captures of Venice to compare with. Instead, the captures over Railroad Valley Playa are used to compare the old and the calibration method. In the following two figures, figure 4.30 and figure 4.31 it is shown that the new calibration method doesn't impact the final result of the atmospheric correction in the same way as for Venice. It can be seen that the new calibration method has a slightly higher ToA radiance below 600 nm for all captures. From 600 nm and onwards they are very similar. As the ToA and BoA correspond it is not surprising that the change in BoA reflectance has the same pattern as the ToA radiance.

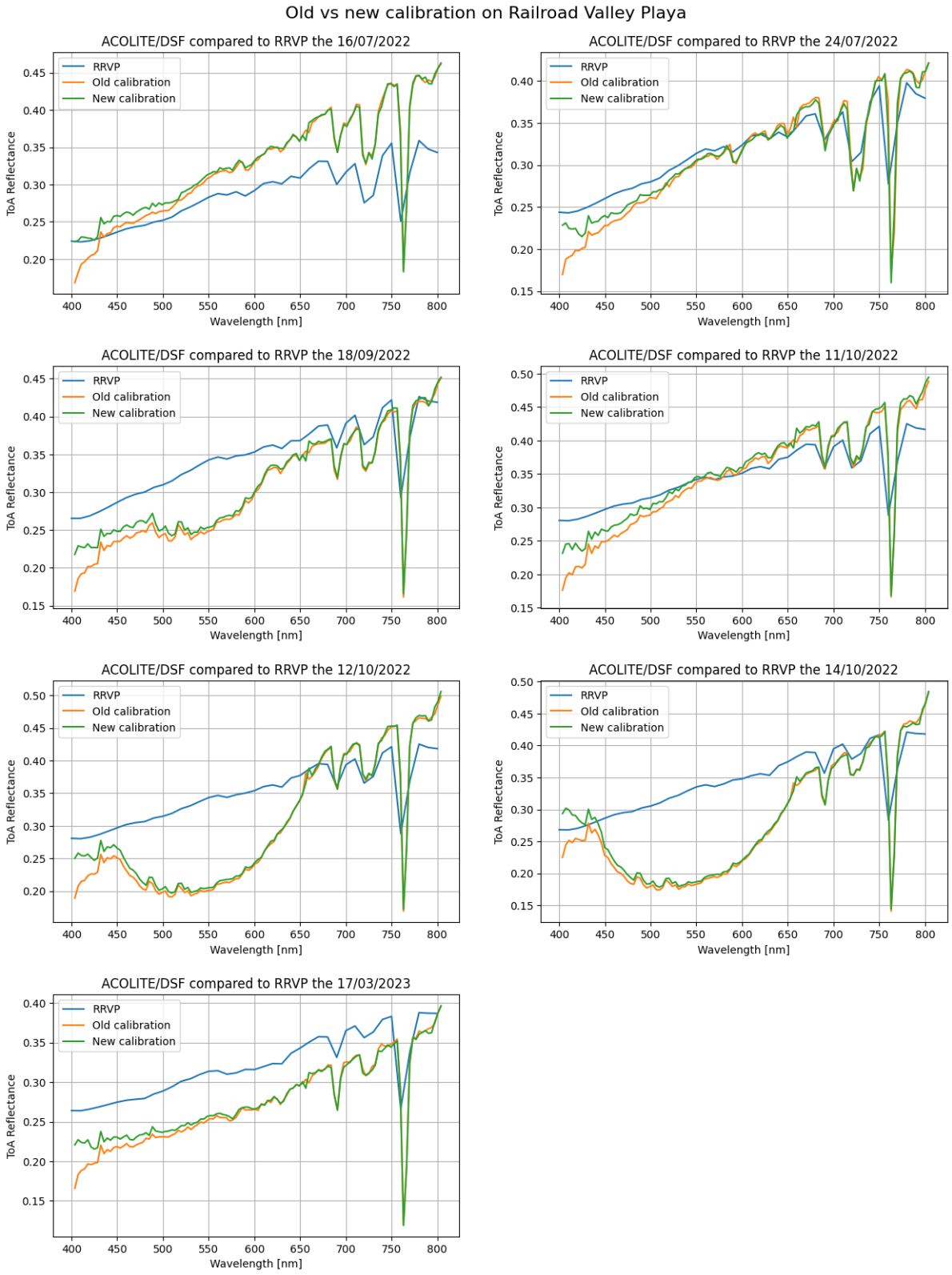

Figure 4.30: The figure compares the old (orange) and the new (green) calibration coefficients applied on the RRVP captures and compared them to the ground station data.

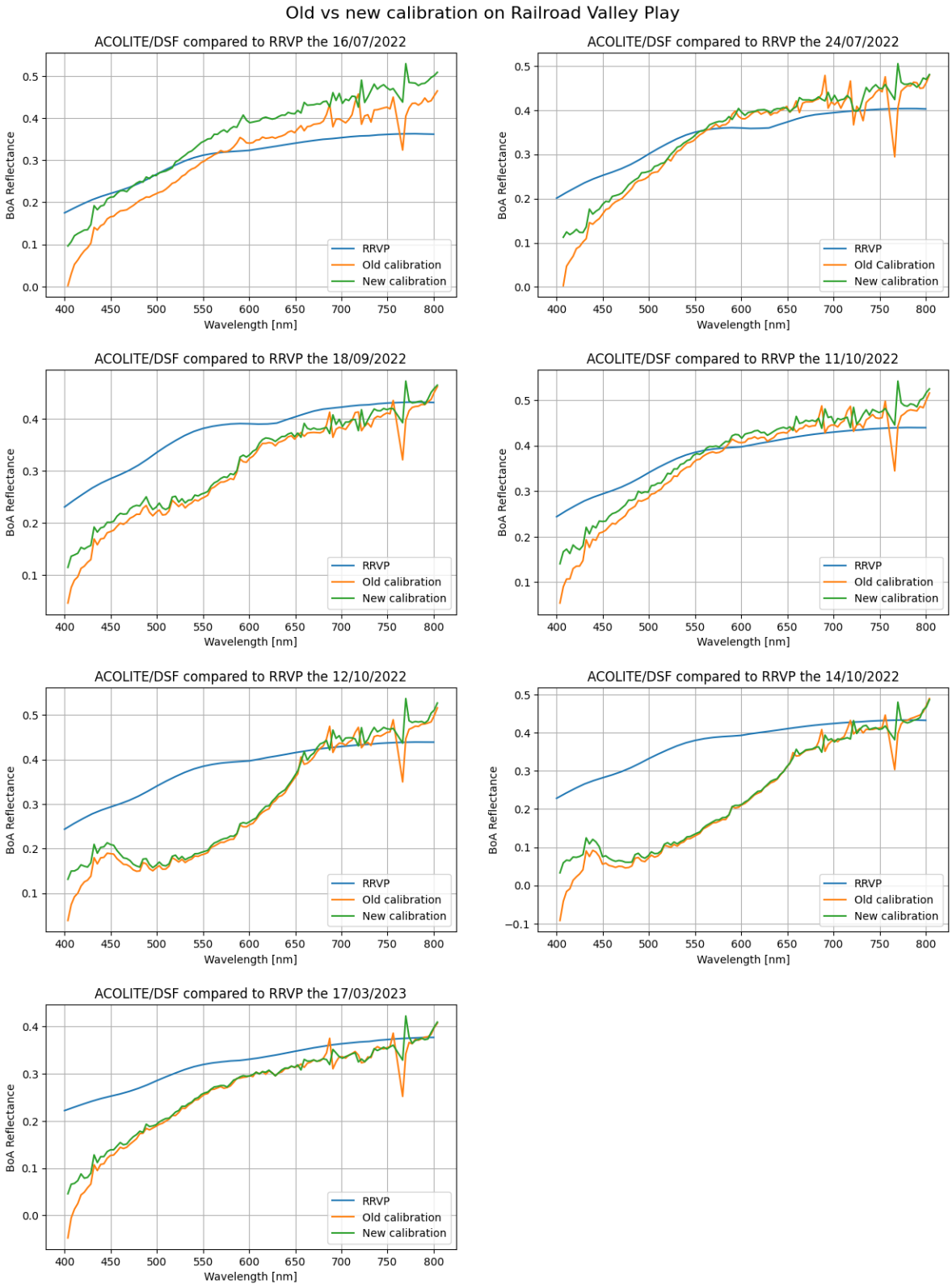

Figure 4.31: The figure compares the old (orange) and the new (green) calibration coefficients applied on the RRVP captures and compared them to the ground station data.

There could be several reasons why the reflectance from Railroad Valley Playa was left less unchanged than the ones in Venice. One of the reasons might be because the remote sensing reflectance is analysed for Venice, whereas for RRVP it is the ToA and BoA reflectance. The one extra algorithm processing BoA reflectance to Rrs might have a bigger impact on the final result than the one processing ToA reflectance to Rrs. The resolution of the reflectance values is as well much lower for Venice, which may cause an illusion that the difference is bigger for Venice than for RRVP.

Nonetheless, the new set of calibration coefficients and functions seems to lift the accuracy of the atmospheric correction in terms of the reflectance values being higher. The reflectance values are not raised in such a way they are spot on, but they are closer to the ground station data than the old calibration coefficients. This is the case for the last six plots, whereas the capture taken on 16/07 has worsened accuracy. Taking the comparison of the new and old methods into account, the new calibration coefficients and functions should be used for the HYPSO-1 captures. However, a further analysis of more Venice captures should be conducted to have more confidence in the new calibration coefficients and functions.

4.7 Savitzky-Golay Filter

The Savitzky-Golay filter is a digital signal processing filter often known as the Savgol filter. It is used for smoothing and noise reduction in data to enhance the data precision while preserving the underlying trend. The filter works by fitting a least-squares polynomial regression to a window of adjacent data points and then using the fitted polynomial to estimate the smoothed value at the centre of the window. The window size and the degree of the polynomial can be adjusted based on the characteristics of the data and the desired level of smoothing [40]

Almost all figures in this thesis such as figure 4.19 depict observable noice in the reflectance calibrated from HYPSO-1. Similarly, the atmospherically corrected data derived from ACOLITE shown in figure 4.15 does as well. It is therefore interesting to see if a filter, this time a Savgol filter, can be used to reduce the noise in the data and improve the accuracy of the atmospheric correction.

The main advantage of the Savgol filter is that it provides good noise reduction properties while minimizing distortion or loss of important features in the signal. It can effectively suppress random noise without significantly affecting the overall shape or timing of the underlying signal. It is desired to test if the Savgol filter can be used to enhance the performance of the atmospheric correction by reducing the noise and smoothing out the data effectively.

The choice of the polynomial order and window size in the filter depends on the characteristics of the data and the specific smoothing requirements. Generally, the order of the filter determines the flexibility or complexity of the polynomial fit used to smooth the data and the window size determines the number of neighboring data points used in the local polynomial fitting.

A higher polynomial can capture more intricate patterns in the data but may also pick up noise

more easily. If the data contains a significant amount of noise, a lower order can help preserve the underlying signal while smoothing out the noise. A higher order polynomials can introduce more smoothing and may result in a loss of fine details or sharp transitions in the data.

The window size can be hard to find, a larger window size will help average out high levels of noise, tend to smooth out more neighbouring data points and have a more robust filter against outliers. However, using a lower window size will preserve fine details, responds more quickly to changes in the input data and the data is less smoothed [41].

There is no definite answer to the optimal settings of the Savgol filter due to it is being used in different applications with various settings. It is however possible to test out different polynomial orders and window sizes to find the optimal settings for the HYPSO-1 data. Figure 4.32 below, shows the original raw cube being filtered before calibration with different polynomial order and window sizes. In the figure to the left, it is zoomed in on the wavelength range 440-560 nm to present a better view that there is very little difference between the different window sizes and polynomial orders. The figure to the right shows that the data remains the same even with higher polynomial order and window size.

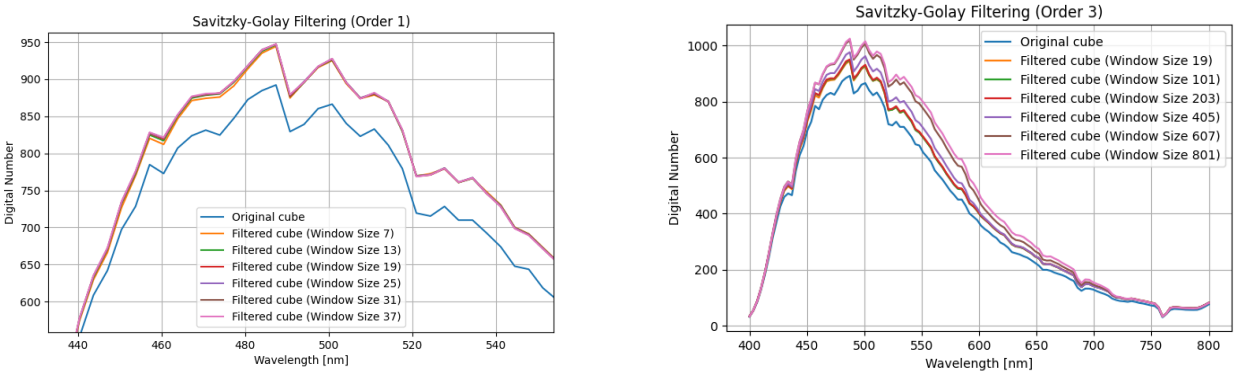

Figure 4.32: The figures shows the raw original cube compared to different Savgol-filtered cubes with different polynomial orders and window sizes.

A similar result is achieved when using orders from 1 to 6 and window sizes from 5 to 801. Even after adjusting the order and window size, there is not much smoothing done by the filter. The result is very similar to the original data with only the value of the data point being raised or lowered. This may happen because of various factors such as signal-to-noise ratio, the presence of outliers, the data scale or simply insufficient variation in the data.

Various filtered cubes with different orders and window sizes are atmospherically corrected and compared to the data before the use of the Savgol filter. Figure 4.33 below, shows the atmospheric corrected Savgol filtered data with order 2 and window size 13. Throughout the different filters, there was hardly any difference in the original and Savgol-filtered data. The figure below shows that there is a slight difference in the data for the capture taken on 04/05, but the reflectance

values have worsened compared to the ground station data.

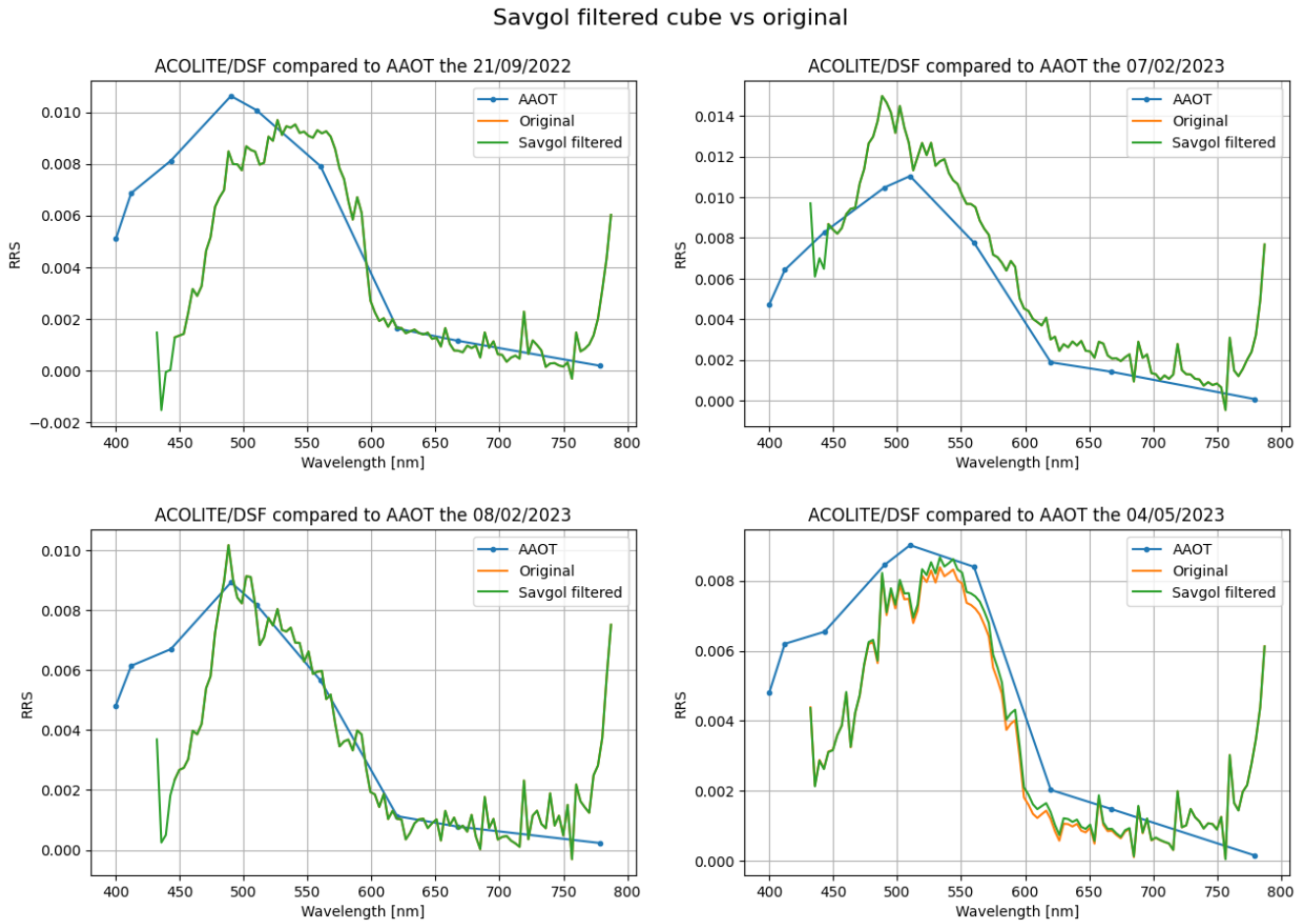

Figure 4.33: The figure compared the original atmospheric corrected data (orange) and the Savgol filtered atmospherically corrected data (green) for Venice.

It was expected that the Savgol filter would help the performance of the atmospheric correction to contain less noise and rather smoother data. Most likely is this not working because of the data characteristics of the HYPSO-1 data. Since the filtering did not work as intended, it will not be used for the atmospheric correction of further data.

Discussion

Contents

In section 1.2 the following three research questions were presented:

- How does the atmospheric correction performed by ACOLITE impact the accuracy of reflectance values derived from HYPSO-1 data compared to ground station data for water applications?

- How does the atmospheric correction performed by ACOLITE impact the accuracy of reflectance values derived from HYPSO-1 data compared to ground station data for land applications?

- How do different atmospheric correction algorithms compare in their accuracy of deriving reflectance from HYPSO-1 data?

In this chapter, the research questions will be discussed and answered based on the findings in the previous chapters.

5.1 Ground Stations

The atmospheric correction performed by HYPSO-1 using ACOLITE was validated using reference measurements from the ground station networks: AERONET and RadCalNet. The Acqua Alta Oceanographic Tower (AAOT) near Venice, Italy, from the AERONET network provided water-leaving radiance measurements. A comparison between level 1.5 and level 2.0 data from AAOT revealed insignificant differences, suggesting that the level 1.5 data could be used for validation. However, it is important to be cautious because there may be errors and limitations in the level 1.5 data.

The water-leaving radiance was converted to Rrs for the most optimal water application validation. While this conversion is valid and widely practised, it introduces an extra step in the validation process, and with it potential for additional error or uncertainties. Ideally, having Rrs measurements directly available from AERONET would eliminate the need for this conversion step, reducing the potential for added uncertainty and simplifying the validation process.

RadCalNet, a radiometric calibration network, offered ToA and BoA reflectance. Railroad Valley Playa in the United States and Gobabeb in Namibia were selected for validation of land application because of the amount of available HYPSO-1 captures over these ground stations. Although

Railroad Valley Playa is a desert and may lack the dark pixels necessary for ACOLITE's dark spectrum fitting method, Gobabeb, located near the ocean, was selected to evaluate the difference.

It is also worth mentioning that HYPSO-1 has a lot of captures of Erie, United States and Palgrunden, Sweden which would be good to use for the validation of ACOLITE. However, the ground station in Erie and Palgrunden was taken in for the winter and because of this, there was no ground truth data available from Autumn 2022 until Summer 2023. While AERONET has measurements almost every day from the ground station, RadCalNet does only have measurements 1/3 - 1/2 of the days in a month, which has also hindered a lot of HYPSO-1 captures to be used for validation due to the lack of any ground truth data. The lack of matchups on the same date for HYPSO-1 captures and for different ground stations have been a challenge in the validation process. This is because there are a lot of good captures by HYPSO-1 that could be used for validation, but are not useable because of the lack of ground truth data.

It is worth mentioning that RadCalNet provided measurements at 10 nm intervals, whereas the AAOT station only offered nine measurement points from 400 to 800 nm. Although having more AAOT measurements at additional wavelengths would have allowed for a more comprehensive validation across the entire light spectrum, the limited data available could still be used for validation. Overall, the comparison of ground-based measurements from AERONET and RadCalNet provided valuable validation and insights into the accuracy of the atmospheric correction performed by HYPSO-1 using ACOLITE.

5.2 Impact of Geolocation

The HYPSO-1 captures has a geolocation offset as shown in figure 4.1, impacting the accurate positioning of pixel coordinates. Georeferencing was performed using the georeferencer tool in QGIS with the use of manually selected ground control points to establish a transformation between the captured images and a reference map. Double digits GCPs distributed over the entire image were used. This process improved the geolocation accuracy of the images compared to the original ones as shown in figure 4.2.

The georeferenced images demonstrated a more precise alignment with the actual locations. The selected GCPs helped with the calculation of pixel offsets, enabling the determination of the ground station's exact location. This precise location information is crucial for comparing reflectance measurements between HYPSO-1 and the ground station, as even a small pixel offset could increase the uncertainty of the comparison.

Optimizing the initial geolocation of raw satellite images would yield substantial advantages, saving time and mitigating errors associated with subsequent georeferencing processes. By ensuring accurate geolocations during image capture, the need for additional georeferencing steps and challenges in selecting suitable ground control points could be eliminated. This streamlined approach would enhance workflow efficiency for pixel analysis and diminish potential uncertainties arising from inaccurately chosen GCPs during georeferencing. Reliable geolocation is important as it forms the foundation for various spatial analyses, enabling users of the images to reduce errors,

enhance the quality of results, and advance applications in remote sensing and geospatial analysis.

In summary, the geolocation offset in the HYPSO-1 captures was mitigated through the georeferencing process using QGIS and GCPs. The resulting geolocation information enabled a more accurate comparison and validation of reflectance measurements between HYPSO-1 and the ground station. However, there could still be slight differences in the georeferenced position and the actual position of the ground station which could lead to inaccurate comparisons. This is crucial in the conclusion of the performance of ACOLITE.

5.3 ACOLITE perfomance

Evaluating ACOLITE's atmospheric correction performance on the Venice, RRVP, and Gobabeb captures reveals a combination of challenges and successes. The satellite mission's emphasis on harmful algal blooms (HABs) in water applications implied that a greater number of captures over water were anticipated, particularly for Venice. However, difficulties with the capture target system, unfavourable weather conditions, and operational bugs led to fewer captured images than initially desired. Increasing the volume of captured images would allow for a more thorough evaluation and validation of ACOLITE's atmospheric correction capabilities.

One of the biggest issues with ACOLITE is the negative and low reflectance values around the wavelengths 400-475 nm. This is believed to not be ACOLITE's fault, but more likely a result of the pre-processing of the HYPSO-1 data. This can happen if the ToA calibration is too low or if there is an overestimation of the aerosol optical depth. It is evident from analyzing the output of ACOLITE for various satellite captures such as Sentinel-2, Landsat or PRISMA, that data is useable from 400 nm and beyond [38][42]. This means that about 19 % of the data is not useable for the validation of ACOLITE. This is a big issue.

Another issue is the peculiar drop and rise in reflectance around 760-770 nm was observed. This phenomenon can be attributed to the absorption of oxygen and water vapour in the atmosphere, leading to low gas transmittance. Consequently, only a limited amount of radiation reaches the satellite, resulting in reduced light reflected. A rise in reflectance was observed after 770 nm, known as the red-edge effect caused by the strong absorption of red light by chlorophyll. This absorption leads to low reflectance in the red portion of the spectrum, followed by a sudden increase in reflectance. When interpreting reflectance values within the 760-800 nm range, it is crucial to consider these factors as one of the measurement points from AERONET was at 779 nm. You could argue that this data is not valid or useable as well, leaving the total the total percentage of useable data at around 30 %.

The captures from Venice showcased ACOLITE's performance in water applications. Nevertheless, for a more comprehensive evaluation of ACOLITE's performance, a larger dataset of valid captures would be advantageous. Unfortunately, two additional captures of Venice were taken, but not usable as the satellite did not orient towards the site during the two captures. From the four of the total six captures available, the Rrs appeared to be precise on the dates 07/02 and 08/02, with only negligible differences in the other two captures, suggesting decent, consistent and reliable results

overall. However, it is hard to conclude anything reliably with only four captures.

In the case of RRVP, ACOLITE's performance was impacted by the lack of dark pixels in the image. The DSF method used by ACOLITE relies on the availability of dark pixels for proper functioning. As a result, the atmospherically corrected images appeared very bright and yellow at first. However, adjustments to the aerosol optical thickness estimate and the RGB wavelengths used for the correction helped mitigate the reflectance and RGB images issue to some extent, respectively. Comparisons between the ground station measurements and ACOLITE's outputs indicated that the ToA reflectance values generally matched well for most captures, although discrepancies were observed at specific wavelengths. The BoA reflectance also exhibited reasonable alignment, except for a few captures where overcorrection occurred at smaller wavelengths. Considering the variations observed in the output of ACOLITE from capture to capture, it can be challenging to place trust in the obtained results. Though the variation could possibly have been there from the raw data.

Gobabeb presented a land application with the appearance of water pixels, ACOLITE's performance was improved due to the presence of more dark pixels in the image compared to RRVP. The atmospherically corrected images of Gobabeb exhibited a more accurate representation of the desert, with a true desert tone. Comparisons between the ground station measurements, calibrated HYPSO-1 data (used as input to ACOLITE), and ACOLITE's outputs showed close alignment in the ToA and BoA reflectance values. Overall, the ToA and BoA reflectance values indicated a good performance of ACOLITE's atmospheric correction.

To finally answer the first two research questions, it is important to consider factors such as using level 1.5 data, unit transformation, inaccurate georeferencing or wrong pixel selection to mention some, could impact the results significantly and is worth taking into consideration when summarizing the performance. ACOLITE's atmospheric correction on the water application lead to higher accuracy than the correction performed on land surface. Venice had few captures but showed close alignment to the ground truth most of the wavelengths, RRVP suffered from the lack of dark pixels, leading to various corrections, but adjustments in ACOLITE's settings showed potential for improving the results. Gobabeb, with its greater availability of dark pixels, demonstrated the successful performance of ACOLITE's atmospheric correction, producing accurate representations of the desert.

All in all, the results are promising for the wavelengths with useable data and that has to be considered. Comparing the results from HYPSO-1 with the results from Sentinel-3 and PRISMA, it is evident that there are differences between ACOLITE and ground truth for their data as well [23] [38]. The process of atmospheric correction is complex, and it is extremely difficult to have a 100% accuracy, leaving ACOLITE to most likely be the best option available for atmospheric correction of HYPSO-1 data. To further improve the correction, the HYPSO-1 data should be invested to see if the negative reflectance values can be removed. This would be a huge improvement for the data.

5.4 Comparison of different methods

The accuracy of satellite-derived measurements largely depends on the method of atmospheric correction applied. Three atmospheric correction methods were considered for HYPSO-1 data in this study: the 6S method, ACOLITE, and Empirical Line Fits (ELF). The comparative evaluation of these methods was conducted against data obtained from the ground station.

The 6S method, despite being primarily for water applications, was observed to produce reflectance values higher than those produced by ACOLITE and the ground station data. This disparity may be caused by a better or an algorithm with a better fit for HYPSO-1 data. Additionally, the need for linear 1-dimensional interpolation to fill in gaps due to Aerosol Optical Thickness (AOT) variations provides further uncertainties to the process. However, the inherent limitations of the 6S script's resolution compatibility are also noteworthy, which are particularly highlighted when trying to process widespatial format captures such as that of 4^{th} May 2023.

ACOLITE's atmospheric correction, in contrast, displayed a closer alignment with the ground station data, potentially reflecting its advanced algorithms and scripts better adapted to the HYPSO-1 data. Although the shortage of available captures for evaluation limits the breadth of our analysis, the extant data sufficiently suggests that ACOLITE outperforms the 6S method in terms of accuracy.

Meanwhile, the ELF method offered a more statistically inclined approach to atmospheric correction, basing its corrections on a linear relationship between spectral radiance values of a base spectrum for open-ocean water and corresponding HYPSO-1 radiance values. The ELF method's practical performance was less satisfactory. The data corrected by the ELF method diverged significantly from both the ground station and ACOLITE data. The result could perhaps have been different with the use of another ground-truth dataset for the correlation. However, the ELF method's performance was not as good as that of ACOLITE, which was able to produce results closer to the ground station data.

To answer the final research questions, among the three methods examined, ACOLITE exhibited the closest alignment with the ground station data, suggesting better results for atmospheric correction for HYPSO-1 data. Nevertheless, this analysis underscores the importance of method selection for data correction, a crucial factor that impacts the reliability and precision of remote sensing data interpretation.

5.5 New calibration method

The new calibration coefficients introduced in May 2023 have demonstrated potential improvements in the radiometric calibration of HYPSO-1 satellite images. The previous calibration method sometimes resulted in stripes in the images, necessitating additional destriping processing. With the implementation of the new calibration coefficients, it was expected that the radiometric calibration process, and subsequently, the atmospheric correction performed by ACOLITE, will be positively influenced. The differences between the calibrated ToA radiance values obtained using the old

and new calibration coefficients may appear relatively minor, as observed in figure 4.28. However, even slight variations in calibrated radiance values can have a significant impact on subsequent atmospheric correction procedures, potentially affecting the accuracy of the final results.

The latest calibration functionalities incorporate the application of new calibration coefficients, followed by smile correction and destriping on the newly calibrated satellite image cube. The smile correction technique effectively removes vertical stripes that may slightly distort the images, while destriping preserves the integrity of the original image while removing small anomalies. Moreover, the introduction of a widespatial image format for the Venice capture taken on 4th May 2023 necessitated the update of the **h1data_processing.py** script to accommodate the new image resolution. The implementation of the new calibration coefficients and functions within the script enables the processing of images with both resolutions using the latest calibration method.

Comparisons between the old and new calibration coefficients applied to the Venice captures, in comparison with ground station data from AAOT, indicate the potential improvement in the accuracy of the atmospheric correction. The new calibration coefficients exhibit enhanced accuracy for two out of three captures (21st September 2022 and 8th February 2023), while the accuracy for the capture on 7th February 2023 appears to be slightly diminished. Due to the widespatial image format of the 4th May 2023 capture, calibration and atmospheric correction using the new method were not feasible until the script was updated. Additionally, the new calibration coefficients enable the analysis of four additional wavelengths in the lower end of the spectrum without encountering negative reflectance values. These findings suggest that the new calibration coefficients should be adopted for future HYPSO-1 captures, contributing to improved accuracy in atmospheric correction processes.

To maintain confidence in the new calibration coefficients, it would be beneficial to acquire more Venice captures that are not in widespatial format for comparison. In the absence of additional Venice captures, the captures over Railroad Valley Playa were utilized to evaluate the impact of the new calibration method. A comparison of the old and new calibration coefficients applied to the RRVP captures, along with ground station data, revealed slight variations in the ToA radiance below 600 nm, while minimal differences were observed from 600 nm onward.

These results indicate that the new calibration method does not exert the same level of influence on the atmospheric correction results for RRVP captures as observed for Venice. The distinct focus on remote sensing reflectance in Venice versus ToA and BoA reflectance in RRVP, along with differences in resolution, may account for the contrasting impact of the calibration method. Despite this, the new calibration coefficients and functions demonstrate an overall improvement in atmospheric correction accuracy, with reflectance values aligning more closely with ground station data for the majority of captures. Thus, the adoption of the new calibration coefficients and functions is recommended for HYPSO-1 captures.

Conclusion and Future Work

Contents

6.1 Conclusion

This study evaluated the ACOLITE atmospheric correction software to HYPSO-1 data, compared its performance with the 6S and ELF methods, and assessed a new calibration method. Through this, understanding and insights have been provided to guide further research and practical applications.

ACOLITE demonstrated a notable level of performance in processing HYPSO-1 data, despite presenting specific challenges such as negative reflectance values at 400 - 475 nm and irregular reflectance fluctuations from 760 - 800, causing around 30% of the data to be unusable for Venice. However, for RRVP and Gobabeb, there were not negative reflectance values from 400 nm when using surface reflectance. This issue seemed to be related to water application as the negative reflectance values were still present when using surface reflectance for Venice.

The comparison of ACOLITE with the 6S and ELF methods showed that ACOLITE aligned more closely with ground station data. The 6S method tended to produce higher reflectance values, and the ELF method often diverged from ground station data. This finding underlines the importance of method selection in achieving accurate remote sensing data interpretation.

The new calibration method, introduced in May 2023, was also assessed. Incorporating new calibration coefficients and functionalities such as smile correction and destriping, it showed a potential for improvements in the radiometric calibration of HYPSO-1 images. While the application of the new coefficients to RRVP captures showed minimal differences, their use in the Venice captures resulted in closer alignment with ground station data. This outcome suggests the new calibration coefficients may be beneficial for future HYPSO-1 captures.

While the study's findings offer valuable insights, they are based on a limited number of HYPSO-1 captures, particularly for water applications. As such, an increased dataset could provide a more robust evaluation. Moreover, addressing the identified issues with the reflectance values may lead to more efficient use of HYPSO-1 data.

In summary, this study has contributed to the understanding of the ACOLITE atmospheric correction algorithm and a new calibration method in the context of HYPSO-1 data. Future research should focus on increasing the dataset and refining the pre-processing steps to optimize results. These steps could enhance the reliability and applicability of HYPSO-1 data in remote sensing applications.

6.2 Future Work

The study has provided important insights into the use of ACOLITE for HYPSO-1 data correction, the comparison with other methods, and the potential of the new calibration method. However, several opportunities for future work arising from this research, which could further strengthen the understanding and applications for atmospheric correction of HYPSO-1 data.

Firstly, addressing the negative reflectance values around 400-475 nm is crucial. A careful analysis of the pre-processing of HYPSO-1 data should be conducted to understand the origins of these negative values. Adjusting the Top of Atmosphere (ToA) calibration or refining the estimates of aerosol optical depth could potentially mitigate this issue.

Secondly, the dataset for evaluation and validation needs to be expanded. This study was constrained by the limited number of captures, particularly over water bodies such as Venice. The planned HYPSO-1 captures over different locations should be conducted without fail, and operational bugs need to be resolved to increase the number of usable captures. A larger dataset would allow a more comprehensive evaluation of ACOLITE's performance and a better understanding of its potential variability.

Future work should also focus on fine-tuning the new calibration method. While the initial comparisons have shown improvements, a more detailed evaluation is required, incorporating more captures, to validate its efficacy fully.

Most importantly, future work should also include a comparison between the performance of ACOLITE for HYPSO-1 data and other satellite missions like Sentinel or Landsat. Performing matchup analyses with images from these satellites, taken approximately at the same time as HYPSO-1, would provide a valuable comparison benchmark for assessing the accuracy of ACOLITE for HYPSO-1 data. This would be particularly interesting because Sentinel and Landsat have already proven datasets with well-established correction methodologies, and comparing them with HYPSO-1 could provide a clear indicator of how well ACOLITE is performing.

Lastly, future studies should consider comparing ACOLITE's performance with other atmospheric correction methods apart from 6S and ELF. It would be beneficial to explore newer, potentially more advanced methods to assess their applicability to HYPSO-1 data and indicate their performance relative to ACOLITE.

Bibliography

[1] Mariusz E. Grøtte, Roger Birkeland, Evelyn Honoré-Livermore, Sivert Bakken, Joseph L. Garrett, Elizabeth F. Prentice, Fred Sigernes, Milica Orlandić, J. Tommy Gravdahl, and Tor A. Johansen. Ocean color hyperspectral remote sensing with high resolution and low latency—the hypso-1 cubesat mission. *IEEE Transactions on Geoscience and Remote Sensing*, 60:1–19, 2022. doi: 10.1109/TGRS.2021.3080175.

[2] Live Oftedahl. Historical launch of norwegian small satellite, 2022. URL `https://www.ntnu.no/nyheter/en/historical-launch-of-norwegian-small-satellite/`.

[3] Fish Site. Norway invests 10 million kroner to combat algal blooms, October 2019. URL `https://thefishsite.com/articles/norway-invests-10-million-kroner-to-combat-algal-blooms`.

[4] Erlend A. Lorentzen Stine Hommedal. What we know about the so-called "killer alga" in northern norway, 2019. URL `https://www.hi.no/en/hi/news/2019/may/what-we-know-about-the-so-called-killer-alga-in-northern-norway`.

[5] Erik Pekkeriet Gerrit Polder. A spectral imaging system for detection of botrytis in greenhouses, July 2013. URL `https://www.researchgate.net/publication/259215766_A_Spectral_Imaging_System_for_Detection_of_Botrytis_in_Greenhouses`.

[6] Algae Centrifuge. Algae strains, not all algae is green, Visited December 2022. URL `https://algaecentrifuge.com/blogs/news/36630145-algae-strains-not-all-algae-is-green`.

[7] Mathworks. Hyperspectal data correction, Visited November 2022. URL `https://se.mathworks.com/help/images/hyperspectral-data-correction.html`.

[8] Gyanesh Chander, Tim J Hewison, Nigel Fox, Xiangqian Wu, Xiaoxiong Xiong, and William J Blackwell. Overview of intercalibration of satellite instruments. *IEEE Transactions on Geoscience and Remote Sensing*, 51(3):1056–1080, 2013.

[9] Bjørndalen Elena. aerosol - meteorologi i store norske leksikon på snl.no, Visited 21 February 2023. URL `https://snl.no/aerosol_-_meteorologi`. Meteorologisk institutt.

[10] Tryve Holtebekk and Johannes Skaar. spredning - fysikk i store norske leksikon på snl.no, Visited 21 February 2023. URL `https://snl.no/spredning_-_fysikk`.

[11] Government of Canada. Interactions with the atmosphere, Visited 21 February 2023. URL `https://natural-resources.canada.ca/maps-tools-publications/satellite-imagery-air-photos/remote-sensing-tutorials/introduction/interactions-atmosphere/14635`.

[12] Skaar Johannes, Dick B. Øystein, and Kristiansen Jostein Riiser. rayleighspredning i store norske leksikon på snl.no, Visited 21 February 2023. URL `https://snl.no/rayleighspredning`.

[13] Susan Kay, John D Hedley, and Samantha Lavender. Sun glint correction of high and low spatial resolution images of aquatic scenes: a review of methods for visible and near-infrared wavelengths. *Remote sensing*, 1(4):697–730, 2009.

[14] NASA. Detecting pollution from individual ships from space, Visited 22. February 2023. URL https://www.esa.int/Applications/Observing_the_Earth/Copernicus/Sentinel-5P/Detecting_pollution_from_individual_ships_from_space.

[15] NASA. Observing in infrared, 2021. URL https://www.earthdata.nasa.gov/engage/open-data-services-and-software/data-information-policy/data-levels.

[16] Micheal T. Eismann. *Hyperspectral Remote Sensing*. SPIE, 1981. ISBN 978-0-8194-8787-2.

[17] Curtis Mobley. Empricial line fits, March 2021. URL https://www.oceanopticsbook.info/view/atmospheric-correction/level-2/empirical-line-fits.

[18] EFTD Vermote, D Tanré, JL Deuzé, M Herman, JJ Morcrette, and SY Kotchenova. Second simulation of a satellite signal in the solar spectrum-vector (6sv). *6S User Guide Version*, 3 (2):1–55, 2006.

[19] Majid Nazeer, Janet E. Nichol, and Ying-Kit Yung. Evaluation of atmospheric correction models and landsat surface reflectance product in an urban coastal environment. *International Journal of Remote Sensing*, 35(16):6271–6291, 2014. doi: 10.1080/01431161.2014.951742. URL https://doi.org/10.1080/01431161.2014.951742.

[20] Giannis Lantzanakis, Zina Mitraka, and Nektarios Chrysoulakis. Comparison of physically and image based atmospheric correction methods for sentinel-2 satellite imagery. In *Perspectives on atmospheric sciences*, pages 255–261. Springer, 2017.

[21] G Thuillier, M Hersé, D Labs, T Foujols, W Peetermans, D Gillotay, PC Simon, and H Mandel. The solar spectral irradiance from 200 to 2400 nm as measured by the solspec spectrometer from the atlas and eureca missions. *Solar Physics*, 214:1–22, 2003.

[22] E. F. Vermote, N. El Saleous, C. O. Justice, Y. J. Kaufman, J. L. Privette, L. Remer, J. C. Roger, and D. Tanré. Atmospheric correction of visible to middle-infrared eos-modis data over land surfaces: Background, operational algorithm and validation. *Journal of Geophysical Research: Atmospheres*, 102(D14):17131–17141, 1997. doi: https://doi.org/10.1029/97JD00201.

[23] Quinten Vanhellemont and Kevin Ruddick. Atmospheric correction of metre-scale optical satellite data for inland and coastal water applications. *Remote Sensing of Environment*, 216:586–597, 2018. ISSN 0034-4257. doi: https://doi.org/10.1016/j.rse.2018.07.015. URL https://www.sciencedirect.com/science/article/pii/S0034425718303481.

[24] Quinten Vanhellemont. Daily metre-scale mapping of water turbidity using cubesat imagery. *Opt. Express*, 27(20):A1372–A1399, Sep 2019.

[25] Sam Murphy. 6s emulator, Visited 22. February 2023. URL https://github.com/samsammurphy/6S_emulator.

[26] Quinten Vanhellemont. Acolite, Visited 22. February 2023. URL https://github.com/acolite/acolite.

[27] Quinten Vanhellemont. Acolite user manual, QV - November 14, 2022. URL https://github.com/acolite/acolite/releases/tag/20221114.0.

[28] Sivert Bakken. Ntnu-smallsat-lab ground systems, Visited 12. May 2023. URL https://github.com/NTNU-SmallSat-Lab/ground_systems/treenetcdf-and-geojsonimgs-processing.

[29] NASA. Aeronet, Visited 24. February 2023. URL https://aeronet.gsfc.nasa.gov/new_web/index.html.

[30] NASA. Aeronet - AAOT, Visited 31. March 2023. URL https://aeronet.gsfc.nasa.gov/new_web/photo_db_v3/AAOT.html.

[31] NASA. Aeronet - AAOT - Water-Leaving Radiance Data, Visited 31. March 2023. URL https://aeronet.gsfc.nasa.gov/cgi-bin/data_display_seaprism_v3.

[32] Marc Bouvet, Kurtis Thome, Béatrice Berthelot, Agnieszka Bialek, Jeffrey Czapla-Myers, Nigel Fox, Philippe Goryl, Patrice Henry, Lingling Ma, Sébastien Marcq, Aimé Meygret, Brian Wenny, and Emma Woolliams. Radcalnet: A radiometric calibration network for earth observing imagers operating in the visible to shortwave infrared spectral range. *Remote Sensing*, 11(20):2401, Oct 2019. ISSN 2072-4292. doi: 10.3390/rs11202401. URL http://dx.doi.org/10.3390/rs11202401.

[33] RadCalNetPortal. Radcalnet portal, Visited 02. May 2023. URL https://www.radcalnet.org/#!/.

[34] MODTRAN. Modtran, Visited 02. May 2023. URL http://modtran.spectral.com.

[35] QGIS. Qgis, Visited 12. May 2023. URL https://qgis.org/en/site/.

[36] S. Vasilchenko, S.N. Mikhailenko, and A. Campargue. Water vapor absorption in the region of the oxygen a-band near 760 nm. *Journal of Quantitative Spectroscopy and Radiative Transfer*, 275:107847, 2021.

[37] Jack T O'Malley-James and Lisa Kaltenegger. Expanding the timeline for earth's photosynthetic red edge biosignature. *The Astrophysical Journal Letters*, 879(2):L20, 2019.

[38] Federica Braga, Alice Fabbretto, Quinten Vanhellemont, Mariano Bresciani, Claudia Giardino, Gian Marco Scarpa, Giorgia Manfè, Javier Alonso Concha, and Vittorio Ernesto Brando. Assessment of prisma water reflectance using autonomous hyperspectral radiometry. *ISPRS Journal of Photogrammetry and Remote Sensing*, 2022. ISSN 0924-2716. doi: https://doi.org/10.1016/j.isprsjprs.2022.08.009. URL https://www.sciencedirect.com/science/article/pii/S0924271622002179.

[39] USGS. Usgs spectral library version 7, Visited December 2022. URL https://crustal.usgs.gov/speclab/QueryAll07a.php?quick_filter=open_ocean.

[40] Wikipedia. Savitzky-savgol filter, Visited 1. June 2023. URL https://en.wikipedia.org/wiki/SavitzkyâĂŞGolay_filter.

[41] Deepshikha Acharya, Asha Rani, Shivangi Agarwal, and Vijander Singh. Application of adaptive savitzky–golay filter for eeg signal processing. *Perspectives in Science*, 8:677–679, 2016.

[42] Quinten Vanhellemont and Kevin Ruddick. Atmospheric correction of sentinel-3/olci data for mapping of suspended particulate matter and chlorophyll-a concentration in belgian turbid coastal waters. *Remote Sensing of Environment*, 256:112284, 2021.

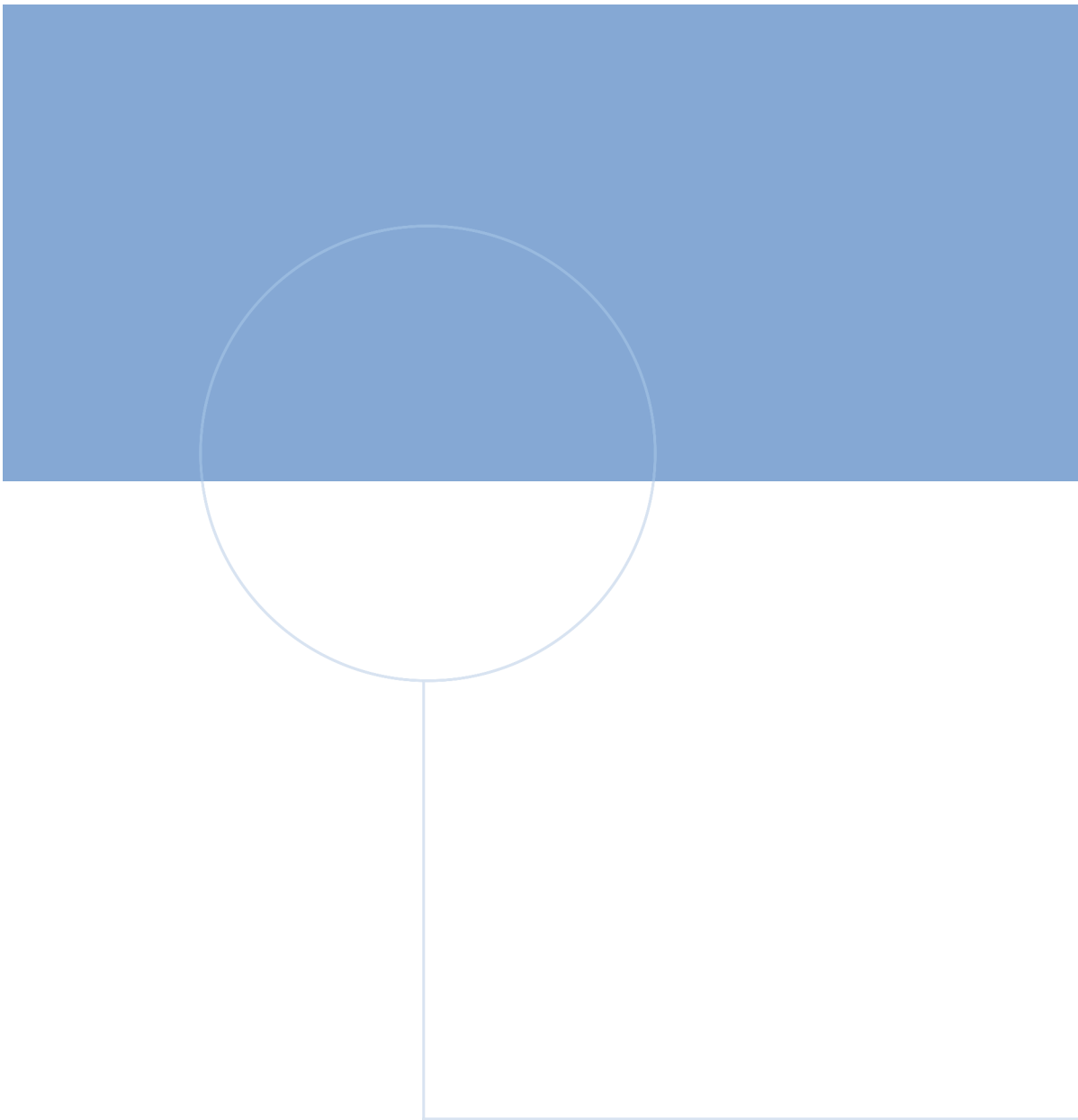

NTNU

Norwegian University of
Science and Technology